SEMMELWEIS EGYETEM

DOKTORI ISKOLA

Ph.D. értekezések

2870.

JURIGA-TÓTH KRISZTINA

Celluláris és molekuláris biofizika
című program

Programvezető: Dr. Kellermayer Miklós, egyetemi tanár
Témavezető: Dr. Simonné Dr. Nagy Krisztina, egyetemi docens
Konzulens: Dr. Jedlovszky-Hajdú Angéla, egyetemi docens

DRUG-CONTAINING IMPLANTABLE ELECTROSPUN MESHES BASED ON DIFFERENT BIOCOMPATIBLE POLYMERS

Ph.D. thesis

Krisztina Juriga-Tóth

Doctoral School of Theoretical and Translational Medicine

Semmelweis University

Supervisor:	Krisztina S. Nagy, Ph.D.
Consultant:	Angéla Jedlovszky-Hajdú, Ph.D.
Official reviewers:	Krisztina Ludányi, Ph.D.
	Zsombor Kristóf Nagy, Ph.D.

Head of the Complex Examination Committee: Alán Alpár, MD, D.Sc.

Members of the Complex Examination Committee: Mihály Kovács, D.Sc.
                                                                                 László Cervenák, Ph.D.

Budapest
2023

Table of Contents

List of Abbreviations

AE:	2-aminoethanol
ATR-FTIR:	attenuated total reflectance Fourier-transform infrared spectroscopy
BCB:	brilliant cresyl blue
BMP-2:	bone morphogenetic protein 2
COX-2:	cyclooxygenase-2
D1R, D2R:	dopamine receptor 1, dopamine receptor 2
DA:	L-dopamine-hydrochloride
DAPI:	4′,6-diamidino-2-phenylindole
DAT:	dopamine transporter
DBA:	dibutyl-amine
DG:	degree of grafting
DMF:	dimethyl-formamide
DMSO:	dimethyl-sulfoxide
Dox:	doxorubicin
DTT:	dithiothreitol
EMEM:	Eagle's minimal essential medium
FBS:	fetal bovine serum
FDA:	U.S. Food and Drug Administration
IC50:	half-maximal inhibitory concentration
ICAM:	intercellular adhesion molecule
IFN:	interferon
IL:	interleukin
iNOS:	inducible nitric oxide synthase
L-DOPA:	levodopa
MCP:	monocyte chemoattractant protein
MDA-MB-231:	triple-negative breast cancer cell line
NAD(P)H:	nicotinamide adenine dinucleotide (phosphate)
NEAA:	non-essential amino acids
OHDA, 6-OHDA:	oxidopamine, 6-hydroxydopamine
PASP:	poly(aspartic acid)

PBS:	phosphate buffered saline
PCL:	ε-polycaprolactone
PDLSCs:	human periodontal ligament stem cells
PEG:	polyethylene glycol
PFA:	paraformaldehyde
Pred:	prednisone
PSI:	polysuccinimide
PVA:	poly(vinyl alcohol)
SEM:	scanning electron microscopy
SH-SY5Y:	human neuroblastoma cell line
TGF:	transforming growth factor
THF:	tetrahydrofuran
TNF:	tumor necrosis factor
VCAM:	vascular cell adhesion molecule
WST-1:	water-soluble tetrazolium salt

1. Introduction

1.1. Engineered biopolymers can replace naturally occurring polymers

Polymer macromolecules consist of repeating monomer units, which are connected together with covalent bonds. Based on the origin, polymers can be classified into synthetic polymers and naturally occurring polymers (biopolymers), but biopolymers can also be produced by chemical synthesis (engineered biopolymers) (1).

Synthetic polymers such as polyvinyl chloride, polyethylene, or polypropylene are produced in laboratories or in higher quantities in manufactories, in contrast biopolymers generally have a natural origin: for example, cellulose (2) or pectin (3) is extracted from plants; gelatin (4), collagen (5), hyaluronic acid (6), and fibrin gels (7) have animal-origin; polylactic acid (8) and xanthan gum (9) are produced by bacteria. Engineered biopolymers such as polyamino acids, elastin-like polypeptides, or silk-like proteins can also be synthetized in laboratories but these mimic the naturally occurring polymers (1).

The application of naturally occurring polymers is restricted due to limited availability since the extraction method is mostly complicated, and it is difficult and time-consuming to reproduce them, not to mention the risk of infections regarding animal-origin. On the contrary, engineered biopolymers are producible in cost-effective ways even on large scale. However, there are only a few among these biopolymers, which are biocompatible and biodegradable at the same time (such as polylactic acid, polycaprolactone, or polyglycolic acid) (10).

Biocompatibility and biodegradability are some of the most important features during the application since these biopolymers are usually potential components of different systems developed for drug delivery, and medical implantations or other biomedical purposes. In these fields, the applied polymer must not be toxic to the host organism, it should not induce any inflammation or irritation or exert a negative reaction in the body, consequently, which properties together are considered as biocompatibility. In addition, for therapeutical applications it is substantial that the polymers should be degraded into smaller biocompatible molecules which can enter the normal metabolic pathways after fulfilling their duty, requiring no surgical procedure for their removal (1).

Considering the limitations and challenges in most of the medical or pharmaceutical aims, there is a possible way to replace the naturally occurring biopolymers with their synthetic-engineered biopolymer analog (11).

1.1.1. Polymer-based based drug-delivery systems

A huge number of active substances have quick elimination from the systemic circulation by liver and renal clearance thus their utilization is limited, therefore a higher dose or more frequent administration is required. However, polymer-based drug-delivery systems can overcome this problem by protecting the substance from early deactivation (11). In addition, by application of these systems the water solubility or the lipophilicity of the active substance can be increased, furthermore targeting and controlled drug administration can be ensured. By this way, the efficacy of the therapy can be improved, hence the amount of the applied substance can be decreased, and side-effects can also be reduced. To construct these systems, usually biodegradable polymers are used since in such cases the release of the drug can be controlled by the degradation of the polymer backbone (11).

The polymer-based drug-delivery systems may be classified into two main categories based on the formulation of the substance: physical encapsulation, adsorption or complexation, and chemical conjugation by covalent bonds (**Figure 1.**) (12).
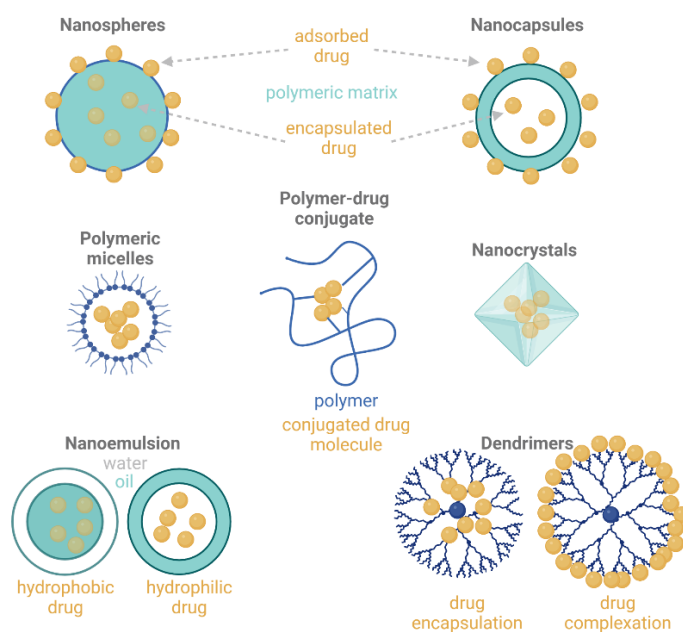
Figure 1.: *Polymeric nanoformulations. The image was made by Biorender based on the work of Viswanthen et al. (12).*

As a matter of encapsulation-based drug-delivery systems, an interstice is formed by association of certain macromolecules, and the substance can be delivered in this interstice or may absorb physically to the surface as well, for example in the case of polymeric nano- or microparticles (spheres and capsules), polymeric micelles, nanocrystals, dendrimers. During the complexation, two or more macromolecules associate with a nonbonded entity, these systems rely on for example London forces, hydrogen bonding, or hydrophobic interactions (at dendrimer complexes) (12).

The resulting complexes produced by physical encapsulation, adsorption, or complexation are often unstable under physiological conditions, therefore polymer-drug conjugates – in which the substances are connected to the polymer chemically with covalent bonds – seem to be more suitable candidates for long-term controlled drug-delivery systems (13).

1.1.2. Polymer-drug conjugates

By conjugation of small-molecule substances to polymer nanocarriers with ester, amide, or disulfide bonds more stable polymer-drug conjugates can be constructed (compared to physical encapsulation, adsorption, or complexation) in order to overcome the problems of poor solubility, short circulation half-time, and toxicity. The conjugation of a drug with a polymer forms a so-called polymeric prodrug due to the substance remaining inactive during the delivery with the assistance of the applied polymer. A polymer-drug conjugate may:

- increase the water solubility
- enhance the bioavailability
- preserve the inactive form
- improve the pharmacokinetics
- reduce the antigenic activity
- provide the possibility of the targeted delivery

of the active substance during the treatment, based on the nature of the polymer (14). Successful conjugation depends on the chemical structure of both the drug and the polymer. The key features are molecular weight and steric hindrance hence it is often necessary to have an appropriate linker group between the active substance and the applied polymer (14).

Polymeric prodrugs can be divided into three major groups. The first group contains conjugates which enable the transformation of the delivered substance into its active form inside the cell. In the second group, the prodrug usually consists of two or more molecules that form the active drug under certain and well-defined conditions. The conjugates of the third group contain targeting agents besides the carrier polymer and the active components (14).

Among the biocompatible and biodegradable polymers, only a few turned out to be an adequate alternative for polymer-drug conjugates. The major challenges regarding these polymers are the nonspecific distribution, *in vivo* circulation instability, inadequate drug-carrying capacity, unsuitable linkers, inefficient drug release, or difficulty during synthetization. Polyethylene glycol and dextran were among the first drug-conjugated polymers introduced as polymer-base of anticancer-drug conjugates in the 1970s (15). Besides these, poly(glutamic acid), polysaccharides (cellulose, chitosan, alginate), and proteins have also been applied as polymeric drug-delivery carriers (15). Although polyamino acids mimic the chemical structure of the natural proteins, there are only few examples in the literature about their use as a drug carrier: polyamino acid-based micelles (16), doxorubicin-peptide conjugates (17), α-amino acid based polymers (18), poly(glutamic acid) based paclitaxel (19), etc.

Nowadays, polymer-based drug-delivery conjugates are commonly developed for tumor therapy, as polymer-based pharmaceuticals have the advantage of high molecular weight since the way of prodrug uptake is different compared to the uptake pathway of the same drug without polymer. The tumor cells usually internalize the conjugates by endocytosis (**Figure 2.**), while small molecules can enter the cells by diffusion. By applying polymers with a targeting moiety, the drug uptake of tumor cells can be enhanced, while side effects of the substance in the healthy cells can be reduced (20).
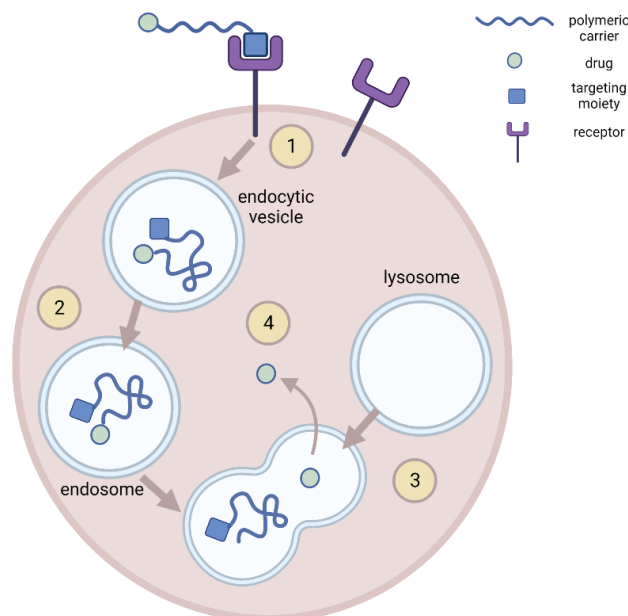
Figure 2.: Receptor-mediated internalization of polymer-drug conjugates: (1) interaction of targeting moiety and receptor, internalization; (2) transport; (3) fusion with lysosomes; (4) degradation and drug release. The image was made by Biorender based on the work of Khandare et al. (14).

With additional nano- or micro-formulation of the polymer-drug conjugates, further improvement can be achieved in the bioavailability of the substance (14). Among these procedures, the latest cutting-edge technique is electrospinning. By using this technique, fibrous products can be produced with the average fiber diameter in the nano- or micrometer range (21).

1.2. Electrospinning technique and electrospinning of biopolymers

Biopolymer-based electrospun fiber mats can be applied as air filter, protective clothing, or in various biomedical and pharmaceutical applications for instance wound dressings, scaffolds for tissue engineering, or drug-delivery systems (21,22).

The first appearance of the term "electrospinning" was in 1994, although Formhals patented the electrostatic spinning process and apparatus in 1934 (23), 1939 (24), and 1944 (25). The first fibrous biopolymer produced by electrospinning was the DNA (26) in 1997.

Generally, the apparatus consists of a capillary tube or syringe with a needle or pipette on the end; a power supply, and a collector or target, which can have different shapes and materials (plain plate or rotating drum, made of copper or covered with aluminum

foil). The power supply is connected to the needle of the polymer solution containing syringe tube, and the target collector is grounded – these parts of the equipment are placed at a short, well-determined distance from each other (**Figure 3.**) (21).
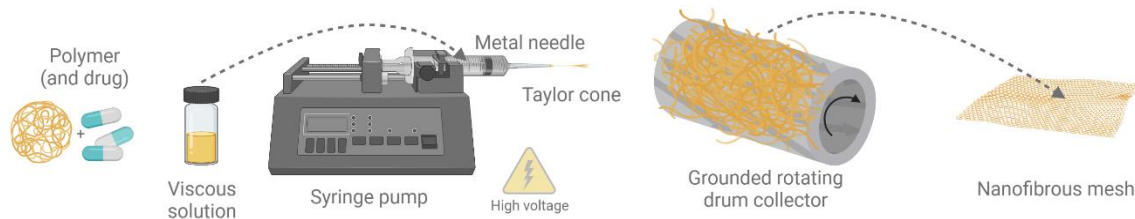
Figure 3.: Electrospinning set-up. The image was made by Biorender.

During the procedure, the polymer solution is pumped through the needle by a syringe pump, which controls the flow rate. At a critical voltage, the Taylor cone appears, and a straight jet of the polymer emerges from the cone. While the jet is reaching the collector a random movement appears due to the instability of the jet in the electric field, the solvent is evaporating, and a dry fibrous polymer mat can be deposited on the applied target (21).

In general, the selection of the suitable polymer for electrospinning is challenging because the features of the product are highly influenced by the chemical and physical properties of the polymer. The important features of the polymer of choice are molecular weight, molecular weight distribution, and glass-transition temperature, as well as the solubility. The morphology of the electrospun fibers and the spinnability is highly affected by the viscosity, viscoelasticity, concentration, surface tension, and electrical conductivity of the polymer solution, the chemical properties of the introduced substances, the feed rate of the solution, the field strength, the geometry of the electrode, the vapor pressure of the solvent, and the humidity (27). Up to now, there are several examples for electrospinning of biopolymers have been described such as polysaccharides (cellulose (28), chitin (29), chitosan (30), alginate (31), and hyaluronic acid (32), dextran (33) and its derivatives), proteins (collagen (34) and gelatin (35), silk (36)) and even DNA (37).

In the case of biomedical and pharmaceutical applications, solubility, biocompatibility, biodegradability, and mechanical properties of the polymer and the fibrous product should always be taken into account (21).

1.2.1. Electrospinning in pharmaceutical applications

Due to the wide variety of applicable polymer materials, various kinds of drugs can be delivered by electrospun nanofibers (e.g., antibiotics, proteins, anticancer drugs, antioxidants). There are three main strategies for creating these drug-delivery systems by electrospinning: embedding/co-electrospinning (drugs are mixed with polymers before electrospinning); coating (drugs are immobilized to the surface of the fibers by electrostatic interaction, van der Waals interaction, or hydrogen bonds); and encapsulation (drugs are loaded into the fibers) (22).

During the co-electrospinning technique (embedding) the drug and the polymer are going through the electrospinning process at the same time. The applied polymer and the solvent are usually selected based on the physicochemical properties of the chosen drug. For example hydrophobic drugs can be mainly dissolved in organic solvents, therefore the applied polymer also has to be soluble in the same solvent, which limits the number of the polymer of choice.

When the drug is electrospun together with the polymer, the drug release is usually fast, and electrospinning may cause destruction in some molecules, which have sensitivity to high voltage and/or organic solvents. To avoid these drawbacks, in the case of sensitive molecules, the post-electrospinning immobilization (coating) can be a safer choice.

Regarding coaxial electrospinning (encapsulation), a special needle is used with inner and outer parts in concentric setup for suitable spatial orientation the drug and the polymer respectively, hence drugs can be delivered in a core-shell structure. The shell can protect the drug from the external environment, and it can enhance the rate of the release (21).

There are also several examples of smart electrospun nanofibers, which can release drugs at a specific location in the body due to external stimulus. These structures can respond to various environmental parameters such as pH value, temperature, light, and electrical- or magnetic fields (22).

Due to the high specific surface of nanofibers, they can provide fast burst release of the drugs. However, by the careful selection of the appropriate polymer and the electrospinning strategy, the drug release can be regulated and tailored.

1.2.2. Drug-conjugated electrospun polymer fibers

A further alternative to control and tailor the release of the chosen drug more precisely is to combine the polymer-drug conjugation with electrospinning.

There are only a few studies in the literature about drug-conjugated polymer-based electrospun delivery systems. For e.g., Sasikala et al. conjugated bortezomib, a chemotherapeutic drug, to poly(D, L-lactide-co-glycolide) and used the electrospinning technique for tumor-triggered controlled drug release (38). Parwe et al. conjugated ciprofloxacin to poly(L-lactic acid) polymer for nanofiber fabrication and evaluation its antibacterial effect (39). Pitarresi et al. created a polyaspartamide-polylactide electrospun scaffold for delivery of ibuprofen, which was conjugated to the copolymer (40), while Jalvandi et al. produced composite nanofibers containing polyvinyl alcohol and conjugated levofloxacin-chitosan for controlled drug release (41). In addition to these works, conjugated electrospun drugs can be used for tissue engineering (42) and for wound dressing as well (43).

In the case of electrospinning of polymer-drug conjugates, the drug is chemically bond to the polymer chain and therefore the kinetics of the drug release can be modulated by the properties of the polymer. The drug release can be either a burst release or it can be determined by the diffusion or the solubility kinetics of the polymer fibers (prolonged drug release). By combining chemical conjugation and electrospinning strategy, the solubility of the slightly water-soluble drugs can be increased due to the large specific surface area of the fibers. At the end of the electrospinning process, according to the rapid evaporation of the solvent and the quick deposition of the fibers, the crystal structure of the substance can alter from totally crystalline to more amorphous.

1.3. Applied polymers – characterization and biomedical applications

1.3.1. Poly(vinyl alcohol) (PVA)

PVA is a biocompatible, white-colored semi-crystalline synthetic polymer, which is commercially available in granular or powder form. The physical attributes of PVA, such as the melting point (180-230 °C), viscosity, pH, and crystal structure are highly dependent on the degree of hydrolysis and the molecular mass of the polymer (44). PVA is usually synthesized by saponification (alkaline hydrolysis) from vinyl acetate

monomers in aqueous sodium hydroxide, due to the fact that vinyl alcohol monomers are unstable. During the polymerization, the ester groups of vinyl acetate is partially replaced by hydroxyl groups (44).

Due to its biocompatibility, non-toxicity, non-carcinogenicity, non-immunogenicity, and its favorable physical and chemical properties such as water solubility in consequence of the high hydroxyl group content, and thermostability, it is a widely used polymer for various pharmaceutical and biomedical applications (44–47).

According to the hydrophilic character of PVA, the polymer can swell in water. When crosslinkers are used (formaldehyde, acetaldehyde, glutaraldehyde, etc.), hydrogels can be prepared for a wide variety of biomedical applications. As a scaffold for tissue regeneration, PVA-based hydrogels must provide adequate mechanical and degradation properties, as well as swelling ratio according to the requirements. Concerning the abovementioned prosperous features and promising mechanical properties (elasticity, high tensile strength, and high elongation at break), PVA-based materials are U.S. Food and Drug Administration (FDA)-approved candidates for artificial replacements of cartilage (48) or certain organs for instance vocal cords (49). Because of the hydrophilic character, high oxygen permeability, transparency, and due to lack of protein adsorption, PVA is an ideal material for hydrogel-based contact lenses (50) and eye-wetting drops (51).

Regarding pharmaceutical applications, PVA hydrogel-based drug-delivery systems (52) and wound dressings (53) have been developed, due to its well-defined, tailorable drug-delivery characteristic (54).

Besides the production of hydrogels, electrospinning is also a successfully applied technique in the case of PVA to create fibrous meshes for biomedical purposes such as skin (55), vascular (56), neural (57), corneal (58), bone (59), cartilage (60), hernia (61) scaffolds and implants applying PVA *per se* or in combination with other or drugs. Concerning drug-delivery applications, several examples can also be found in the literature about the incorporation of drugs (62,63), nanoparticles (64), proteins (65), growth factors, and DNA into PVA fibers alone (66,67) or PVA fibers combined with other polymers such as polylactic acid (68). Usually, hydrophobic drugs are loaded or incorporated into PVA since this hydrophilic polymer can enhance the solubility of a poorly soluble drug after electrospinning them together. The enhanced solubility can

originate from the altered crystal structure of the drug besides the higher specific surface area because of the nanofibrous structure. According to drug-polymer incompatibility, a drug with a hydrophobic character can migrate and localize onto the fiber surface generating burst drug release (69,70).

1.3.2. Polysuccinimide (PSI)

Polysuccinimide is a biocompatible, biodegradable hydrophobic, and amorphous synthetic polymer, which can undergo a hydrolysis at slightly alkaline pH transforming to poly(aspartic acid) (PASP) (71–73). PASP has peptide-like structure due to the amide linkages in the polymer chain, therefore the derivatives during the degradation process behave like amino acids or small peptides. This makes PASP based polymers fully biocompatible as the substances can be used up in amino acid metabolism or can be eliminated easily from the body (74,75).

PSI can be synthesized by either a thermal polymerization reaction from aspartic acid or by a reaction based on maleic anhydride and ammonia. Although the maleic anhydride-based synthesis is fast and cost-effective, this provides PSI only with low molecular weight (1,000-3,000 g/mol) (76). On the contrary, the thermal polymerization of aspartic acid in the presence of an acid catalyst can produce PSI with higher molecular weight (5,000-200,000 g/mol) (74,75,77).

By an imide ring-opening (nucleophile attack) reaction, PSI can be easily modified with different molecules, which own a primary amine group (78). This feature makes PSI and polyaspartamides (modified PSI) promising candidates for polymer-based drug-delivery systems (75,79).

There are several examples in the literature for the modification of PSI regarding medical applications. For instance, Neri et al. modified PSI with ethanolamine to create a plasma expander (74), while Li et al. used L-cysteine to modify the PSI for the treatment of lead poisoning (80). For intracellular drug-delivery purposes, there are modifications using tetraethylenepentamine (81), cyclodextrin (82), dopamine (83), 1-propylimidazole with dimethylpropylammonium (84). After a ring-opening reaction with hydrazine hydrate (82,85–87) aldehyde-containing polyaspartamides can be produced, which are capable to form drug containing hydrogels after cross-linking (88). Several nanomicelles and nanoaggregates were described in the binding of Dox to the PSI chain by a pH-sensitive linker (89–94) for cancer treatment. Research about

polyaspartic acid-based treatment was also carried out regarding neurodegenerative diseases including epigallocatechin gallate conjugated polyaspartic acid micelle (95), and quercetin incorporated polyaspartamides (96). Polyaspartamide-based drug-delivery systems were also developed for gastrointestinal drug-delivery purposes (97,98) or for wound dressings (99).

The PSI-based carriers can hinder the drug accumulation inside the targeted cells, increase the bioavailability and alter the solubility features of the drug (100,101). However, with applying PSI in combination with other polymers, the properties of the polymer carrier can be tailored more precisely according to the adequate aim (102). For example, PEGylated phospholipid-polyamino acid micelle with beclomethasone dipropionate (103) and ethylenediamine and lipoic acid-modified PSI (104) are prepared for pulmonary disease treatment or there are also examples for cancer treatment regarding poly(N-vinylpyrrolidone) and PASP block copolymer-based host-guest inclusion complexes loaded with cisplatin (105).

1.3.3. ε-polycaprolactone (PCL)

PCL is a biodegradable and biocompatible polyester with hydrophobic and semicrystalline characteristics. Its mechanical features and degradation profile are highly dependent on the molecular weight of the polymer, crystallinity, and branching, which can be affected by the different polymerization methods (106,107). PCL can be produced by ring-opening polymerization of caprolactone monomers through different polymerization mechanisms (anionic, cationic, coordination, or radical) (108).

Regarding the degradation, the ester bonds-monomer ratio has also a crucial role. According to the literature, the total degradation of the polymer takes 2 or 3 years under biological conditions (109–112). The ester bonds can be cleaved by lipase enzymes and the derivatives of the polymer can be metabolized in the citric acid cycle (107), therefore, PCL is considered as a biocompatible polymer.

Due to its favourable physicochemical and high load bearing capacity, PCL is a promising candidate for tissue engineering, and drug-delivery purposes according to the FDA (107,113,114). As a result of its slow degradation, long-term prolonged drug release can be achieved by drug incorporation. According to the drug-polymer compatibility, lipophilic drugs can be incorporated homogeneously inside the hydrophobic PCL. There is a wide variety of examples of PCL-based drug delivery

systems in the literature: curcumin-loaded nanoparticles (115), dexamethasone-loaded electrospun mats (116), paclitaxel-loaded polyethylene glycol (PEG) and PCL-based micelles and nanoparticles (117,118). Introducing hydrophilic drugs into PCL, such as in the case of doxycycline-encapsulated PCL microspheres (119), or carboplatin-loaded nanoparticles (120), the drugs can be localized on the surface generating a burst release due to the drug-polymer incompatibility (69). The solubility and the drug release time can be tailored by applying other polymers besides PCL (121). By using polylactic acid and poly lactic-co-glycolic acid-based copolymers the degradation of the drug-delivery system can be shortened (110,122), or the cytotoxic efficacy can be enhanced by applying polyethyleneimine to produce PCL-based graft copolymers with the encapsulation of doxorubicin and p53 plasmid DNA (123). Antibacterial efficacy was developed regarding triclosan-loaded PCL-poly(quaternary ammonium salt) micelles (124).

In addition, some PCL-based electrospun meshes have been researched for different drug-delivery purposes, to exploit the high specific surface area of the fibers. For instance, dexamethasone-loaded PCL meshes were researched for potential ear and ocular treatments (116). Doxorubicin was also electrostatically bounded to PCL meshes by an immersion method for possible cancer therapy in the future (125), or tetracycline was loaded into PCL fibers for potential treatments of periodontal and rheumatic disease (126). The drug delivery purposes can be easily combined with tissue engineering aims as regards PCL-based electrospun nanofibrous meshes. Although PCL is hydrophobic and cells are not capable of adhering to its surface, by adding different bioactive factors, such as proteins or growth factors to the system, or using it in combination with other polymers (127), its applicability for tissue regeneration can be enhanced (128–132). There are PCL-based tissue-engineered scaffolds in the literature regarding soft and hard tissues as well according to their different mechanical requirements. The slow degradation feature of PCL makes it a good candidate for hard tissue implants that can be used in orthopedics (133–135) or dentistry (136) in the future. In addition, the possible wound-healing applications of PCL alone (137) or with other polymers (138,139) were also described, besides other potential soft tissue-based regeneration like bladder repair (140) or nerve regeneration (141) due to the prosperous mechanical properties of PCL (107).

1.4. Applied substances

According to the previous chapters, several drugs with different physicochemical properties can be incorporated into polymers to tailor the drug release profile or even the pathway of the cellular uptake by the abovementioned electrospinning process. Regarding the following substances: dopamine (DA), doxorubicin (Dox), and prednisone (Pred), there is a strong demand to alter the drug release kinetics to enhance the bioavailability and to avoid the inconvenient side effects during a potential therapy.

1.4.1. The role of dopamine (DA) and dopamine receptors in biomedical applications

As a neurotransmitter or signalling molecule, DA plays a key role in the communication between neuronal cells (**Figure 4.**) (142).
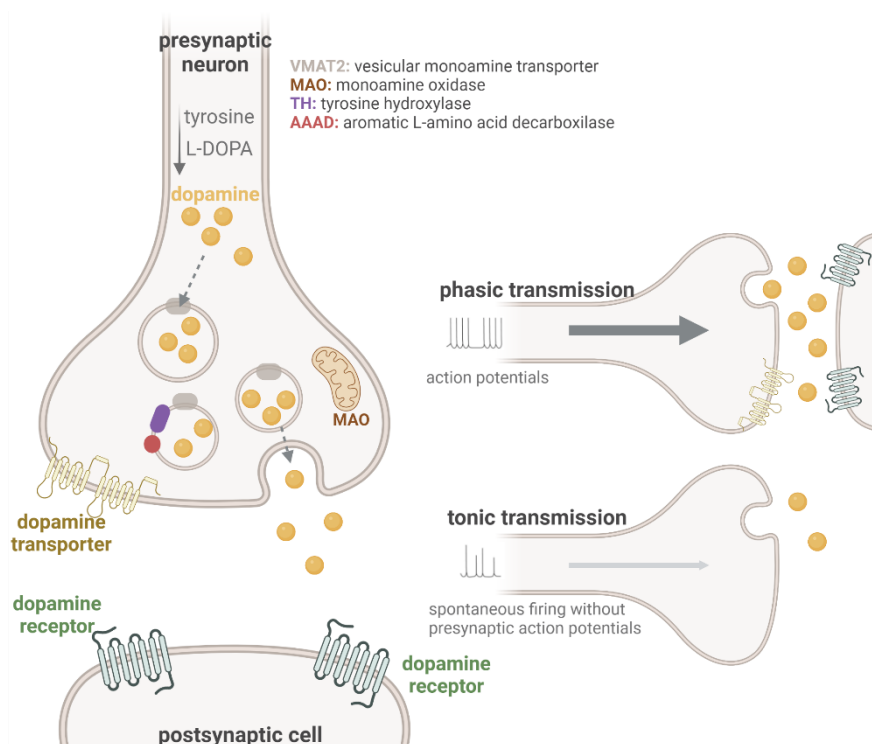
Figure 4.: *Dopamine: synthesis and phasic/tonic transmissions. The image was made by Biorender based on the work of Klein et al.* (142).

Regarding its synthesis, levodopa (L-DOPA), which is the inactive form of DA (143), can be produced from tyrosine directly, or from L-phenylalanine through tyrosine in an indirect way (144,145) in the cytosol of dopaminergic neurons. DA is stored in an acidic environment in synaptic vesicles, which can stabilize and prevent its oxidation to

toxic quinones (146) and protect it from further metabolization (147,148). From the synaptic vesicles, DA can be released into the synaptic cleft through exocytosis driven by membrane potential changes (149), volume transmission, diffusion (150), and both phasic and tonic transmissions. During the phasic release, the action potential generates a fast and transient DA appearance at the presynaptic terminal. As regards the tonic transmission, the DA release is mainly regulated by other neuronal cells and by the reuptake of neurotransmitters – this process is not action potential related, therefore the DA release is milder compared to the phasic transmission (151). The reuptake of extracellular DA is regulated by dopamine transporters (DAT) and monoamine transporters as well (152,153). The extracellular DA can bind postsynaptic receptors or presynaptic receptors (D2R, D3R) as well. DA receptors are commonly targeted in clinical pharmacology during therapies for various neural diseases such as schizophrenia, Parkinson's disease, bipolar disorder, or depression. The DA receptors, which are members of the G protein-coupled receptor superfamily, mediate all the physiological functions of DA through both G protein-dependent and independent mechanisms (154). According to the structure and properties, DA receptors can be classified into D1-like receptor (D1, D5) and D2-like receptor (D2, D3, D4) subtypes. D1 and D2 receptors are expressed mainly in the brain, but it is rare if both are expressed by the same cells (155,156). D1-like and D2-like DA receptors have different affinities to DA (D2R >> D1R) and respond to the DA concentration in different ways: D1-like receptors are activated by high concentrations of DA (phasic release), while D2-like receptors are stimulated by low levels of DA (tonic release) (157–159). The D1-like receptors are coupled to the G protein $G\alpha_{s,olf}$, which activates adenyl cyclase and generates increasing intracellular concentration of the second messenger cyclic adenosine monophosphate, while D2-like receptors are coupled to the G protein $G\alpha_{i,o}$, which directly inhibits the formation of cyclic adenosine monophosphate by inhibiting the enzyme adenylyl cyclase (160). The cyclic adenosine monophosphate is responsible for the activity of the protein kinase A, which is involved in many intracellular signalling pathways triggered by the binding of a ligand to its transmembrane receptors including DA receptors (142,161).

Since DA receptors are strongly involved in dopaminergic signalling, and DA is responsible for a wide variety of diseases and functions (memory, attention, learning,

movement, hormonal regulation, immune system), DA-based research is emerging to find potential therapies to cure diseases such as Parkinson's disease, Huntington's disease, schizophrenia, attention deficit of hyperactivity (142).

Because DA is a primer amine group-containing monoamine molecule, it can be used for easy cost-effective modification of PSI to produce DA-containing polyaspartamides (162,163) or PSI-DA conjugates for drug-delivery purposes (78,164).

According to the literature, DA was already conjugated to other kinds of polymers (DA-Dox-polymer (165), DA functionalized thiophene-fluorene copolymer (166)). Moreover, there are some studies aimed to develop DA-containing electrospun fibers for different biomedical purposes, e.g. polylactic acid-DA-SiO$_2$ (167) or Zein nanofibers with L-DOPA (168). Nevertheless, it is important to mention that DA cannot pass through the blood-brain-barrier.

Regarding the above-mentioned literature, the *in vitro* experiments are mainly carried out using neuronal cells, such as the SH-SY5Y human neuroblastoma cell line, hence its differentiated and undifferentiated forms are commonly used as cell models in neuroscience. The SH-SY5Y cell line has catecholamine uptake system and possesses DAT as well (169). Regarding these cells, the intracellular DA concentration is relatively low but the DA uptake ability provided by DAT (170) is higher than their capacity to store, therefore these cells could be very sensitive to the increased cytosolic DA content (171).

According to this, some examples can be found for the investigation of the effect of DA and its metabolites on this cell line. For e.g., Haque et al. showed that L-DOPA and its metabolites containing two OH residues exerted toxic effect on SH-SY5Y cells due to the generation of highly reactive quinones. After 24 h, the IC50 values for L-DOPA- and DA-induced cytotoxicity were 194 and 184 μM respectively. There were almost no changes in cytotoxicity induced by L-DOPA and DA co-incubated with a DA transporter blocker (172).

Lopes et al. investigated the cytotoxicity of oxidopamine (6-OHDA) in the case of differentiated and non-differentiated SH-SY5Y cells. 6-OHDA is a neurotoxin it is used to generate Parkinson's circumstances due to it causing dopaminergic and noradrenergic cell death. This toxin also enters the dopaminergic neuron via DAT and causes oxidative stress (173). The median toxic dose for undifferentiated cells was evaluated as

35 μM after 24 hour-long 6-OHDA treatment. Their study claims that DAT inhibition did not protect the undifferentiated cells against oxidative stress, in contrast to differentiated cells where DAT inhibition gave protection possibly because undifferentiated cells have low levels of DAT (174), which corroborates with previous results (175,176).

Ham et al. investigated the neuroprotective effect of spirafolide against DA-induced apoptosis in human SH-SY5Y cells. The treatment with only 0.6 mM DA for 24 hours, showed diminution of cell number by 60% (177). Kawajiri et. al treated differentiated SH-SY5Y cells with 50 μM DA hydrochloride for 24 hours. The cell viability decreased to approximately 60% (178).

In the literature, other prosperous features of DA were utilized beside its pharmaceutical effect: for e.g. DA can form strong covalent and noncovalent bonds with inorganic and metallic materials, Kim et al. used the catechol functional group of DA to immobilize heparin (Hep-DA conjugate) and BMP-2 on the surface of PCL fibers to enhance the proliferation and osteogenic differentiation of PDLSCs (179). Lee et al. also used DA for the immobilization of BMP-2 on a titanium surface, but in a different approach: they used the capability of DA for oxidative polymerization to make mussel-inspired polydopamine (180).

1.4.2. Doxorubicin (Dox) as an anti-cancer drug

Doxorubicin is an anticancer anthracycline drug molecule, which was the first to receive clinical approval for intravenous introduction in liposomal form as a therapy against different tumors including bladder, stomach, lung and breast cancer, leukemia, lymphomas, pediatric tumors, etc. (181,182). Dox exerts its effect at least by two different mechanisms: it can intercalate between DNA strands and inhibit the topoisomerase II enzyme production inhibiting the replication process. On the other hand, Dox generates free radicals, which are also toxic for the cells since they can attack the DNA and the cell membrane as well (182,183).

Dox can be produced by genetically modified *Streptomyces* spp., however, there are more than 2000 analogs to overcome its cardiotoxic side effect (182,184,185), or it can be combined with cardioprotective agents and encapsulation by drug carriers can also applied for this purpose (184,186). By using different carriers, such as liposomes, the therapeutic index can be enhanced through favorable pharmacological distribution since

the liposomes are accumulated in tumors and only a reduced amount of Dox can reach the heart muscle, which has tight capillary junctions (187). On the other hand, the application of conventional liposomes is limited because of the short circulation half-life, therefore pegylated liposomes were developed for more prolonged circulation (Doxil, Caexyl) (182). However, pegylated-liposome-based Dox delivery also has a side effect: hand-foot syndrome. Later nonpegylated liposomal Dox with stable, long circulation time was developed without the side effect of pegylated liposomes (Myocet, Nudoxa) (182). The development of Dox-containing systems for cancer therapy is still ongoing and emerging in recent years. Among them, stealth liposomes (188), immunoliposomes (189), temperature-, light-, pH-, and enzyme-sensitive liposomes (182,190) can also be found. Block co-polymer-based (191), hydroxyapatite-based hydrogel implants (192) were also investigated. Moreover, Dox-delivery systems based on different polymer-Dox conjugates (193,194) including PSI-Dox conjugates can also be found in the literature, although most of these nanocarrier conjugates possess a pH-sensitive linker between Dox and PSI (89–93,195–197). Recently, implant-based local Dox therapies (198–200) open a new perspective as they can provide appropriate Dox concentration *in situ* during the therapy through a well-determined drug release profile with reduced side-effects. For potential implants, several examples can be found in the literature for Dox containing fibrous meshes with different polymer-carriers such as PCL and polylactic acid (201), functionalized PCL (202–204), functionalized PVA and PCL core-shell nanofibers (205), functionalized polylactic acid (206), poly lactic-co-glycolic acid/polyethylene glycol fibers (207), poly-l-lactic acid fibers (208), polydopamine and alginate fibers (209), chitosan/PVA and polylactic acid/chitosan nanofibers (210), and silk fibroin nanofibers (211) amongst numerous others for this aim.

Since the commonly applied Dox-containing treatments usually involve other substances along with Dox, for e.g., prednisone (182,212), the combination of different drugs with Dox in a layer-by-layer implantable mesh can be a promising path.

1.4.3. Prednisone (Pred) and its anti-inflammatory effect

Prednisone, which is the inactive form of prednisolone, is a glucocorticoid that mainly exerts its anti-inflammatory effect by suppressing the immune system during various therapies such as asthma, rheumatoid arthritis, dermatitis (213,214). In addition, it is

often applied even in different anti-cancer therapies (212) due to reducing the side effects generated by chemo- or radiotherapy (215), inducing apoptosis in the case of lymphoid cancers, and influencing tumor growth according to the applied dose and the cancer type (215). Pred, like other glucocorticoids, exerts its effects through the glucocorticoid receptor, a member of the nuclear receptor superfamily of transcription factors (216). The binding of glucocorticoids to the glucocorticoid receptor generates conformational changes hence the receptor can be released from the heat shock protein complex in the cytoplasm, and translocated to the nucleus where the receptor influences the gene transcription leading to its immunosuppressive effect (217).

Besides several other effects and features (218), glucocorticoids can influence the immune response by decreasing the levels of pro-inflammatory (immune cell activation capability) molecules (interleukine (IL)-1β, IL-2, IL-4, IL-5, IL-6, IL-8, IL-12, IL-18, COX-2, E-selectin, iNOS, interferon (IFN)-γ, TNF-α, ICAM, MCP-1, and VCAM (219)) and anti-inflammatory cytokines (IL-1 receptor antagonist, IL-4, IL-10, IL-11, IL-13). Cytokines are small proteins secreted by numerous different types of cells to influence the interaction and communication among them. Proinflammatory cytokines, which are responsible for the up regulation of inflammatory reactions, are mainly secreted by activated macrophages, while anti-inflammatory cytokines control the function of the above-mentioned pro-inflammatory cytokines. Leukemia inhibitory factor, interferon-α, IL-6, and transforming growth factor (TGF)-β can be part of both anti- and pro-inflammatory cytokines according to the different circumstances. IL-1, TNF-α, and IL-18 can also inhibit the pro-inflammatory cytokines. In addition to the grouping system based on pro- and anti-inflammatory cytokines, these molecules can be categorized into lymphokines, monokines, chemokines, and interleukins based on the secreting cells (lymphocytes, monocytes, leukocytes) and their activity (chemotactic activities; acting on other leukocytes) or can be separated according to the place of action (autocrine, paracrine, endocrine) (220).

Pred has poor water solubility, therefore in order to successfully apply as an immunosuppressor, there is a strong need to enhance the bioavailability by different carriers or formulation processes (221,222). Amongst these methods, the electrospinning formulation can be a promising technique. Regarding Pred-containing nanofibers, Poller et al. created polyvinylpyrrolidone-based nanofiber tablets to enhance

the solubility and the bioavailability of Pred (223), and Wang et al. produced Pred-loaded electrospun poly (ε-caprolactone-*co*-l,l-lactide) copolymer against intimal hyperplasia after coronary artery bypass graft surgery to tailor the drug release (224). Besides prednisone, recently prednisolone-loaded electrospun fibers were also fabricated for the same purpose: to conquer the low aqueous solubility and bioavailability and to find alternatives to the commercially available orally disintegrating tablet formulation of prednisolone. For e.g., Celebioglu et al. compared electrospun cyclodextrin/prednisolone inclusion complexes and pullulan/prednisolone nanofibrous webs (225), Tawfik et al. made prednisolone-containing PVA nanofibers (226) and Jafari-Aghdam formulated methylprednisolone acetate-Eudragit RS100 nanofibers for this aim (227). Besides the drug-delivery purposes, there are other biomedical aims regarding prednisolone such as different scaffolds: for e.g., Zhang et al. prepared polycaprolactone/polysialic acid hybrid nanofibers for the treatment of spinal cord injury (228) or Yao et al. produced methylprednisolone-loaded polyurethane fibrous patches for infracted myocardium restoring (229).

Prednisone-containing nanofibrous systems can be promising candidates for local drug-delivery therapies, therefore the side effects which occurs during the systemic introduction can be moderated.

2. Objectives

The aim of my thesis was to create implantable nanofibrous polymer-based drug-delivery systems for biomedical applications and to characterize their physicochemical and mechanical properties as well as their biological effect on cell cultures.

The main objectives were the followings:

1. to prepare electrospun meshes from dopamine (DA)-conjugated (chemically bound) polysuccinimide (PSI) and investigate the effect of the degree of grafting (DG) on the fiber diameter and the mechanical features (specific load capacity and initial modulus) of the meshes;

2. to examine the dissolution of PSI-DA conjugates and to compare the kinetics of DA release from the nanofibers with different DG;

3. to investigate the effect of DA-conjugated nanofibrous PSI meshes on the viability of two relevant cell types: a primary cell culture (e.g. periodontal ligament stem cells) and a neurogenic cell line (e.g. SH-SY5Y neuroblastoma cell line), and to study the potential internalization of the polysuccinimide-dopamine conjugates;

4. to load prednisone into poly(vinyl alcohol), polysuccinimide, and ε-polycaprolactone electrospun meshes and to investigate the effect of different amounts of prednisone on fiber diameter, mechanical performance (specific load capacity, initial modulus and maximal elongation) and the effect of polymers with different polarity on drug release, as well as on anti-inflammatory effect *in vitro;*

5. to prepare doxorubicin (Dox)-loaded and Dox-conjugated nanofibrous PSI meshes and compare their properties regarding drug release, cytotoxicity and cellular internalization *in vitro*.

3. Methods

3.1. Preparation of neat and drug-containing polymer meshes

3.1.1. Synthetization of polysuccinimide

PSI was synthesized from the powder form of L-aspartic acid. The catalyst during the thermal polycondensation reaction was o-phosphoric acid, which was applied at a weight ratio of 1:1 along the L-aspartic acid. The substances were homogenously mixed in a round-bottom flask, which was installed to a vacuum rotary evaporator (Rotadest IKA RV-10). The mixture of L-aspartic acid and o-phosphoric acid was progressively heated up to 180 °C in an oil bath and the pressure was progressively reduced to at least 4 mbar (Vacuubrand PC 3001 vario pump). After the 8-hour-long thermal polycondensation reaction, the brown viscous melt of the polymer was dissolved in dimethyl-formamide (DMF). After the completed dissolution, the solution was gently precipitated in distilled water during constant stirring. The white-color precipitation was filtered by a glass filter and resuspended in distilled water at least 4 times until the pH reached neutral. After this, the polymer was dried in a heated exsiccator (40 °C) until a constant mass was obtained.

3.1.2. Synthetization of PSI-DA conjugates and PSI-Dox conjugate

The PSI-DA conjugates were synthesized at different degrees of grafting (DG), which refers to the molar ratio between the succinimide monomer units and the DA (**Equation 1.**), while in the case of PSI-Dox conjugate, there was only one composition (DG800).

$$Degree\ of\ grafting\ (DG) = \frac{n_{monomer}}{n_{drug\ molecule}} \tag{1}$$

For the modification, dried PSI powder was dissolved in dimethyl-sulfoxide (DMSO) (25 w/w%). Thereafter, L-dopamine-hydrochloride and dibutyl-amine (DBA) were separately dissolved in DMSO and added to the homogenous PSI/DMSO viscous solution. In the case of PSI-Dox conjugate the doxorubicin-hydrochloride and DBA were dissolved in DMF. DBA was used in order to avoid the protonation of the primer amino group of the drugs. The degree of DA grafting in final PSI-DA conjugates was 1, 2, and 4. In a unique case, 2-aminoethanol (AE) was also grafted to the main polymer chain to improve the solubility features of the dopamine-containing conjugate. The ratio

of DA and AE was 1:2. During the synthesis process, AE was also dissolved in DMSO at the same time as L-dopamine-hydrochloride and DBA (**Figure 5.**). In the case of PSI-Dox conjugate, the amount of Dox on the polymer chain was 0.005 w/w% (approximately in accordance with DG800).
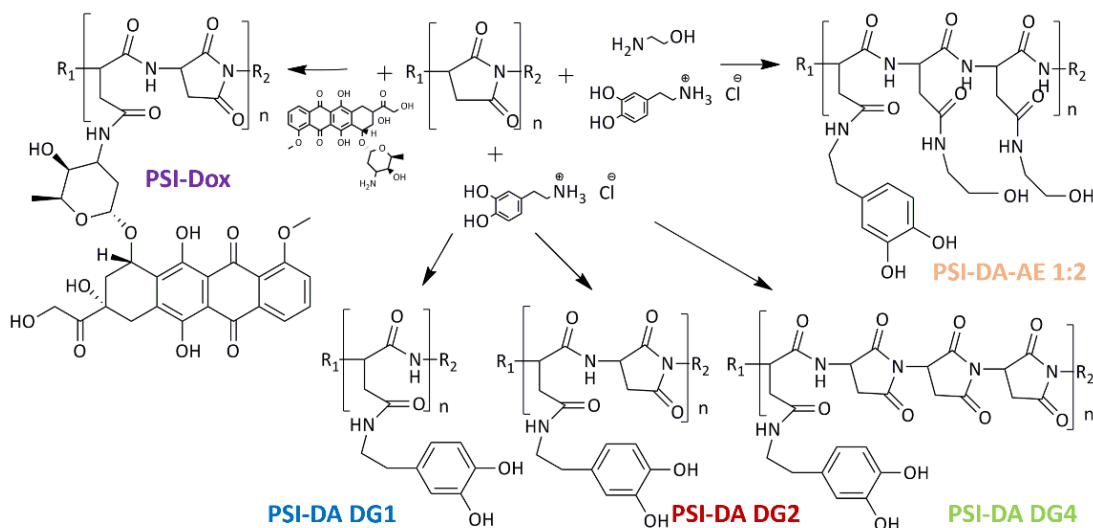
Figure 5.: *Chemical composition of different PSI-DA conjugates and the PSI-Dox conjugate. R_1: NH$_2$ group; R_2: COOH group; n: repeating unit (**KT1** and **KT2**). The image was made by ChemDraw.*

The final viscous solutions were heated up to 60 °C and stirred for 1 week in closed-tempered tubes (IKA RCT basic). After 7 days of incubation, the PSI-DA DG1, DG2, and DA-AE 1:2 samples were filled into cellulose dialysis membranes (with 14 kDa cut off) at room temperature in order to exchange the organic medium for water. After 1 week of dialysis and several changes of water, PSI-DA DG1 and DG2 conjugates were extracted, milled, and dried in a heated exsiccator at 40 °C until a constant mass was obtained.

Regarding the PSI-DA-AE 1:2 conjugates, the polymer was extracted and freeze-dried after the dialysis.

The PSI-DA DG4 samples after the 1-week-long reaction, were precipitated in water and dried in the heated exsiccator.

The PSI-DA conjugates were dissolved in their proper polymer solutions before the electrospinning process according to the fine-tuning of a bead-free fibrous product (**Table 1.**). Besides the DMF and tetrahydrofuran (THF), in the case of PSI-DA DG1

conjugate, ethanol (EtOH) was also added to the final solution to enhance the beadless electrospinning.

*Table 1.: Spinning and solvent parameters of the different PSI-DA conjugates (needle-collector distance: 15 cm; speed of rotating drum: 10 rpm) (**KT1**).*

Polymer-drug conjugates	Solvent (Volume ratio)	Concentration (w/w%)	Voltage (kV)	Flow rate (ml/h)
PSI-DA DG1	DMF-EtOH-THF 2:1:1	30	11	0.3
PSI-DA DG2	DMF-THF 4:1	40	14	0.3
PSI-DA DG4	DMF-THF 4:1	35	10	0.4
PSI-DA-AE 1:2	H_2O	50	13	0.3

The PSI-Dox conjugate was filled into a syringe right after the 7-day incubation to instantly electrospun the viscous solution.

3.1.3. Preparation of drug/polymer solutions to electrospinning

In the case of drug-loaded fibers, the drugs were also dissolved in their proper polymer solutions right before the electrospinning process according to **Table 2.:** Spinning and solvent parameters of the PSI-Dox conjugate and the Pred or Dox-loaded polymers (needle-collector distance: 15 cm, except in the case of PCL: 20 cm; speed of rotating drum: 10 rpm) (**KT2**).**Table 2.**

*Table 2.: Spinning and solvent parameters of the PSI-Dox conjugate and the Pred or Dox-loaded polymers (needle-collector distance: 15 cm, except in the case of PCL: 20 cm; speed of rotating drum: 10 rpm) (**KT2**).*

Polymer-drug conjugate or drug/polymer mixtures	Solvent (Volume ratio)	Concentration (w/w%)	Voltage (kV)	Flow rate (ml/h)
PVA or Pred/PVA	H_2O:DMF (8:2)	10	16	0.3
PSI or Pred/PSI	DMF	25	14-16	1
Dox/PSI or PSI-Dox	DMF	25	14-16	1
PCL or Pred/PCL	DMF:THF (1:1)	15	12.5	1

In the case of PVA, the polymer was first dissolved in ultra-pure water and heated up to 90 °C during stirring. After a homogenous solution was reached, the Pred (0.5 or 1 w/w%) was dissolved in DMF and mixed with the PVA solution. In the case of PSI, the Pred (0.5 or 1 w/w%) or Dox (0.005 w/w%) was dissolved in the PSI/DMF 25 w/w% polymer solution before the electrospinning process. Regarding PCL, the polymer was dissolved in the solution of DMF:THF 1:1 V/V, and after the dissolution, Pred (0.5 or 1%) was also added to the viscous solution, right before the electrospinning process. After a homogenous solution was obtained, the drug/polymer viscous solutions were filled into the syringe of the electrospinning setup.

3.1.4. Electrospinning process

Nanofibrous structures were prepared from the viscous solutions of PSI-DA conjugates with different degrees of grafting (DG1, DG2, DG4), and PSI-Dox conjugates by a homemade electrospinning equipment (**Figure 6.**). Besides the conjugates, the drug-loaded polymers (Pred/PVA, Pred/PSI, Dox/PSI, Pred/PCL) were also formulated by electrospinning.
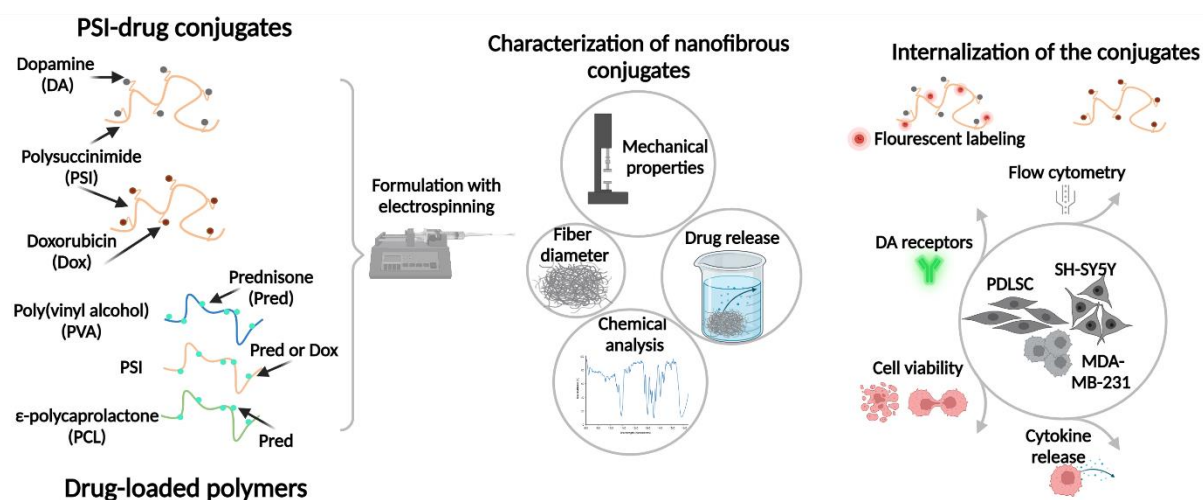
Figure 6.: *Summary of the applied methods and investigations. The image was made by Biorender.*

First, a syringe attached to a needle was loaded with the viscous solution of the polymer-drug conjugates or drug/polymer mixtures and this set-up was placed into a syringe pump (NE-500 Model, New Era Pump Systems Inc., USA). The positive electrode was connected to the metal needle tip and the ground (negative electrode) was

attached to the target collector, which was wrapped in aluminum foil. The rotating drum collector was placed at a well-determined distance (15-20 cm) in front of the metal needle. The voltage was provided by a direct current power supply (ES 30 Model, Gamma High Voltage Inc., USA). The adjustments and circumstances of the electrospinning process can be seen in **Table 1.**, and **Table 2.**

3.2. Physicochemical and mechanical characterization of the electrospun meshes

The schematic representation of the applied methods for the characterization of DA, Dox and Pred-containing fibrous meshes can be seen in **Figure 6.**

3.2.1. Chemical characterization by Attenuated Total Reflectance Fourier-Transform Infrared Spectroscopy (ATR-FTIR)

For the investigation of the chemical composition of the samples, FTIR measurements were carried out using a diamond ATR head (Jasco FT/IR-4700A, ATR Pro ONE, JASCO Ltd.). The investigated range was between 400 cm^{-1} and 4000 cm^{-1} at a resolution of 2 cm^{-1}. A deuterated triglycine sulfate detector was applied, and 80 scans were accumulated per sample. Background spectra (H_2O, CO_2) were subtracted after the measurements.

The transmittance of powder and fibrous form of the PSI-DA conjugate samples was determined beside the powder form of Pred, Dox, and the polymers (PVA, PSI, PCL); the fibrous form of the polymers (PVA, PSI, PCL), as well as the fibrous form of Pred/polymers (Pred/PVA, Pred/PSI, Pred/PCL); Dox/PSI, and PSI-Dox conjugate to detect the potential change in the chemical structure during the electrospinning process.

3.2.2. Chemical characterization by ^{1}H-NMR

To confirm the success of the conjugation NMR spectroscopic measurements of the electrospun PSI-Dox conjugate sample were carried out applying a 600 MHz Varian DDR NMR spectrometer (Agilent Technologies, Palo Alto, CA, USA) by Szabolcs Béni at the Department of Pharmacognosy of Semmelweis University. Before the measurements, the PSI-Dox fibrous mesh was dissolved in DMSO-d6. The measurement parameters were the following: internal standard: tetramethylsilane; temperature: 22 ± 0.5 °C; pulse angle: 30°; delay: 2 sec; spectral width: 8.5 kHz; data

points: 16.5 K; scans: 1024. The ^{1}H-NMR data were analyzed by the Top Spin 3.6.4 software (Bruker, USA).

3.2.3. Powder X-ray Diffractometry (XRD)

To investigate the crystal structure of the samples X-ray diffraction spectra of the samples were recorded (PANalytical X'Pert3 Powder diffractometer, Malvern Panalytical B.V., The Netherlands) at the Department of Pharmaceutics at Semmelweis University by Bence Tóth. The powder form of the polymers (PVA, PSI, PCL) and Pred, the physical mixtures of the powder forms of the polymers (PVA, PSI, PCL) and Pred, as well as the Pred/polymer (Pred/PVA, Pred/PSI, Pred/PCL) fibrous meshes were measured by XRD. During the measurements the following parameters were used: Cu Kα radiation; 45 kV accelerating voltage; 40 mA anode current (range: between 2 and 40° (2 θ)), 0.0084° step size, 100 s times/step, reflection mode. The sampler holder was spinning by $1 \, s^{-1}$. Incident beam optics parameters: programmable divergence slit; 15 mm constant irradiated length; anti-scatter slit at fixed 2°. Diffracted beam optics: X'Celerator Scientific ultra-fast line detector; 0.02 soller slit; programmable anti-scatter slit with a 15 mm constant observed length. Data were collected by the PANalytical Data Collector Application, version 5.5.0.505 (Malvern Panalytical B.V., The Netherlands).

3.2.4. Determination of the average fiber diameter of the electrospun meshes

A Quanta400F Scanning Electron Microscope (SEM, University of Technology and Economics, Budapest) was used at a 2-20 kV accelerating voltage to study the morphology and the average diameter of the electrospun fibers. The fibrous samples were previously coated with gold (MCM-100 Model metal ion spraying device) to achieve higher contrast. The average diameter of the fibers was determined using the Fiji (ImageJ v1.53) program by measuring the diameters of 100 fibers altogether from 3 parallel enlarged images, which were taken at a magnification of 5000x regarding each type of electrospun sample (**Figure 7.**).
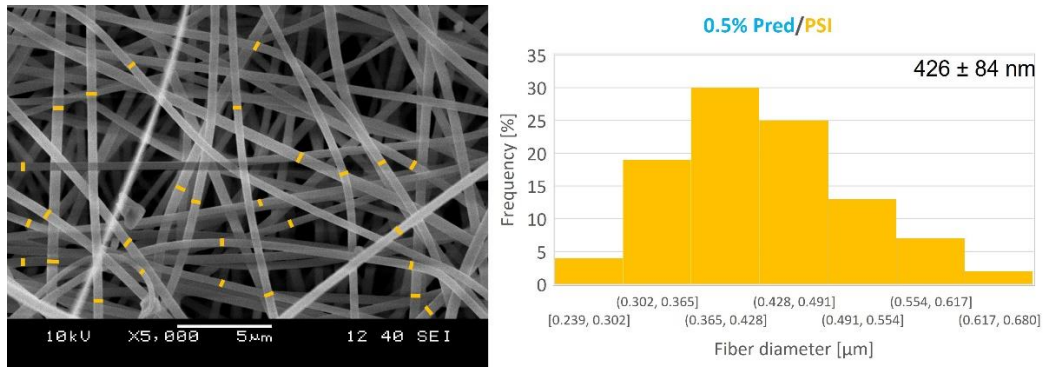
*Figure 7.: Average fiber diameter of fibrous 0.5% Pred/PSI sample (**KT2**).*

3.2.5. Investigation of mechanical properties of electrospun meshes

The mechanical performance of the 1 cm x 6 cm rectangle-shaped electrospun test pieces (PSI-DA samples with different degrees of grafting, as well as Pred/PVA, Pred/PSI, Pred/PCL with 0.5 or 1% Pred, was investigated during unidirectional strain-controlled experiments (Instron 5942 mechanical tester (Instron, USA); applying 50 N maximal load capacity, 0.5 mm/min elongation rate to sample-torn at room temperature) (**Figure 8.**). Six parallel measurements were carried out regarding each type of fibrous samples.
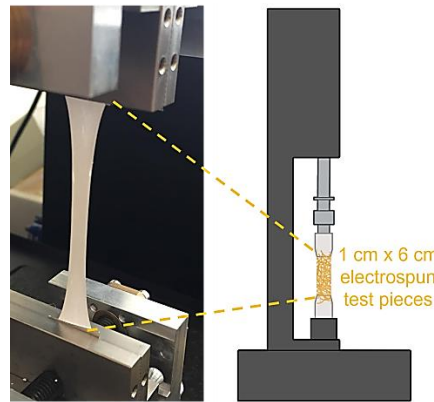
Figure 8.: Set-up for unidirectional strain-controlled mechanical tests.

Based on the experimental data, the specific load capacity and the initial modulus of the samples were determined. The specific load capacity (**Equation 2.**) and the area density (**Equation 3.**) were calculated according to the following formulas:

$$Specific\ load\ capacity\ \left[\frac{Nm^2}{g}\right] = \frac{Maximal\ load\ [N]}{Area\ density\ \left[\frac{g}{m^2}\right]} \qquad (2)$$

$$Area\ density\ \left[\frac{g}{m^2}\right] = \frac{Mass\ of\ the\ sample\ [g]}{Surface\ of\ the\ sample\ [m^2]} \qquad (3)$$

The initial modulus of the samples can be determined from the slope of the linear function, which was fitted to the initial ascendant period of the load-extension curves.

3.3. Disintegration, solubility, and drug release of fibrous meshes

3.3.1. Disintegration of fibrous, neat PVA, PSI, and PCL polymer meshes

The disintegration of neat PVA, PSI, and PCL polymer meshes was investigated by measuring the amount of the transmitted light (lux), which was detected by a COSILUX LM2 device (Tungsram, Hungary). The fibrous samples were placed into a phosphate-buffered saline (PBS) (pH 7.4, I=150 mM) solution containing Petri dish, and small weights were placed onto the edges of the samples to prevent floating. The sample containing Petri dish was placed on the top of the detector. Above the Petri dish, a micro-camera equipped with a lamp (DigiMicro 1.3, DNT, DE) was placed, which took photographs to follow the changes in the mesh morphology (**Figure 9.**). The illuminance of the transmitted light was detected for 180 h. The relative transparency change was calculated in each detected time point.
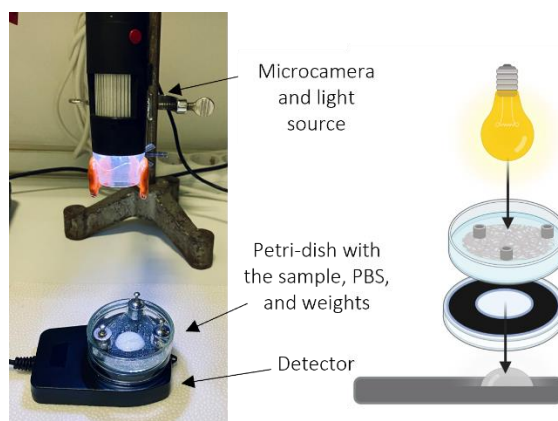
*Figure 9.: Set-up for the investigation of the neat fibrous polymer disintegration (**KT2**).*

3.3.2. Solubility and drug release regarding nanofibrous polymer-drug conjugates and drug-loaded meshes

To determine the solubility of the PSI-DA meshes with different degrees of grafting, the fibrous conjugate samples were placed into a silk filter, immersed in PBS solution (pH 7.4, I=150 mM) and stirred at normal human body temperature (36 °C) for 2 days by a magnetic stirrer (**Figure 10. A**).
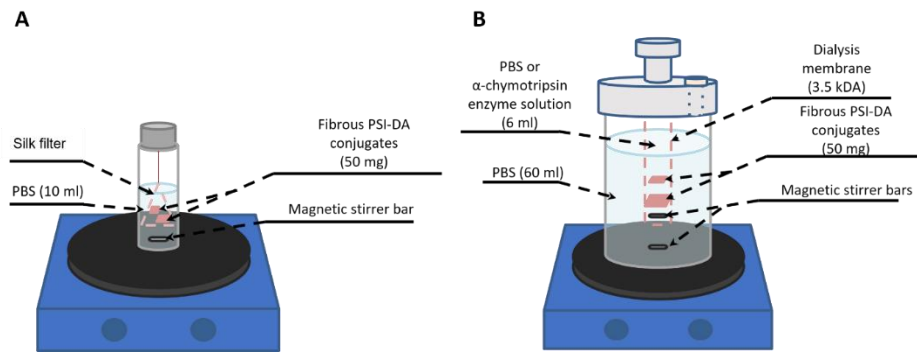
*Figure 10.: Solubility (A) and DA release setup (B) (**KT1**).*

To determine DA release from the fibrous PSI-DA meshes with different degrees of grafting, the fibrous PSI-DA conjugate was loaded, but into a dialysis membrane (Spectra/Por 3 regenerated cellulose, cut off: 3.5 kDa) instead of a silk filter, in order to separate the polymer-DA conjugates from the small molecules such as released DA molecules. In this manner, only the released DA could be measured outside of the membrane, due to that the larger molecules could not pass through the pores of the dialysis membrane. A magnetic stirrer bar was also placed into the dialysis membrane to exclude the effect of diffusion. The drug release was also investigated in PBS (pH 7.4; I=150 mM) and in the presence of α-chymotrypsin enzyme as well. The samples were also stirred at human body temperature for 2 days (**Figure 10. B**).

In the case of the Dox release from fibrous PSI-Dox conjugate meshes, the drug release was investigated similarly as in the case of PSI-DA conjugates, but besides the 7.4 pH PBS, 6.5 pH PBS was also used to mimic the more acidic environment of the tumorous and inflamed tissues (**Figure 11. A**).
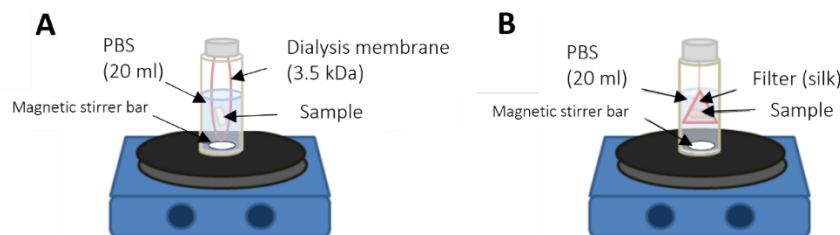
*Figure 11.: Drug release setup in the case of PSI-Dox conjugate (A) and drug-loaded polymer samples (B) (**KT2**).*

To determine the drug release in the case of drug-loaded nanofibrous polymer meshes (Pred/PVA, Pred/PSI, Dox/PSI, Pred/PCL), a silk filter was used to hold together the larger pieces of the samples similarly to the investigation of the solubility of PSI-DA

conjugates. The volume of the PBS (pH 7.4; I=150 mM and pH 6.5; I=150 mM) was 20 ml, and the samples were stirred with a magnetic stirrer at a human normal body temperature (36 °C) for 2 weeks (**Figure 11. B**).

The absorbance of the external liquid samples was measured by an Agilent 8453 UV-VIS spectrophotometer (Agilent Technologies, USA). Regarding both the solubility and the drug release investigations of DA, the absorbance values were measured at 280 nm, 470 nm, and 690 nm. In the case of Pred, the samples were measured at 244 nm, while Dox-containing samples were measured at 481 nm.

To calculate the concentrations from the absorbance values, calibration lines were determined using concentration series of DA (between 0.001 and 1 mol/l), Pred (between 0.001 and 0.2 mmol/l at both pH values (7.4; 6.5), and Dox (between 0.001 and 0.1 mmol/l at both 7.4 and 6.5 pH).

3.4. *In vitro* experiments

3.4.1. Cell cultivation

For the *in vitro* tests, three cell cultures were used: human primary cell cultures of periodontal ligament stem cells (PDLSCs), a human neuroblastoma cell line (SH-SY5Y), and a triple-negative breast cancer cell line (MDA-MB-231). PDLSC cells are derived from the connective tissue adjacent to human wisdom teeth, which were removed from healthy patients at the Department of Dentoalveolar Surgery at Semmelweis University according to the ethical guidelines (ethical permission: 25459/2019/EKU). PDLSCs were isolated by the members of the Department of Oral Biology at Semmelweis University.

The SH-SY5Y and MDA-MB-231 cell lines were purchased from the European Collection of Authenticated Cell Cultures (Salisbury, UK).

PDLSCs and SH-SY5Y cells were cultured at the Department of Oral Biology at Semmelweis University.

The culturing medium of PDLSCs consists of Eagle's Minimal Essential Medium (EMEM) supplemented with 10% fetal bovine serum (FBS), 2 mM L-glutamine, 100 units/ml penicillin, and 100 mg/ml streptomycin.

The SH-SY5Y culturing medium is composed of Ham's F12 and EMEM (1:1 V/V) supplemented with 15% FBS, 2 mM L-glutamine, and 1% Non-Essential Amino Acids (NEAA), 100 units/ml penicillin and 100 mg/ml streptomycin.

The culturing medium of the MDA-MB-231 cell line contains EMEM supplemented with 10% FBS, 2 mM L-glutamine, 100 units/ml penicillin, and 100 mg/ml streptomycin. MDA-MB-231 cells were cultured at the *in vitro* laboratory of the Department of Genetics, Cell- and Immunobiology of Semmelweis University.

All the cell cultures were maintained in a humidified incubator (Nuaire, USA) in tissue culture flasks under standard culture conditions (37 °C, 5% CO_2, 100% humidity).

For passaging the cells, 0.05% trypsin-EDTA solution was used during a 5-minute-long incubation at 37°C.

3.4.2. Immunofluorescence labeling

For investigating the presence of D1 and D2 DA receptors on PDLSC and SH-SY5Y cells, 10 000 cells/cm^2 were seeded and grown on previously sterilized glass coverslips in 24-well plates and then fixed with 4% paraformaldehyde (PFA) in PBS. The cell membrane was permeabilized with 0.1% Triton X in PBS. After rinsing (PBS), the cells were incubated in 5% normal donkey serum in PBS at room temperature for blocking, then the fixed cells were incubated with 1:500 dilutions of anti-D1R (rabbit polyclonal IgG, Abcam) and anti-D2R (goat polyclonal IgG, Abcam) primary antibodies overnight at 4 °C. Afterwards, the cells were treated with 1:1000 dilutions of Alexa 488 conjugated secondary antibodies (goat anti-rabbit IgG and rabbit anti-goat IgG, Molecular Probes) for fluorescence visualization. After washing with PBS and distilled water, the fixed cells were dried and mounted with Prolong Gold antifade reagent with 4′,6-diamidino-2-phenylindole (DAPI) (Molecular Probes).

The fixed and fluorescently labelled cells were examined with a Nikon Eclipse E600 fluorescence microscope (Nikon Instruments) at the Department of Oral Biology. Images were captured from the cells with a cooled SPOT RT Color 2000 CCD camera (Diagnostic Instruments) and by using the SPOT Advanced image acquisition software (Diagnostic Instruments).

3.4.3. Cell viability assay

During the cell viability test regarding the concentration ranges of the drugs, 10 000 cells/cm² PDLSC and SH-SY5Y cells were seeded in 100 µl cell culturing medium in 96-well plates (Thermo Scientific). After 24 hours of incubation, stock solutions of DA and water-soluble PSI-DA-AE 1:2 conjugates were diluted with supplemented cell culturing medium according to the investigated concentration range between 0 and 200 µmol/l and were added to the cells. In the case of Pred and Dox, MDA-MB-231 cells were seeded into white-walled optical bottom 96-well plates (Thermo Scientific, USA) in the concentration of 5 000 cells/well (13 513 cells/cm²). The stock solutions regarding Pred and Dox were previously diluted with DMSO (2 mol/l) due to the poor water solubility of these drugs. The DMSO-containing stock solutions were further diluted 200-fold with supplemented cell culturing medium and adequate concentrations were prepared according to the required concentration ranges (Pred: 0-400 µmol/l, Dox: 0-100 µmol/l).

Before the introduction of neat and drug-containing fibrous samples to the cells, these samples were previously sterilized with a hot air sterilizer and UV radiation. In these cases, the volume of the applied culturing medium was calculated and considered according to a well-defined final concentration regarding the adequate drugs.

Cell viability was assessed after 24 and 72 hours of treatment with different drugs in different concentration ranges, and neat, DA or Dox-containing fibrous membranes by using WST-1 cell proliferation reagent (Roche, CH; dilution of 1:20) in the case of PDLSC and SH-SY5Y cells, and CellTiter-Glo Luminescent Cell Viability reagent (Promega, USA) in the case of MDA-MB-231 cells.

The WST-1 reagent contains water-soluble tetrazolium salts, which are cleaved to formazan molecules by mitochondrial dehydrogenase enzymes in the metabolically active cells, and this reaction is accompanied by the formation of NAD^+ from NADH. The absorbance of the formazan was measured by a microplate reader (Model 3550, Bio-Rad Laboratories, Japan) at 450 nm with a 650 nm reference wavelength at the Department of Oral Biology. In the case of the CellTiter-Glo reagent, luminescent signal is generated by luciferase enzyme in the presence of ATP (after the lysis of the cells). The luminescence, which is directly proportional to the number of living cells, was measured by a microplate fluorometer at 560 nm (Fluoroskan™ FL Microplate

Fluorometer and Luminometer, Thermo Scientific, Waltham, MA, USA) at the Department of Genetics, Cell- and Immunobiology of Semmelweis University.

Statistical evaluation of the viability data was carried out using the Kruskal-Wallis nonparametric ANOVA followed by a median test. A difference was considered statistically significant if $p < 0.05$.

3.4.4. Examination of cell morphology and cellular internalization

PDLSC and SH-SY5Y cell cultures were observed using phase-contrast microscopy (Nikon Eclipse TS100, Nikon, Japan) with a 10x objective. Images were taken with a high-performance CCD camera (COHU, USA) and the Scion image software at the Department of Oral Biology.

Regarding the MDA-MB-231 cell line, cells were observed by Axio Observer A1 inverted microscope (Zeiss, Germany) and the AxioVision LE64 Rel.4.9.1. software at the Department of Genetics, Cell- and Immunobiology of Semmelweis University.

Regarding two-photon microscopy, PDLSCs and SH-SY5Y cells were labelled with a fluorescent vital dye (Vybrant DiD, Invitrogen) before seeding at $10\,000$ cells/cm^2 density on an 8-chamber slide. After 24 and 72 hours of treatments, the cells were fixed with 4% PFA according to the above-mentioned fixation protocol and mounted with Prolong Gold antifade reagent with DAPI (Molecular Probes). During the observations, a Femto2d two-photon microscope (Femtonics, Hungary) was used with a Spectra Physics Deep See laser at 800 nm at the Department of Biophysics and Radiational Biology of Semmelweis University. Photos were taken by using a 10x objective and utilizing the MES4.4v program.

For visualizing the PSI-DA conjugates internalized by PDLSCs and SH-SY5Y cells, and Dox or PSI-Dox internalized by MDA-MB-231 cells, confocal microscopy was used. To visualize the PSI-based DA-containing conjugates inside the cells, the polymer was labelled with the brilliant cresyl blue (BCB) fluorescent stain at a grafting degree of 1:500 (BCB500) (**Figure 12.**) before the electrospinning process.
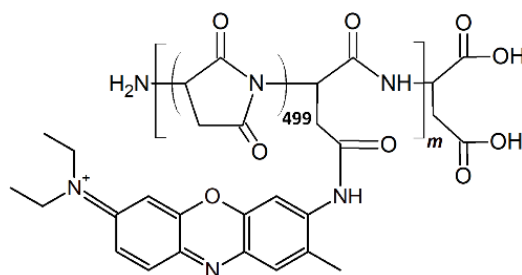
Figure 12.: *Chemical composition of BCB conjugated PSI (PSI-BCB500); m: recurring module (**KT1**). The image was made by ChemDraw.*

For these experiments, cells were seeded onto round-shaped microscope coverslips and placed into 6-well plates. After 24 h of growth, the PDLSC and SH-SY5Y cells were treated with 4 different samples: PSI, PSI-DA1-BCB500, PSI-DA2-BCB500, and PSI-DA4-BCB500. Regarding MDA-MB 231 cells, Dox, fibrous PSI, and PSI-Dox conjugate were introduced to the cells. After 72 h of treatment, the cells were fixed (4% PFA) and mounted with Prolong Gold antifade reagent with DAPI (Molecular Probes). The cellular internalization of the BCB conjugated PSI-DA and unstained PSI-Dox polymers and free Dox itself was observed under a Nikon Eclipse Ti2 Inverted Research Microscope (60x objective) at the Department of Biophysics and Radiational Biology of Semmelweis University. The pictures were recorded by the Abberior Imspector program, and analyzed with Fiji (ImageJ v1.53) software.

3.4.5. Flow cytometry

Internalization of the conjugates by the cells was verified by flow cytometry. For this experiment, the cells were seeded into 6-well plates. Regarding PDLSCs, and SH-SY5Y cells, after 24 h of culturing, 1000 µM stock solutions were prepared from BCB, DA, PSI-BCB500, PSI-DA1-BCB500, PSI-DA2-BCB500, PSI-DA4-BCB500 in DMSO. The DMSO-based solutions were diluted by 10 times with supplemented cell culturing medium before introducing them to the cells. After 72 h of the treatments, the cells were detached from the surface with TripLE Express enzyme solution (Gibco), then resuspended in a fresh cell culturing medium and centrifuged at 1200 rpm. After the elimination of the supernatant, the cells were resuspended in PBS and centrifuged 2 times.

The flow cytometry measurements were performed using a CytoFLEX S flow cytometer (Beckman Coulter, Inc. USA) by Éva Pállinger and Nóra Fekete at the

Department of Genetics, Cell- and Immunobiology of Semmelweis University. The population, which was negative for the propidium iodide staining, was denoted as viable cells. During the investigation, unlabelled and untreated cells were used for the identification of the autofluorescence of the cells. The BCB supravital stain was the positive control for internalization regarding the investigation of PSI-DA conjugates.

3.4.6. Cytokine release

To investigate the anti-inflammatory effect of Pred in different concentrations (0-400 µM), and the potential anti-inflammatory effect of neat (PVA, PSI, PCL) and Pred-containing polymer meshes (Pred/PVA, Pred/PSI, Pred/PCL), the presence and the amount of 13 cytokines in the MDA-MB-231 cell-supernatant were investigated (BioLegend LEGENDplex (13 plex), San Diego, USA) at the Department of Genetics, Cell- and Immunobiology of Semmelweis University. The investigated cytokines were the following: IL-1β; IFN-α2; IFN-γ; TNF-α; MCP-1; IL-6; IL-8; IL-10; IL-12p70; IL-17A; IL-18; IL-23; IL-33.

For this examination, first, MDA-MB-231 cells were seeded (300 000 cells/well; 2 ml cell culturing medium). 24 hours later, the medium was replaced by fresh serum-free medium containing Pred (0-400 µM) or neat polymer meshes, or Pred-containing PVA, PSI, and PCL fibrous meshes (400 µM regarding Pred). After 48-hour long treatments, the supernatant was removed, centrifuged (10 min, 1500 g), and stored at -80 °C.

The investigation of the cytokine level in the supernatants was implemented according to the manufacturer's protocol by Nóra Fekete at the Department of Genetics, Cell- and Immunobiology of Semmelweis University. The measurements were carried out using a flow cytometer (CytoFlex S, Beckman Coulter, Inc. USA) and the data were converted by Árpád Kovács using the LEGENDplex 0.8 software.

4. Results

4.1. Physicochemical and mechanical characterization of electrospun meshes

4.1.1. Chemical characterization by ATR-FTIR and NMR spectroscopy

In **Figure 13.** the FT-IR spectra of the different DA-containing powder conjugates (**Figure 13. A**) and their fibrous form (**Figure 13. B**) can be observed. The main characteristic peaks are highlighted in the images.
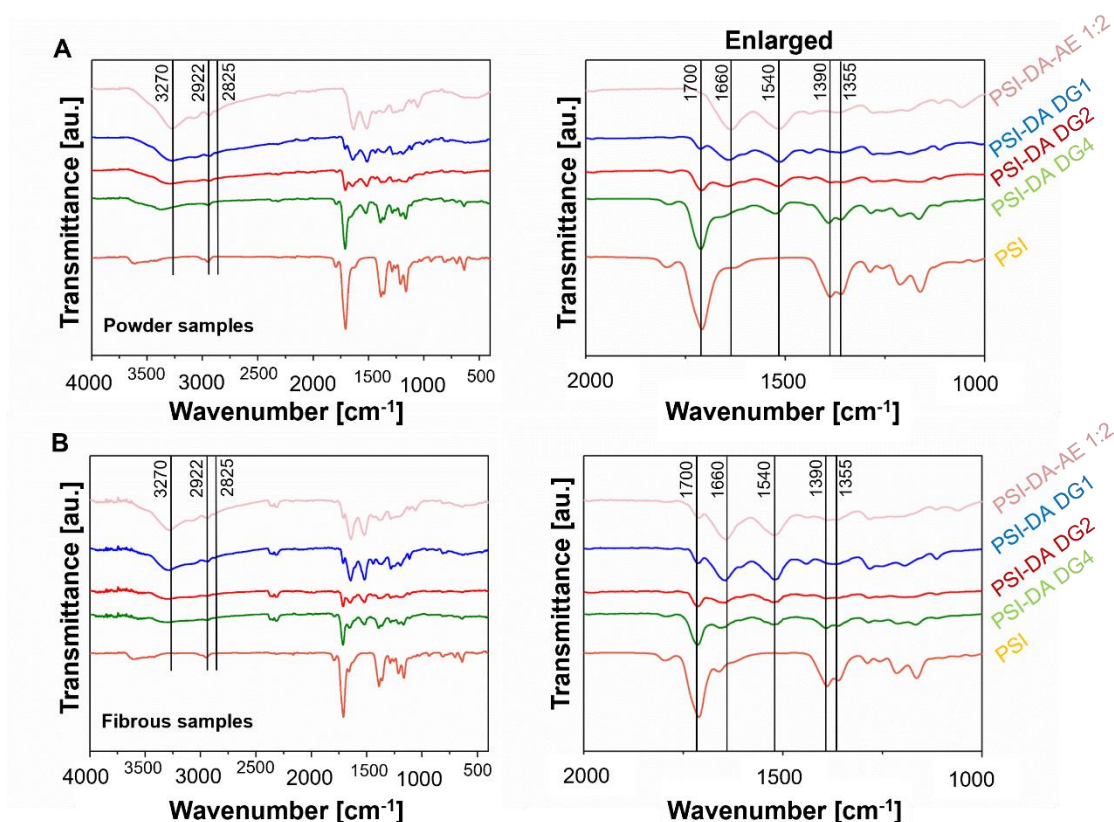
Figure 13.: *FT-IR spectra of PSI-DA conjugate powders (A) and fibrous meshes (B)*
*(**KT1**).*

The peak, that can be observed at 1700 cm^{-1} belongs to the imid bond of the succinimide ring, which is related to the asymmetric stretching vibration of C=O in –(OC)$_2$N–. Additional characteristic peaks of imid groups can be found at 1384 cm^{-1} (C=O delta vCN), at 1207 cm^{-1} ((C=O)-NH group vCN vibration, and at 1160 cm^{-1} ((C=O)-NR-(C=O) group).

The characteristic peak at 1600 cm^{-1} wavenumber is related to the amide bonds, which is a demonstration of the succinimide ring-opening. 1390 cm^{-1} belongs to the bending vibration of C–O and at 1355 cm^{-1} the stretching vibration of C–N in –(OC)$_2$N– can be observed. The wavenumber of 1660 cm^{-1} and 1540 cm^{-1} belong to the C=O and C–N bending vibration of amide groups. The increase regarding these above-mentioned amide-related peaks compared to the PSI spectrum, refers to the succinimide ring-opening during the successful DA-modification.

The wide peak at 3270 cm^{-1} belongs to the asymmetric stretching vibration of the seconder and primer –OH groups. In addition, peaks at 2922 cm^{-1} and 2825 cm^{-1} belong to the asymmetric and symmetric vibration of CH$_2$ groups, which also refers to the aminoethanol modification, such as the primer –OH groups.

Based on the FT-IR spectra, PSI was successfully modified with DA and AE with different degree of grafting, and the formulation by electrospinning does not affect the chemical structure of the conjugates.

In the case of Pred-containing fibrous PVA, PSI, and PCL samples, the results of the FT-IR measurements can be seen in **Figure 14**.
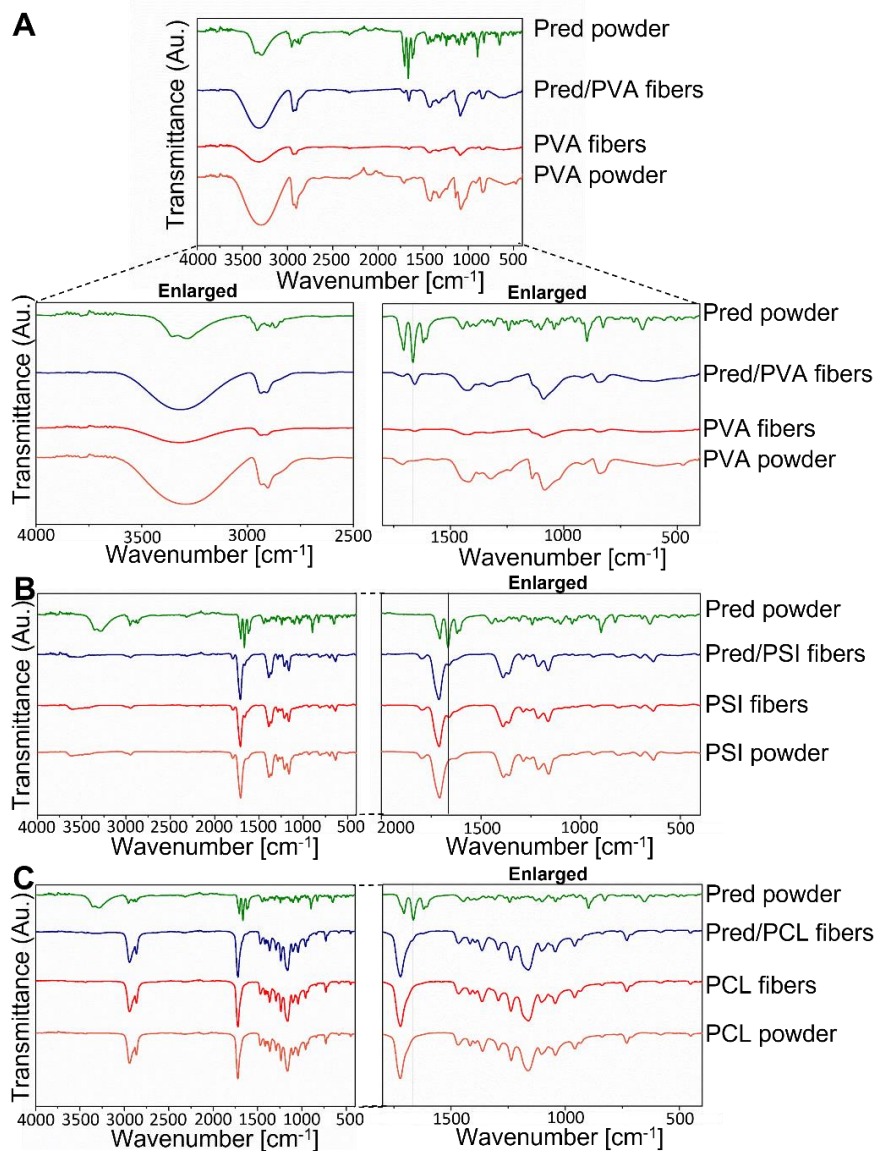
Figure 14.: *FT-IR spectra of neat and Pred-containing PVA (A), PSI (B), and PCL (C)*
*(**KT2**).*

Considering the spectrum of neat and Pred-containing PVA samples, the peaks of the introduced drug can be clearly observed at 1680 cm^{-1}, and in the range between 750-2000 cm^{-1}, while in the case of PSI, this main characteristic peak of Pred (1680 cm^{-1}) is fully overlapped with the strong characteristic peaks of PSI polymer around 1700 cm^{-1}. Regarding neat and Pred-containing PCL samples, this specific peak (1680 cm^{-1}) also appears, although this peak is slightly noticeable due to the small amount of Pred.

Regarding Dox-containing samples, in one case the Dox was physically mixed with PSI before the electrospinning (Dox/PSI), without any conjugation, and another type of

43

mesh was produced by electrospinning: PSI-Dox conjugate. In **Figure 15.**, the FT-IR spectra of these Dox-containing fibrous samples can be seen beside the neat PSI powder and mesh.
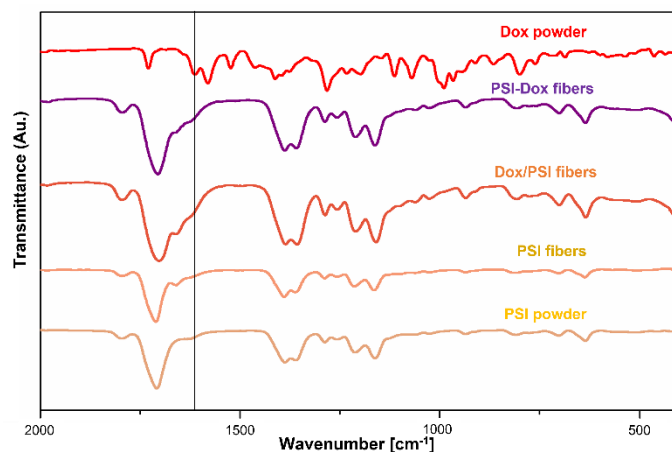
*Figure 15.: FT-IR spectra of neat and Dox-containing PSI samples (**KT2**).*

In the case of Dox-containing samples (Dox/PSI and PSI-Dox), the characteristic peaks of Dox can be observed between 1500 and 1700 cm^{-1}. These peaks do not overlap with the main characteristic peaks of PSI (1612 and 1580 cm^{-1}), which are related to the stretching of C=C bonds. However, only a slight appearance can be observed due to the relatively small amount of Dox in the fibrous meshes. Around 1282 cm^{-1}, a slightly increased peak of Dox can be seen regarding Dox-containing samples compared to the neat PSI spectra.

According to the FT-IR analysis, Dox/PSI and PSI-Dox samples do not differ notably from each other, therefore, ^{1}H-NMR spectrum (**Figure 16.**) was also analysed to prove the conjugation of Dox on the PSI polymer chain.

*Figure 16.: NMR spectra of PSI-Dox conjugate (**KT2**).*

The range between 0.8-2.1 ppm, and 3.9-4.8 ppm was enlarged, to analyze the peaks of the different protons of Dox (1.02, 1.06, 1.16, 1.92, 2.97 ppm), which mainly appear in this range. The peaks related to the succinimide rings can be seen at 3.23 ppm, and 2.74 ppm (methylene peaks), as well as at 5.28 ppm (methine group). The peak at 4.65 ppm is related to aspartamide (methine proton), while 0.9, 1.25, 1.34, and 1.56 ppm peaks refer to the presence of dibutyl amine. The presence of the methine proton and Dox-related peaks proves the modified succinimide monomers (aspartamide) and refers to the successful Dox-conjugation.

4.1.2. Powder X-ray Diffractometry (XRD)

Electrospinning may induce amorphization in the case of drug molecules with limited water solubility, such as Pred. To investigate the potential crystal structure change, physical mixtures of neat PVA, PSI, and PCL polymers and Pred were investigated before and after electrospinning by XRD (**Figure 17.**).

Figure 17.: XRD spectra of neat and Pred-containing polymers before and after electrospinning (**KT2**).

According to the results (**Figure 17.**), the Pred itself is entirely crystalline. Regarding the applied polymers, due to the formulation by electrospinning in the case of neat PVA samples, the peak at $2\theta=23°$ vanished, therefore the crystal fraction of PVA was reduced. On the contrary, regarding PSI and PCL samples, electrospinning had no significant effect on the crystal structure.

Regarding the physical mixture of Pred and polymers (PVA, PSI, PCL), the characteristic peaks of the drug are remarkable on the XRD spectra between $2\theta=13-20°$, which means that the physical mixing has no effect on the crystal structure of the drug. In contrast, the characteristic peaks of the drug totally disappeared in the case of Pred/PSI and Pred/PCL samples after electrospinning, while in the case of Pred/PVA fibers, the disappearance of the characteristic peaks of the drug is incomplete.

4.1.3. Morphology of the electrospun fibers by microscopy, and determination of fiber diameter

The images taken by scanning electron microscopy (SEM) (**Figure 18. A**) from the fibrous PSI-DA conjugates show that the fibers are uniformly thick with a relatively narrow distribution of fiber diameter. No damages and defects can be observed on the

SEM photos due to the well-determined solvent composition development, which was tuned during the electrospinning process.
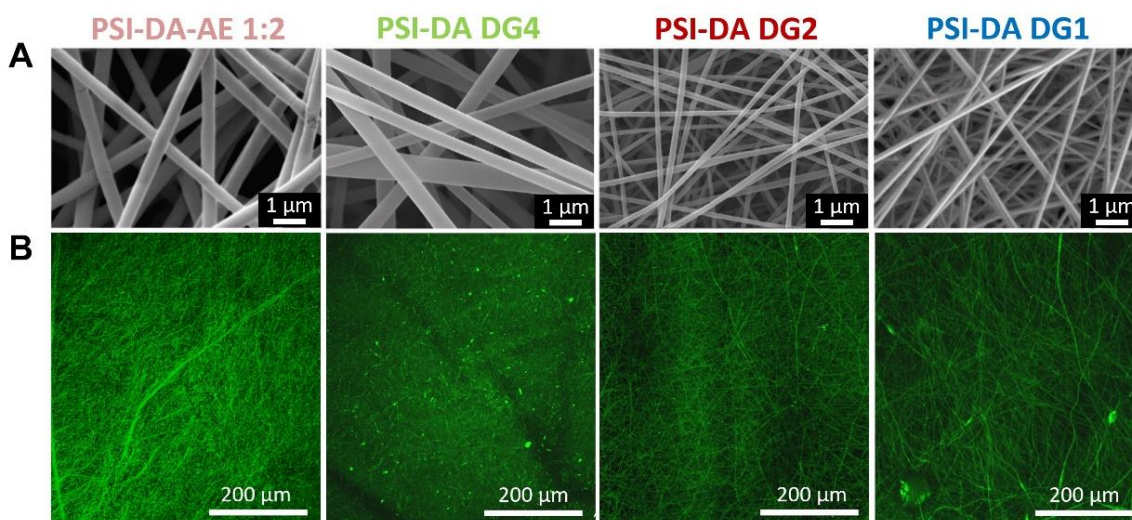
Figure 18.: *SEM (A) and two-photon microscopic images (B) of fibrous PSI-DA conjugates image. (Scale bars: 1 μm (A); 200 μm (B)) (**KT1**).*

A larger area of the fiber-structure of PSI-DA meshes can be observed by two-photon microscopy due to the smaller magnification and hence PSI-based fibrous conjugates show an autofluorescence signal due to the polymer structure (**Figure 18. B**). While PSI-DA DG4, PSI-DA DG2, and PSI-DA-AE 1:2 fibrous meshes have a uniform structure in two-photon microscopic images, at the same time, PSI-DA DG1 samples contained beads and showed diversity in shape and diameter.

Table 3.: *Average diameter of the different PSI-DA fibers (n=100) (**KT1**).*

	PSI-DA-AE 1:2	PSI-DA DG4	PSI-DA DG2	PSI-DA DG1
Average fiber diameter [nm]	431 ± 46	613 ± 172	179 ± 27	78 ± 15

According to the determination of the fiber diameter, the results show that the thickness of the fibers is decreasing by the increasing amount of DA on the PSI (**Table 3.**). The PSI-DA-AE 1:2 samples are theoretically between DG2 and DG4 regarding DA content. In addition, the average diameter of these fibers is also between the values of DG2 and DG4 samples.

Regarding neat (0% Pred) and Pred-containing (0.5% or 1%) PVA, PSI, and PCL samples, the images taken by SEM also present fibers without defects. The distribution of the fiber diameter is homogenous, except PCL-based samples (**Figure 19.**).
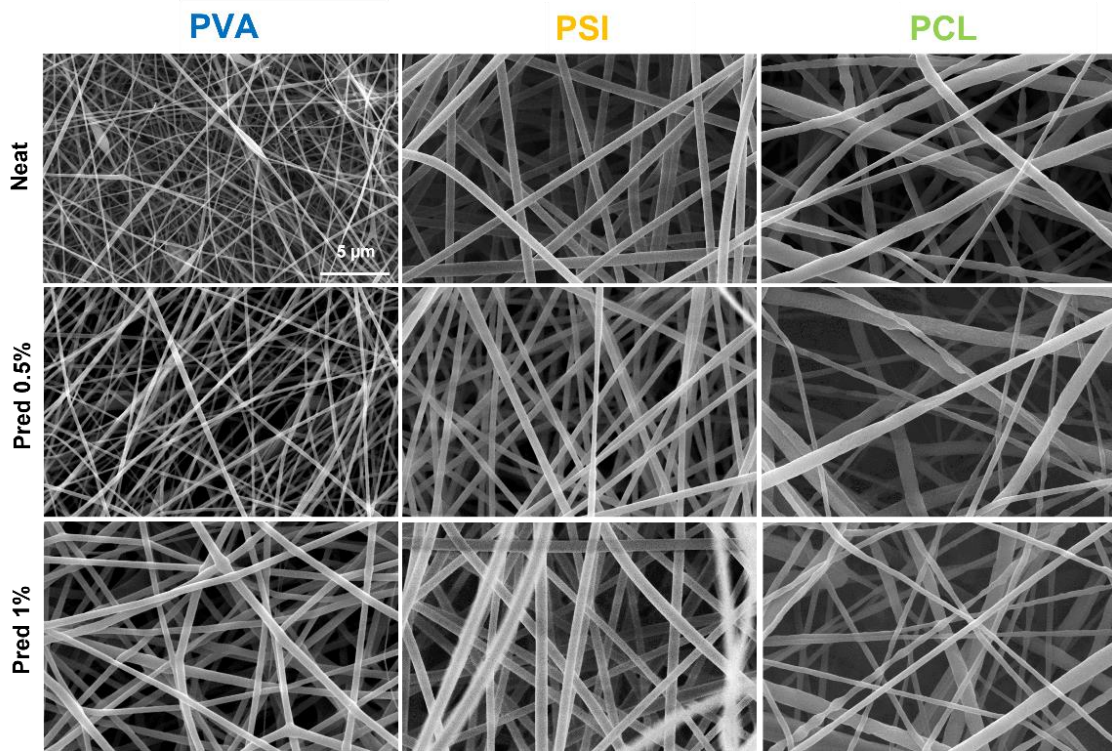
*Figure 19.: SEM images were taken from fibrous neat and Pred-containing PVA, PSI, and PCL samples. The same magnification was applied for each image (Scale bar: 5 µm) (**KT2**).*

Incorporating different amounts of Pred (0.5% or 1%) into PSI and PCL fibers had no noticeable influence on the structure and the appearance of the fibers, while the Pred loading showed a high impact on the appearance of PVA-based fibers (**Figure 19.**).

*Table 4.: Fiber diameter of neat and Pred-containing PVA, PSI, and PCL meshes (n=100) (**KT2**).*

Pred content	PVA [nm]	PSI [nm]	PCL [nm]
Neat	157 ± 61	584 ± 113	583 ± 255
0.5%	212 ± 56	426 ± 84	546 ± 261
1%	497 ± 117	616 ± 102	610 ± 299

According to the fiber diameter measurements, the Pred loading into PVA fibers induces an increase in the average diameter of the fibers, which seems to be directly proportional to the amount of Pred (**Table 4.**).

In **Figure 20.**, SEM images taken from Dox-containing PSI-based samples can be seen.
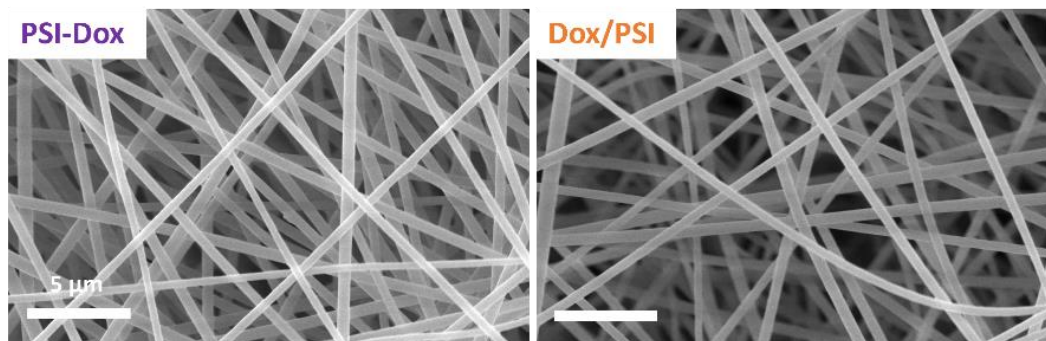
*Figure 20.: SEM images are taken from fibrous PSI-Dox and Dox/PSI meshes. The same magnification was applied for each image. (Scale bar: 5 μm) (**KT2**).*

The appearance of the fibers looks uniform and smooth, and no significant difference can be observed between neat PSI (**Figure 19.**), Dox-loaded PSI fibers (Dox/PSI), and the PSI-Dox conjugate fibers (**Figure 20.**) according to the photos and the fiber diameter measurements as well (Dox/PSI: 467 ± 107 nm; PSI-Dox (545 ± 90 nm).

4.1.4. Mechanical properties of the electrospun fiber meshes

The specific load capacity of the fibrous membranes was also investigated as the strength and mechanical performance of these membranes are crucial parameters as regards biomedical applications. The thickness of these fibrous meshes cannot be properly determined because the volume of the fibers is around 10% of the macroscopical volume of the meshes. In order to avoid the generally used ultimate strain values and considering that Young's modulus cannot be calculated due to the lack of the thickness value of the sample, instead of these parameters, the specific load capacity and the initial modulus of the samples were calculated (**Equation 2.** and **3.**).

In the case of PSI-DA conjugates with different degrees of grafting, the specific load capacity values and the representative load-extension curves can be seen in **Figure 21.** beside the determination of the initial modulus values.
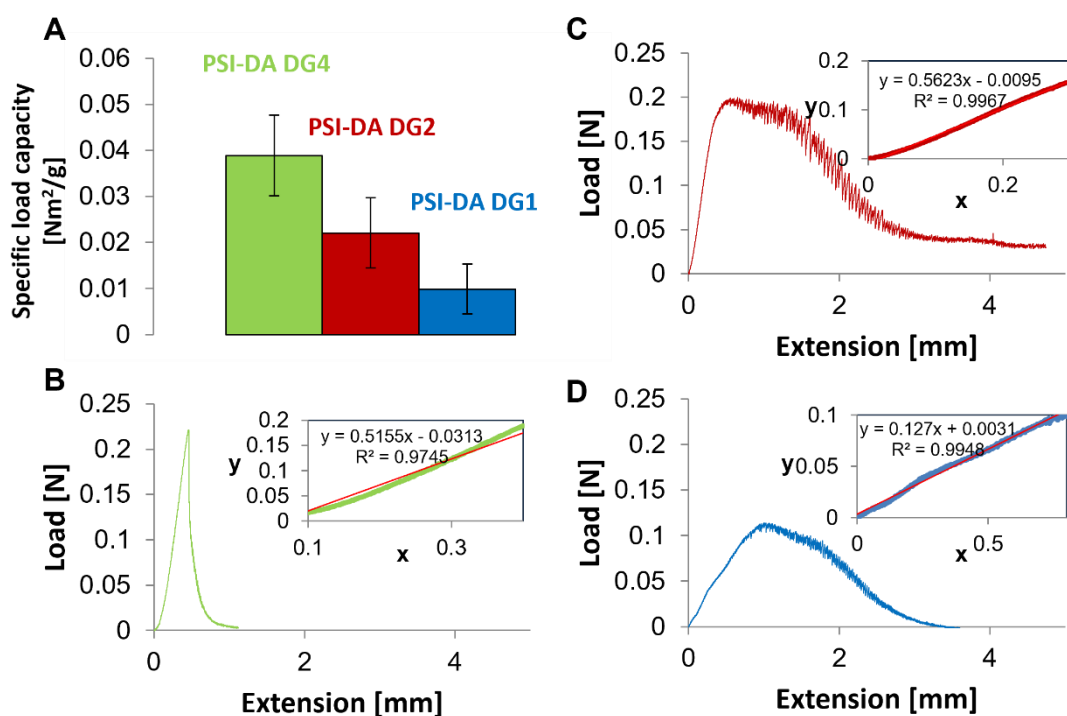
Figure 21.: *Specific load capacity (A) and typical load-extension curves (C; B; D) of fibrous PSI-DA membranes with the fitted line to the initial linear ascendant period of the curves used for the determination of the initial modulus (x: extension [mm]; y: load [N]) (**KT1**).*

The calculated specific load capacity values and the determined initial modulus values with the fiber diameters of the fibrous PSI-DA meshes can be seen in **Table 5.**

Table 5.: *Mechanical properties of DA-containing fibrous membranes (**KT1**).*

Sample	Fiber diameter [nm]	Specific load capacity [$Nm^2·g^{-1}$]	Initial modulus [$N·mm^{-1}$]
PSI-DA DG4	613 ± 172	0.039 ± 0.008	0.448 ± 0.061
PSI-DA DG2	179 ± 27	0.022 ± 0.007	0.490 ± 0.066
PSI-DA DG1	78 ± 15	0.010 ± 0.005	0.303 ± 0.130

The results show that the higher DA content (DG4 < DG2 < DG1) of the fibers concerns decreased specific load capacity. According to the data, a correlation can be observed between the fiber diameter and the specific load capacity: with the increasing amount of DA, the fiber diameter decreases, and it results in decreased specific load capacity.

Regarding the Pred-loaded (0.5%, 1%) polymer samples, the typical specific load-elongation curves can be seen on **Figure 22.**
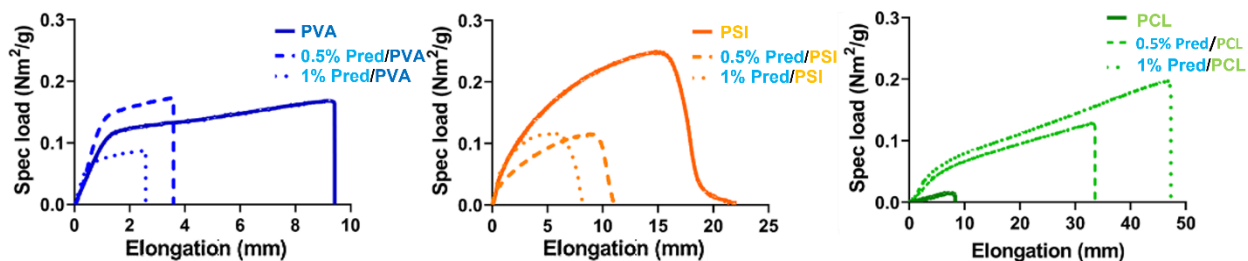
*Figure 22.: Specific load-elongation curves of fibrous Pred-containing PVA, PSI, and PCL meshes (**KT2**).*

In the case of PVA, by incorporation of increasing amount of Pred, the maximum elongation of the meshes is decreasing in comparison with the neat PVA meshes. Regarding PSI fibers, the incorporation of Pred also leads to a decrease in the maximum elongation of the samples, the same as in the case of PVA. The typical deformation curve of PSI without drug content looks similar to those of a thermoplastic polymer, however, in the presence of Pred, the first linear ascendant period (elastic or Hookean region) of the curves is altered. In addition, with the increasing amount of the incorporated Pred, the yield point (endpoint of Hookean region) is shifted to a lower elongation value. Moreover, by incorporating an increasing amount of Pred, the PSI samples were torn at lower elongation values.

The specific load-elongation curves of neat and Pred-loaded PCL meshes show plastic deformation. By the incorporation of an increasing amount of Pred, the elongation of the samples increases. PCL samples show a short Hookean linear ascendant period. Compared to other polymers (PVA, PSI), the elastic modulus of PCL-based samples is the lowest, but these samples were torn apart at the highest deformation.

The data, which were calculated from the specific load-elongation curves of the samples, are presented in **Table 6.** in line with the fiber diameter of the samples.

*Table 6.: The parameters of the mechanical performance of neat and Pred-containing electrospun meshes (**KT2**).*

Polymer	Property	Fiber diameter [nm]	Specific load capacity [$Nm^2 \cdot g^{-1}$]	Initial modulus [$Nm^2 \cdot (mm \cdot g^{-1})$]
PVA	Neat	157 ± 61	0.151 ± 0.006	2.794 ± 0.339
	0.5%	212 ± 56	0.164 ± 0.009	1.972 ± 0.212
	1%	497 ± 117	0.081 ± 0.005	0.650 ± 0.104
PSI	Neat	584 ± 113	0.233 ± 0.009	0.701 ± 0.019
	0.5%	426 ± 84	0.126 ± 0.005	1.680 ± 0.099
	1%	616 ± 102	0.136 ± 0.009	2.373 ± 0.270
PCL	Neat	583 ± 255	0.018 ± 0.004	0.007 ± 0.001
	0.5%	546 ± 261	0.139 ± 0.004	0.043 ± 0.003
	1%	610 ± 299	0.165 ± 0.012	0.050 ± 0.006

According to the results, the incorporation of Pred into PVA meshes has a high impact on the mechanical performance of the meshes. By increasing the amount of the drug, the specific load capacity values are decreasing, such as the initial modulus of the meshes, along with the fiber diameter. By the incorporation of the increasing amount of Pred into PSI meshes, the specific load capacity values are decreasing, but the initial modulus values are increasing. In the case of PCL-based fibrous meshes, both the specific load capacity and the initial modulus values increase with the Pred concentration.

4.2. Disintegration, solubility, and drug release of fibrous meshes

4.2.1. Disintegration of fibrous, neat PVA, PSI, and PCL polymer meshes

Since PCL and PSI are insoluble in water-based solutions in contrast to PVA, but PSI can hydrolyse in a slightly alkaline environment, the aim of these polymers was to deliver the drug inside the human body while protecting it from early deactivation or degradation processes. According to the result of the disintegration investigation (**Figure 23.**), we can observe the dissolution of the neat fibrous polymer meshes by measuring the relative transparency.
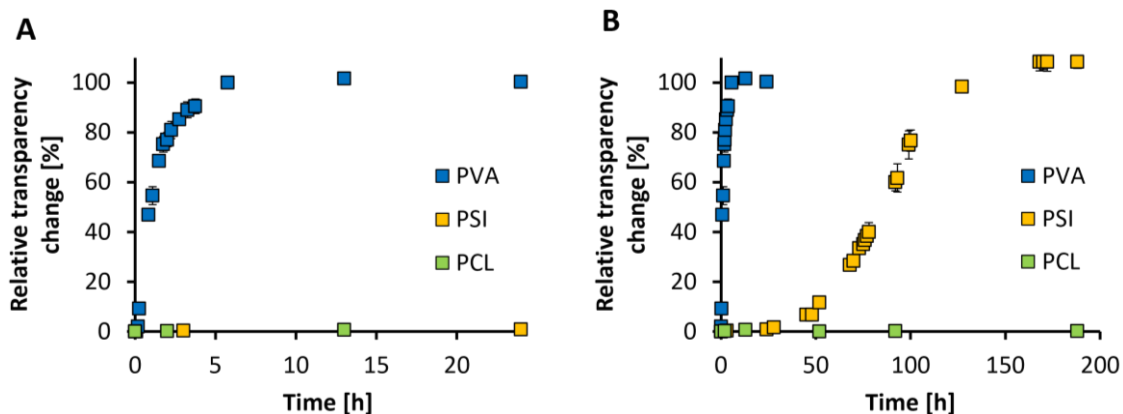
Figure 23.: *Disintegration of neat PVA, PSI, and PCL meshes after 188 h (A) and 24 h (B) (**KT2**).*

The relative transparency change of PVA fibers reaches the maximal value within 6 hours while, the hydrolysis of the PSI samples occurs approximately after 100 h and the sample became fully transparent by 200 h. On the contrary, PCL fibers are not transparent even after 200 h of dipping.

4.2.2. Solubility of fibrous PSI-DA conjugates and drug release from the fibrous conjugates and drug-loaded polymer fibers

In the next step, the dissolution kinetics of PSI-DA conjugates (**Figure 24. A**) and the DA release (**Figure 24. B, C, D**) from the fibrous polymer conjugates were investigated.
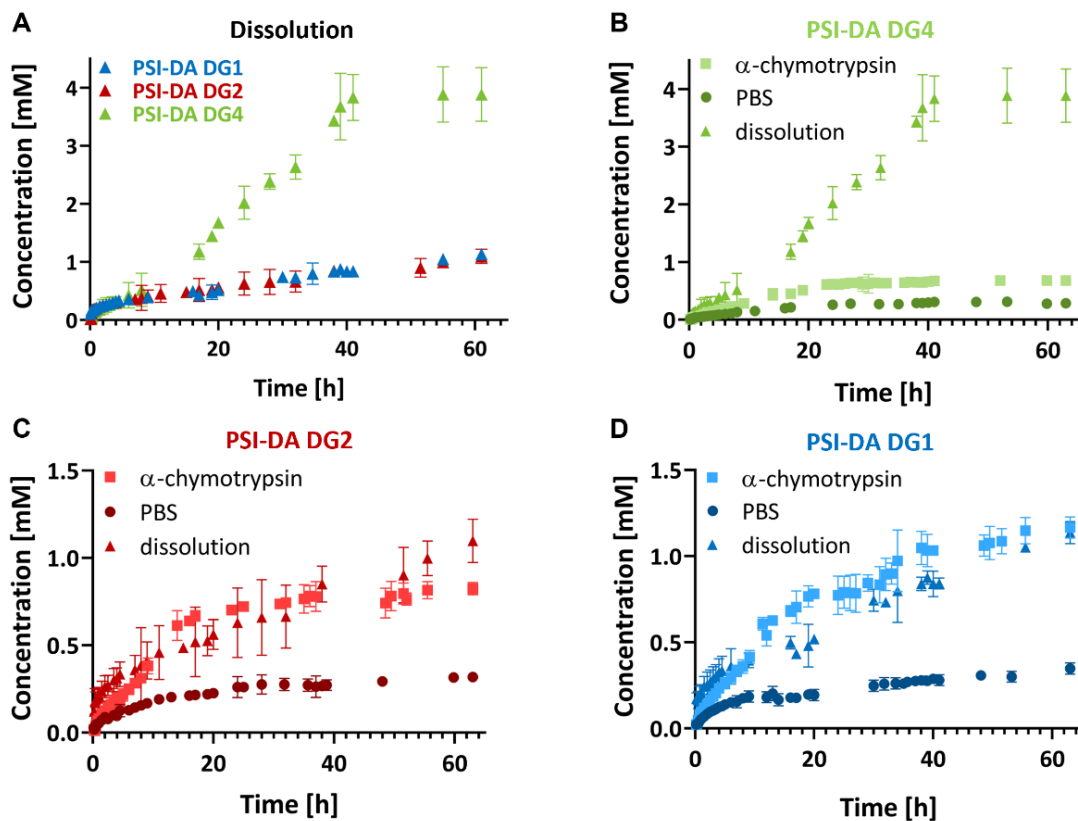
*Figure 24.: Dissolution of PSI-DA conjugates in PBS (A) and DA release from fibrous PSI-DA DG4 (B), PSI-DA DG2 (C), and PSI-DA DG1 (D) conjugates under different conditions (**KT1**).*

Besides the polymer of choice, the conjugated drug can also affect the physicochemical parameters of the polymer regarding the solubility and the kinetics of the dissolution. The conjugation of AE at the same time with DA to the PSI chain, increases the solubility of the polymer. This type of fibrous conjugate immediately dissolves in water or PBS, therefore in this part, PSI-DA-AE 1:2 conjugates have not been investigated.

The fibrous meshes with different DA content showed almost similar dissolution kinetics. The PSI-DA-DG4 dissolved the most rapidly and provided the highest solubility after approximately 3 days during the investigated period. Moreover, a sudden increase in the DA concentration can be observed after 8 hours (**Figure 24. A**).

The release kinetic curves (**Figure 24. B, C, D**) show the proteolytic activity of the α-chymotrypsin enzyme, which is capable to cleave the amide bonds next to an aromatic ring. The enzyme provides 2-3 times higher DA release compared to PBS without enzyme in the case of all types of conjugates.

The percentage of the dissolved conjugates and the released DA in PBS and in the presence of the α-chymotrypsin enzyme can be seen in **Table 7.** The values were calculated according to the theoretical content of DA on the polymer chain based on our previous publication (164).

***Table 7.:** Percentage of the dissolved conjugates and the released DA after 65 hours (**KT1**).*

Polymer conjugate	Dissolved conjugates [%]	Released DA (PBS) [%]	Released DA (α-chymotrypsin) [%]
PSI-DA DG4	42.3	20.5	49.2
PSI-DA DG2	7.6	14.5	38.0
PSI-DA DG1	6.6	13.4	45.1

The amount of the released DA in almost every case, is higher than the amount of the DA on the dissolved conjugates, the only exception is the PSI-DA DG4 conjugate (**Table 7.**).

Amongst the PSI-DA conjugates with different degrees of grafting, the PSI-DA DG4 releases the most DA after 65 h, namely 42.3%, and there is no significant difference regarding DA release between PSI-DA DG2 and PSI-DA DG1 fibrous meshes. In the presence of the α-chymotrypsin enzyme, the tendency between the different conjugates is similar: PSI-DA DG4 conjugate can release the most DA (49.2%), but in the presence of enzymes PSI-DA DG1 sample can provide more released DA than PSI-DA DG2, almost reaching the level of PSI-DA DG4.

In the case of Dox-containing drug-delivery systems (Dox/PSI and PSI-Dox), the main long-term goal can be a therapeutic usage of these meshes after a potential breast cancer surgery. Therefore, to mimic the proper conditions, the drug release of Dox-loaded (Dox/PSI) and Dox-conjugated (PSI-Dox) meshes were investigated at two different pH values: pH 6.5 stands for the slightly acidic environment around tumors, and pH 7.4 represents the healthy tissue conditions (**Figure 25.**). The aim of the Pred-containing meshes is to support the effect of Dox and hinder the inflammation after a potential surgery, therefore these samples were also investigated at both abovementioned pH values (**Figure 26.**).
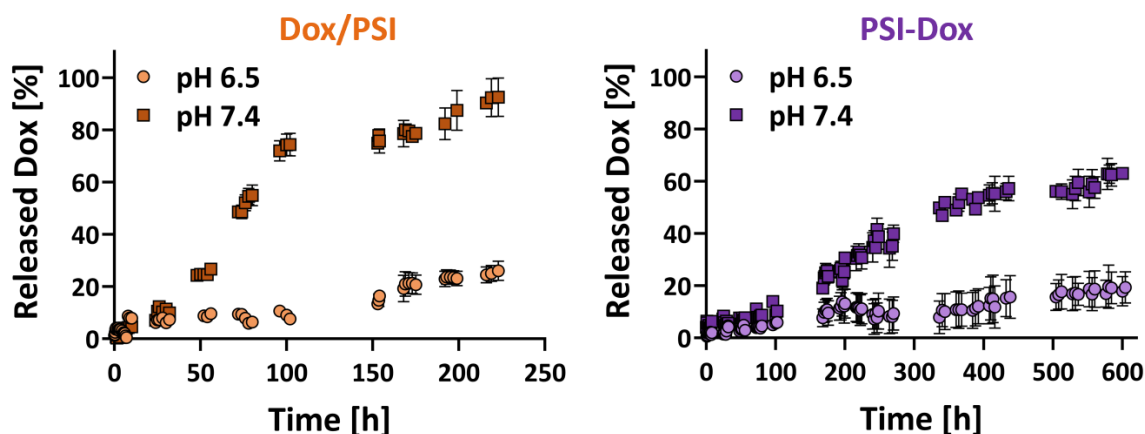
*Figure 25.: Drug release from fibrous Dox/PSI and PSI-Dox meshes (**KT2**).*

Regarding the Dox-loaded PSI meshes (Dox/PSI), and PSI-Dox conjugate meshes (**Figure 25.**) the Dox release in both cases is higher at pH 7.4 compared to pH 6.5. On both diagrams, a sudden increase can be observed in the drug release after 48 h in the case of pH 7.4. In addition, the release of Dox from PSI-Dox conjugate samples is noticeably slower, than in the case of Dox-loaded PSI fibers (Dox/PSI).
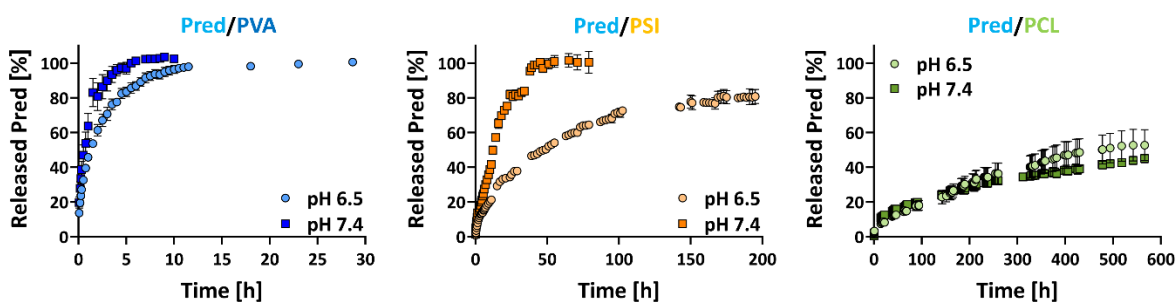
*Figure 26.: Pred release from Pred-loaded PVA, PSI, and PCL meshes (**KT2**).*

The release of Pred from fibrous polymer meshes were compared in the case of 3 different polymers: PVA, PSI, and PCL (**Figure 26.**). Regarding Pred/PVA nanofibrous meshes, the release of Pred is the fastest compared to the other polymers. During the first 2-hour-long interval, 80% of the drug is released at pH 7.4, while the drug release reaches 60% of the total Pred content at pH 6.5, consequently at a lower pH value, the Pred release from PVA fibers is slightly slower. The total release time in the case of pH 7.4 is around 6 hours, while at pH 6.5 it takes approximately 12 hours.

In the case of Pred/PSI meshes, the release is far slower compared to PVA-based fibers, but the effect of pH is much more significant. At pH 7.4, the drug release is completed in 42 hours, while at pH 6.5 the released Pred content is about 77% after 155 hours and remains at this level until the end of the investigated period.

56

The slowest release can be observed in the case of Pred/PCL fibers, compared to PVA and PSI samples. No effect of the environmental pH value can be detected applying PCL fibers. After a sudden initial increase in the Pred release during the first 1 hour, a linear, controlled and relatively slow release can be observed. After 25 days of investigation, the released Pred is around 55% at both investigated pH values.

4.3. *In vitro* experiments

4.3.1. Detection of D1 and D2 receptors of PDLSCs and SH-SY5Y by immunofluorescence labeling

The expression of two typed of DA receptors (D1R; D2R) was studied on both PDLSCs and SH-SY5Y cells to investigate whether these cells are capable to react and having sensitivity to DA (**Figure 27.**).
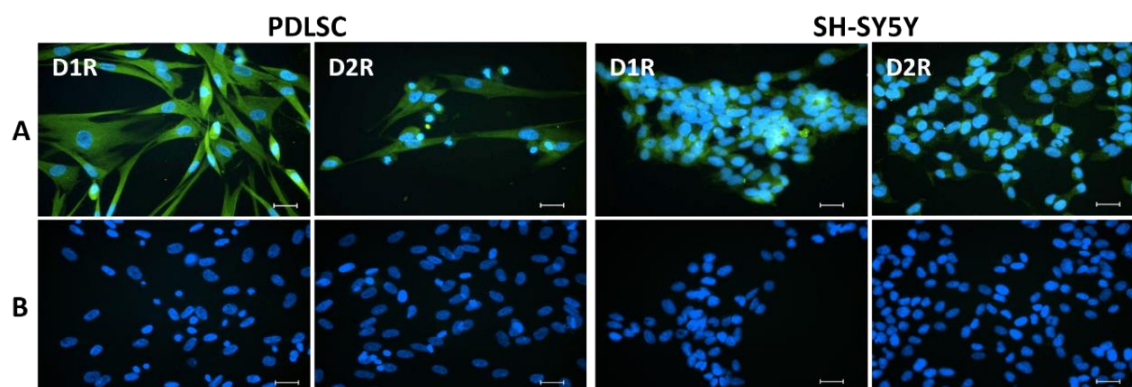
*Figure 27.: Immunofluorescence labeling of D1R and D2R DA receptors (green, cytoplasm) on PDLSCs and SH-SY5Y cells (A) with 2nd antibody controls (B). The nuclei were stained with DAPI (blue). Confocal microscopy images, scale bar: 20 μm (**KT1**).*

The staining control (**Figure 27. B**) proves the validity of the specific binding in the case both cell types.

Our immunofluorescence labeling results proved that both of the D1 and D2 DA receptors are expressed on PDLSCs and on SH-SY5Y neuroblastoma cell as well.

4.3.2. Effect of different drugs on cell viability assays and microscopy investigation of cell morphology

The effect of different DA concentration on viability of PDLSCs and SH-SY5Y cells was assessed by *in vitro* tests. For this investigation, free DA and PSI-DA-AE 1:2

conjugates were also applied in a wide concentration range for 24 and 72 h (**Figure 28. A, B**).
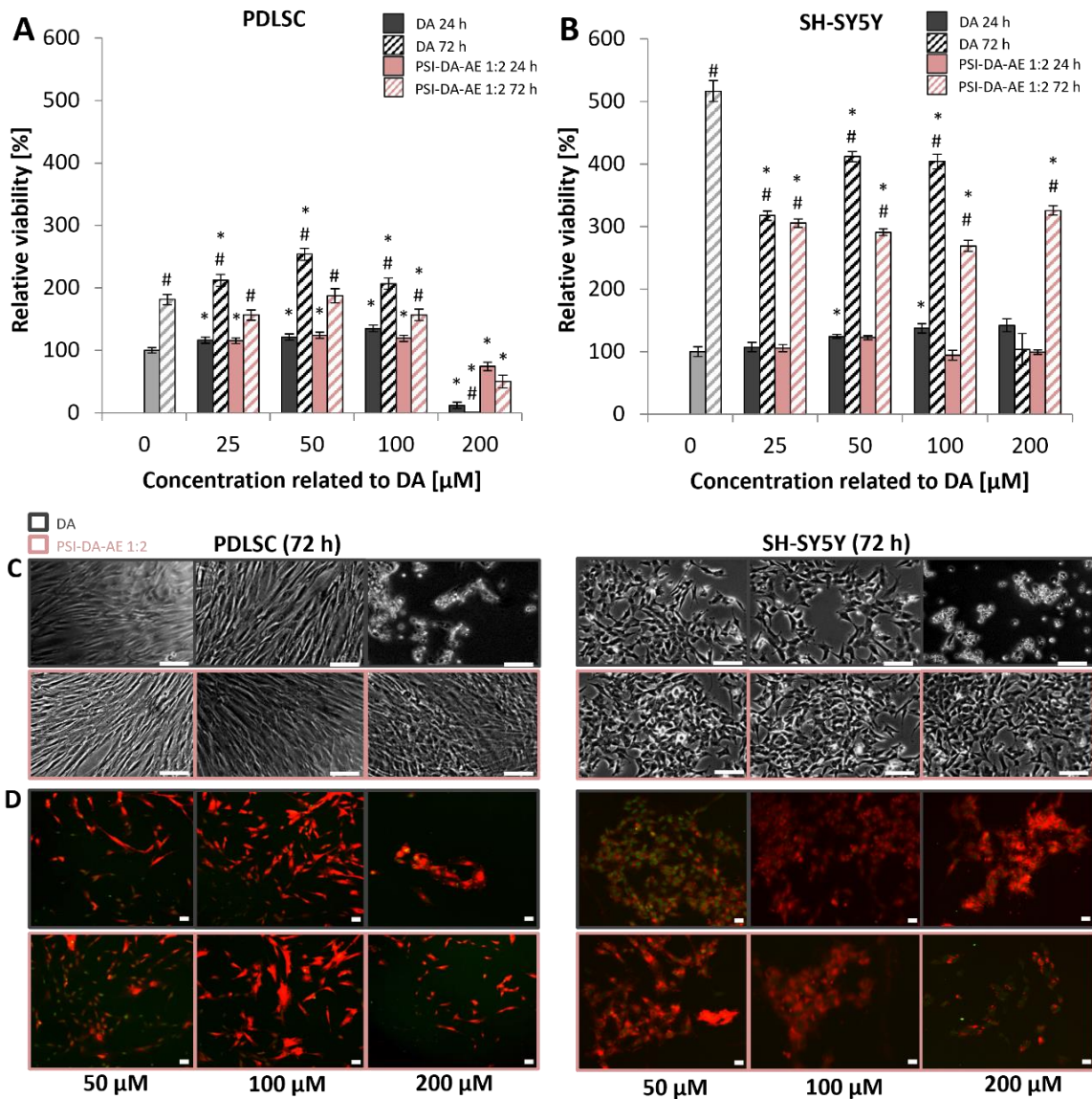
Figure 28.: *DA-concentration dependent cell viability regarding PDLSCs (A) and SH-SY5Y cell line (B). The data are represented as arithmetic mean ± standard error of mean. *Significant difference to the daily control. #Significant difference to the 24 h of treatment. Phase contrast microscopy (C) and two-photon microscopy images (D) taken after 72 h of treatments. Scale bar: 100 µm (C); 200 µm (D). In two-photon microscopy images, the red sign indicates the cytoplasm of the cells stained with Vybrant DiD and the green sign stand for the cell nuclei stained with DAPI (**KT1**).*

Based on our results, both DA and PSI-DA-AE 1:2 conjugate have no significant effect on the cell viability up to the concentration of 100 µM regarding both cell types and

both exposure times. However, at 200 µM concentration (related to DA) significant differences can be seen between the effect of free DA and its conjugated form regarding both cell types.

In the case of PDLSCs, the viability significantly decreased in the presence of free DA after 24 hours, while in the case of the treatment with the conjugated form, only a slight decrease can be observed.

On the other hand, SH-SY5Y cells were not affected significantly by either 200 µM free DA or its conjugated form during 24 h of treatment. 200 µM DA eliminated all PDLSCs after 72 h and also prevented the proliferation of SH-SY5Y cells. The PSI-DA-AE 1:2 conjugate did not affect the SH-SY5Y cell viability even after 72 h of treatment.

In summary, both cell types show a DA concentration-dependent decrease in cell viability.

By phase-contrast microscopy we could confirm the results of the cell viability tests (**Figure 28. C**). Up to 100 µM DA concentration, confluent cultures of PDLSCs can be observed with normal cell morphology after 72 h. However, the PDLSC cultures, which were treated with 200 µM free DA, contained round shaped and floating cells indicating cell death. The undifferentiated SH-SY5Y cells normally show short neurites and generally grow in clumps, which can be seen in the images regarding the low DA concentrations. On the contrary, cell death can be observed at 200 µM free DA concentration, but SH-SY5Y cultures treated with conjugated DA, show no morphological changes even with 72 hour-long exposure to 200 µM concentration (related to DA).

By applying two-photon microscopy (**Figure 28. D**), a larger area can be detected, therefore the distribution of the cells can be properly observed. According to the images, PDLSCs showed healthy, elongated shapes, and normal morphology, additionally, connections can be observed between the cells in several cases. SH-SY5Y cells also showed typical behavior, thus these cells formed clusters and generated clumps. These photos can confirm the cell viability results: the higher number of the observed cells is in a line with higher cell viability values.

Besides the above-mentioned *in vitro* tests, the effect of the different concentrations of Dox and Pred on viability of MDA-MB-231 breast cancer cells was also investigated in

order to determine the optimal concentration for the electrospun implantable meshes (**Figure 29.**).
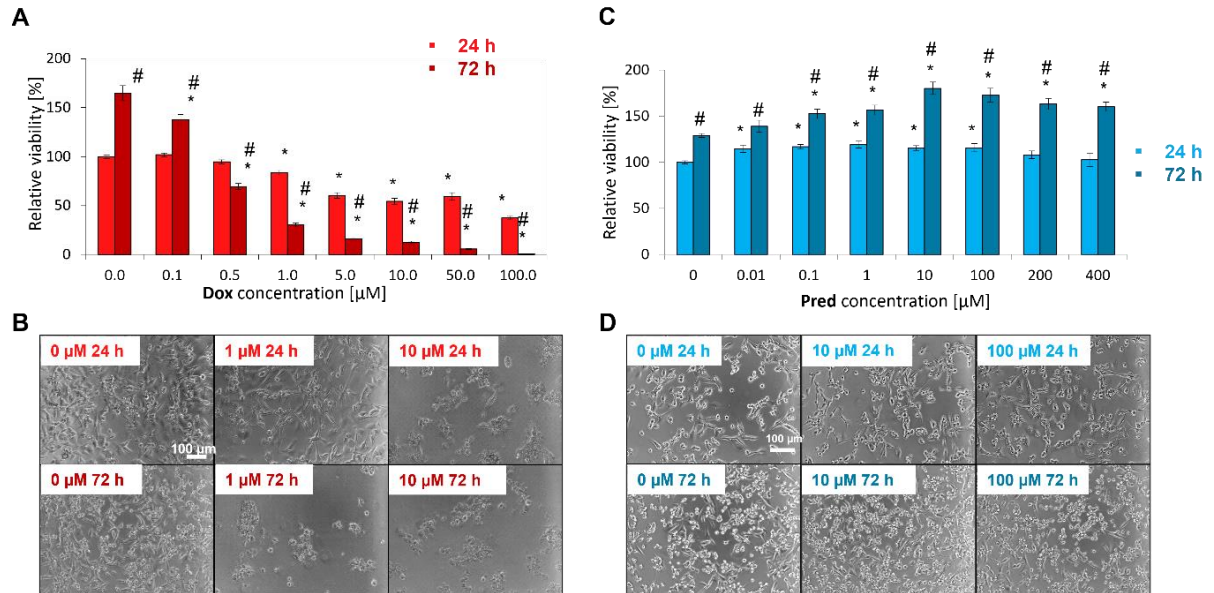
Figure 29.: *Cell viability (A, C) and morphology (B, D) of MDA-MB-231 cells in the presence of different concentrations of Dox (A, B) and Pred (C, D) for 24 and 72 hours. The data are represented as arithmetic mean ± standard error of mean. *Significant difference to the daily control. #Significant difference to the 24 h of treatment. Scale bar: 100 μm for all photos (B, D). (**KT2**).*

According to our results, 10 µM Dox can decrease the viability of the cells by 50% (IC50) after 24 hours of treatment, while the IC50 value for a 72-hour-long treatment is between 0.5 and 1 µM (**Figure 29. A**). Based on the phase-contrast microscopy images, after 24 hours of treatment with 0-0.5 µM Dox, the MDA-MB-231 cells show normal morphology, and almost confluent cultures can be seen, while applying higher concentrations of Dox, the number of cells with normal morphology decrease, and round-shaped floating cells can occur (**Figure 29. B**), which is in correlation with the viability results.

Regarding treatments with Pred, it does not show cytotoxic effect in the applied concentration range on MDA-MB-231 cells after 24 or 72 hours of treatment (**Figure 29. C**). In concordance with these measurements, phase contrast images show cells with normal morphology in each experimental group (**Figure 29. D**).

4.3.3. Effect of drug-containing fibrous polymer meshes on cell viability

After the investigation of the effect of the concentration range of different drugs on cell viability, the neat fibrous polymers were tested to investigate their cytotoxic effect (**Figure 30.**).
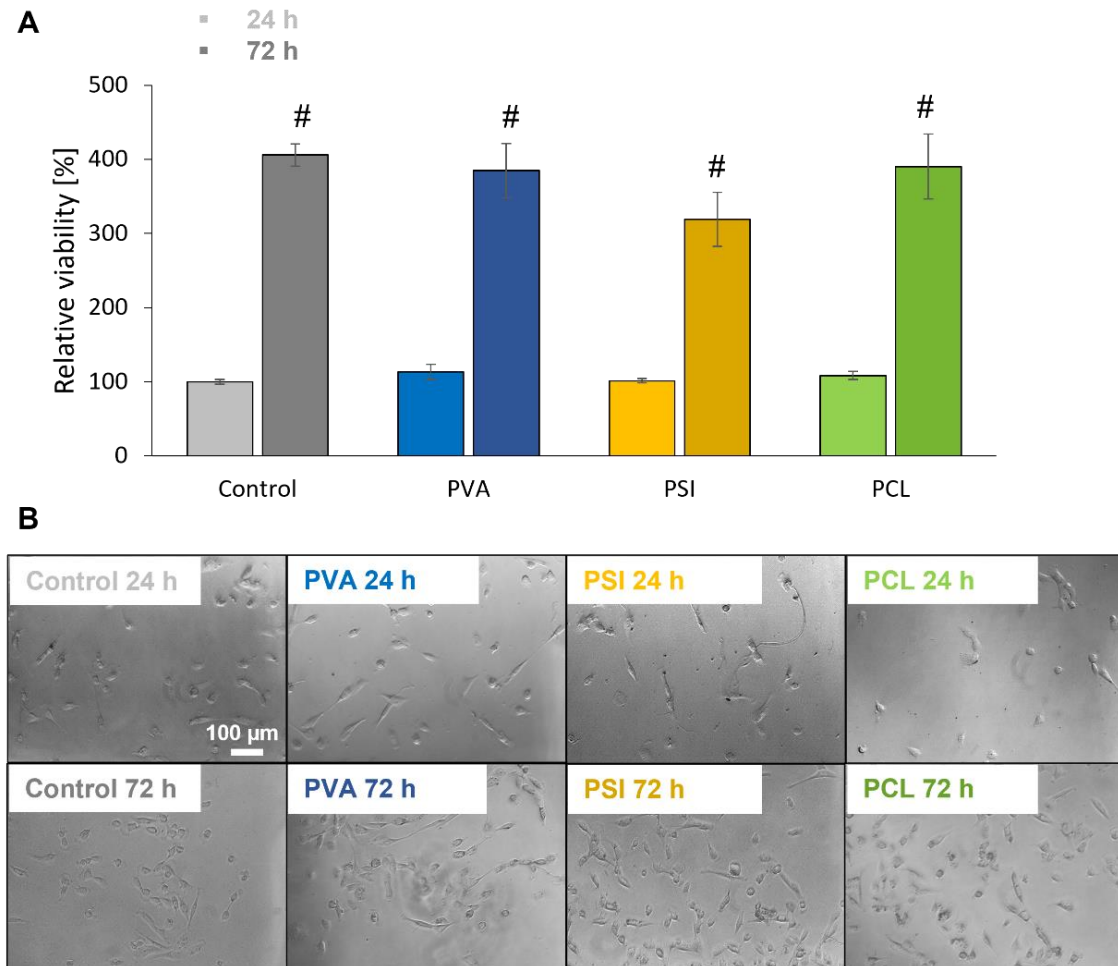
Figure 30.: Viability assay (A) and morphology (B) of MDA-MB-231 cells treated with neat PVA, PSI, and PCL nanofibrous meshes. The data are represented as arithmetic mean ± standard error of mean. #Significant difference to the 24 h of treatment. Scale bar: 100 μm for all photos (B). (KT2).

According to the results regarding neat PVA, PSI, and PCL fibers, none of them exert cytotoxic effect on MDA-MB-231 cells (**Figure 30. A**). The data show that there is no significant difference in cell viability compared to the daily control in the case of each polymer. The MDA-MB-231 cells were capable to appreciably proliferate in the presence of nanofibrous neat PVA, PSI, and PCL meshes from 24 h to 72 h of

treatment. The phase-contrast images confirm the cell growth between two time points and show normal cellular morphology in each case (**Figure 30. B**).

After these preliminary-investigation with neat-fibrous meshes, the potential cytotoxic effect of drug-containing meshes were assessed (**Figure 31.** and **Figure 32.**).
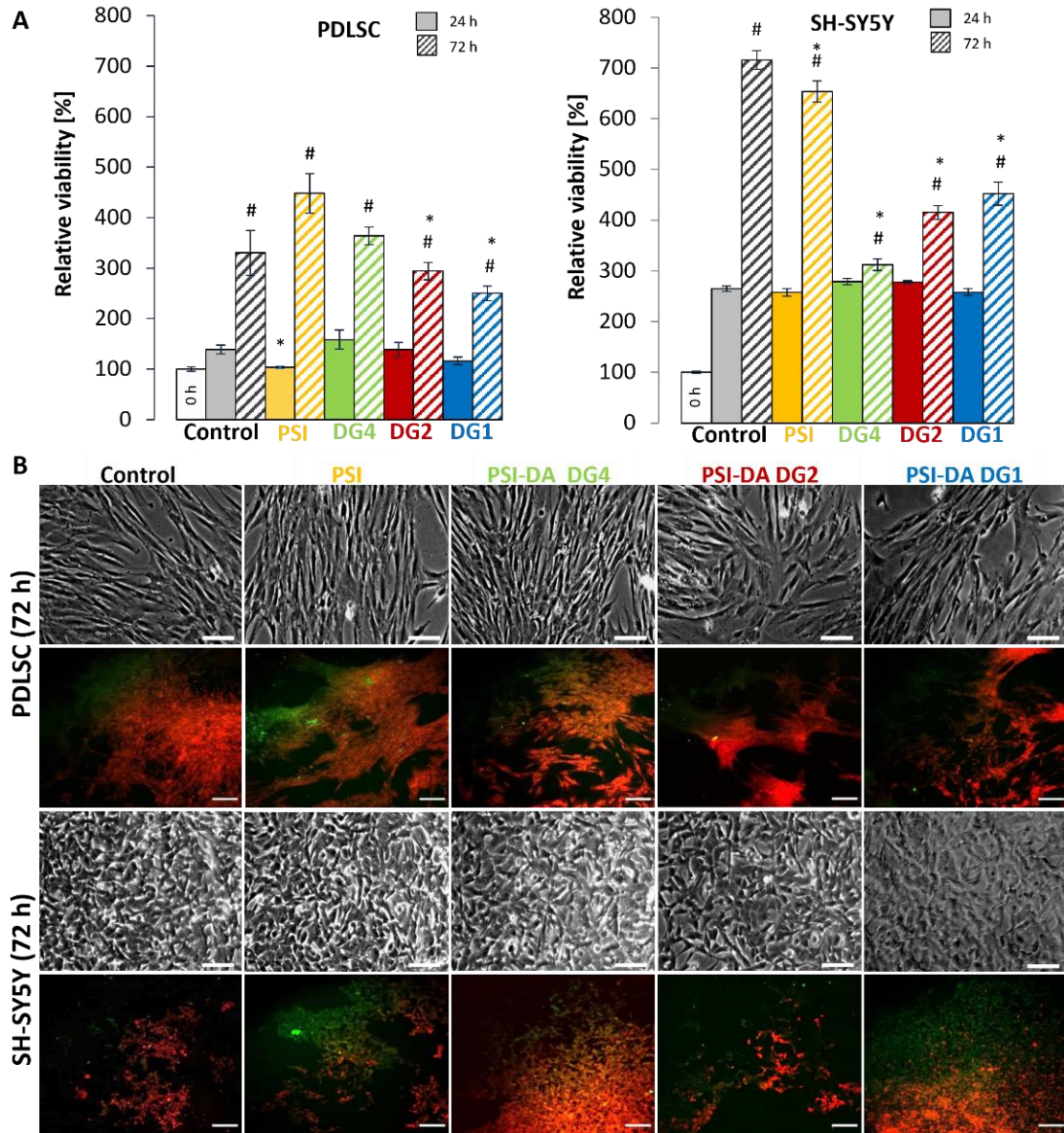
*Figure 31.: Relative viability (A) and cell morphology (B) after 24 and 72 h of treatment with fibrous PSI and PSI-DA conjugates at 300 µM related to DA. *Significant difference to the daily control. #Significant difference to the 24 h treatment. Phase contrast microscopy images (above; scale bar: 100 µm) and two-photon microscopy images (below; scale bar: 200 µm) were taken after 72 h of treatments. The red sign indicates the cytoplasm of the cells stained with Vybrant DiD and the green autofluorescence indicates the presence of the polymer (KT1).*

We observed that both PDLSCs and SH-SY5Y cells were capable to proliferate from 24 h to 72 h of the exposure to the fibrous PSI-DA meshes (**Figure 31. A**) despite the relatively high 300 μM concentration related to DA. This exceeds the concentration value that these cells are capable to tolerate regarding free form of DA according to the previous cell viability investigations (**Figure 28.**). Consequently, the cells are capable to proliferate in the presence of higher concentrations related to DA when DA is conjugated to the PSI.

Although there are no significant differences between the different DA-containing conjugates after 24 h of treatment, comparing the examined two different cell types, reverse tendencies can be observed after 72 h of exposure. With the decreasing grafting degree (which corresponds to increasing DA content), the viability of PDLSCs showed a decreasing viability tendency, while on the contrary, the viability of SH-SY5Y cells tended to increase.

Concerning both cell types, the images made by phase-contrast microscopy and two-photon microscopy (**Figure 31. B**) show high confluency levels with normal cell morphology after 72 h of exposure in each experimental group. In addition, a high number of connections between the cells can be observed in each case.
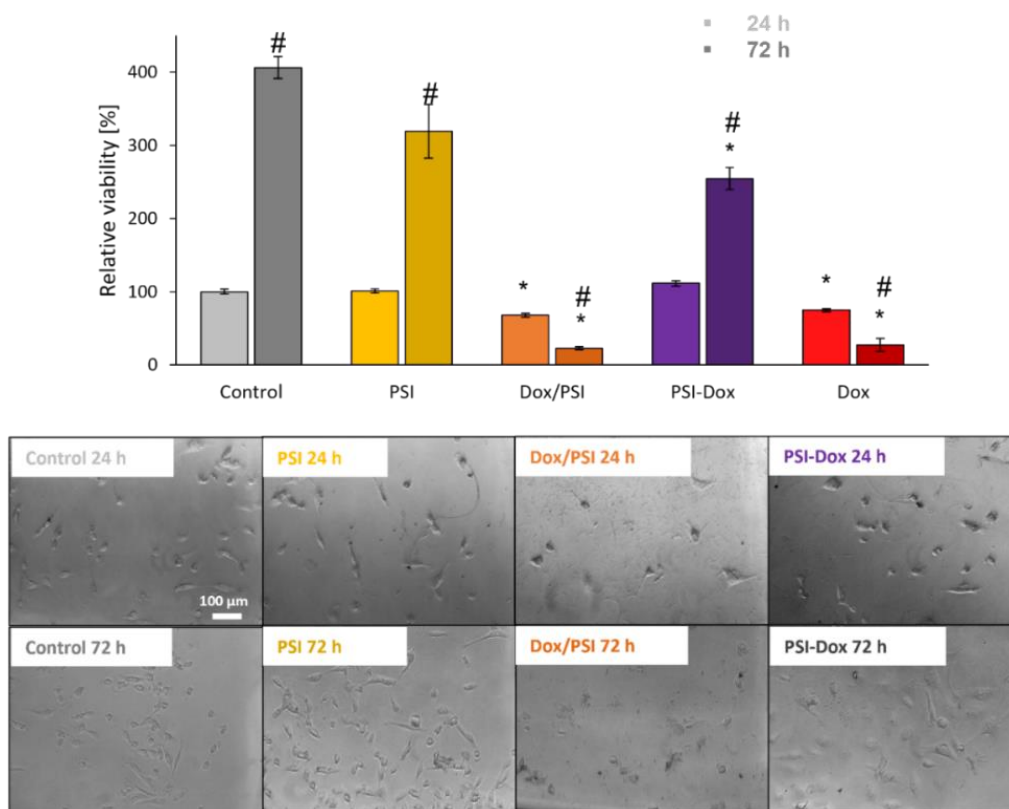
*Figure 32.: Cytotoxicity and morphology of MDA-MB-231 cells treated with Dox-conjugated and Dox-loaded PSI fibers. *Significant difference to the daily control. #Significant difference to the 24 h treatment. Scale bar: 100 μm for all photos. (**KT2**).*

We also studied the cytotoxic effect of the Dox-containing nanofibrous meshes. Both PSI-Dox conjugates and Dox-loaded PSI (Dox/PSI) fibers were introduced to MDA-MB-231 cells in 1 μM concentration related to Dox (**Figure 32.**) based on our previous cell viability results applying different concentrations of Dox (**Figure 29. A**).

According to our results (**Figure 32.**), Dox/PSI fibrous meshes decreased the viability of MDA-MB-231 cells by 32% after 24 hours of treatment compared to the untreated control – this value was 95% after 72 hours of exposure. The same tendency and similar viability values can be observed when the free form of Dox was applied. However, when fibrous PSI-Dox conjugate was introduced to the cells, their viability did not change during the first 24 hours of treatment, and it decreased only by 38% after 72 hours. Based on the phase-contrast images, MDA-MB-231 cells with normal morphology can be observed after 24 hours in each case. In contrast, after 72 hours,

significantly less cells can be seen in the case of treatment with Dox or Dox-containing samples, and round-shaped floating cells also appear, indicating the cell death.

4.3.4. Internalization of PSI-DA conjugates

As both free DA and Dox have a concentration-dependent effect on cell viability according to our previous results, in addition PSI-DA and PSI-Dox conjugates also influence cell behavior, we could assume that not only the free DA and Dox but also their conjugates can be uptaken by the cells.

To investigate the internalization of the PSI-DA conjugates with different degrees of grafting, fluorescent BCB-labeled PSI-DA conjugates were added to the cells, which can be detected inside the fixed cells by confocal microscopy (**Figure 33.**).
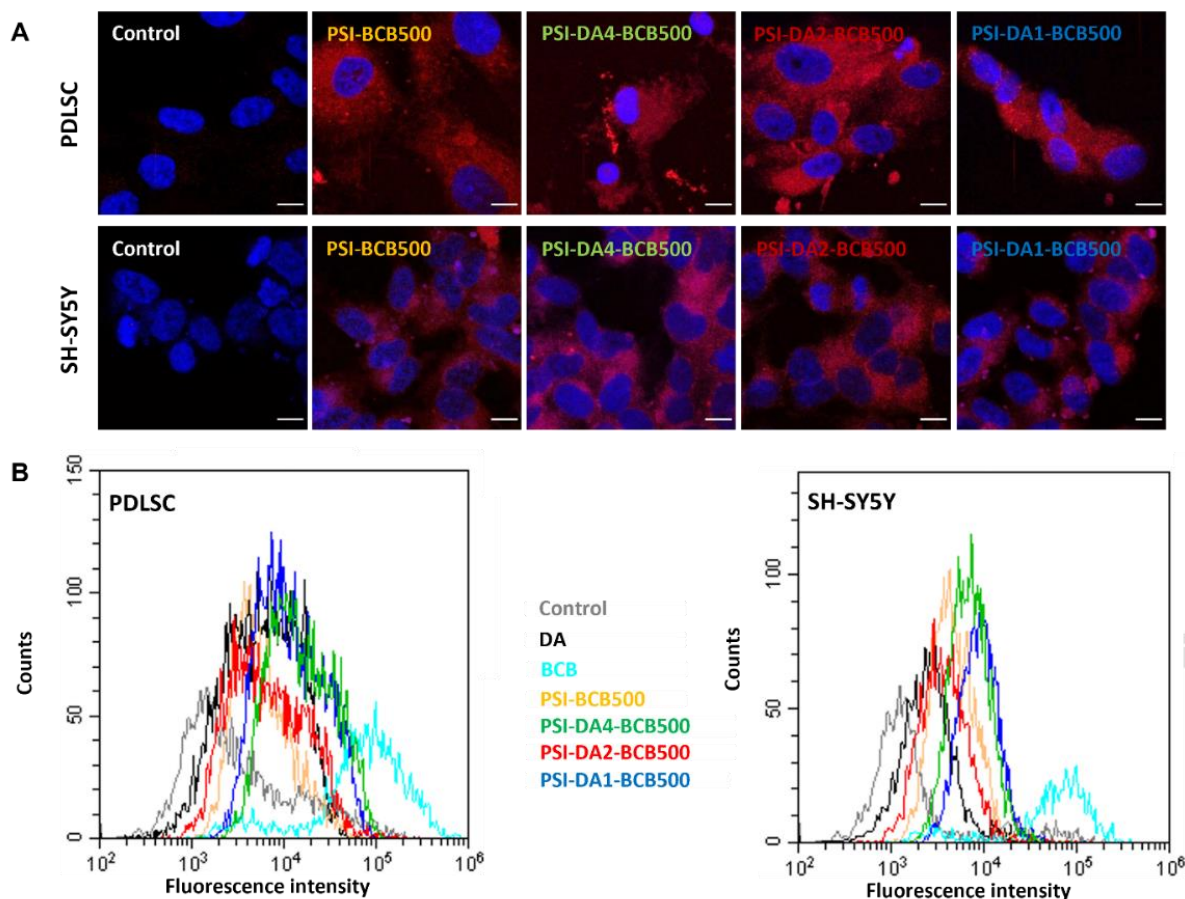
Figure 33.: *Visualization of the internalization of BCB stain conjugated PSI-DA conjugates by confocal microscopy (A). Scale bar: 10 µm; nuclei (DAPI, blue); BCB in the cytoplasm (red). Validation of the internalization by flow cytometry (B) (**KT1**).*

In the photos, the homogenous fluorescent signal of BCB (red color) can be observed in the cytoplasm of both cell types proving the internalization of the PSI-DA conjugates (**Figure 33. A**).

The fluorescent signal and the uptake of the PSI-DA conjugates can be quantified and affirmed by flow cytometric analysis (**Figure 33. B**). To identify the autofluorescence, unlabeled cells were used as the negative control. Pure, free BCB-treated cells in the same concentration related to BCB, found in BCB-labeled PSI-DA conjugates, stood for positive control. In all cases, except the negative control, significant BCB fluorescence was observed. The results show that the fluorescence intensity signal of BCB-labeled conjugates is between the negative control (untreated cells) and the positive control (cells treated with pure, free BCB stain).

In the case of PSI-Dox conjugates, there is no need of pre-labelling the polymer with a fluorescent agent to investigate the uptake, due to the fluorescent signal of Dox (at 470 and 560 nm).
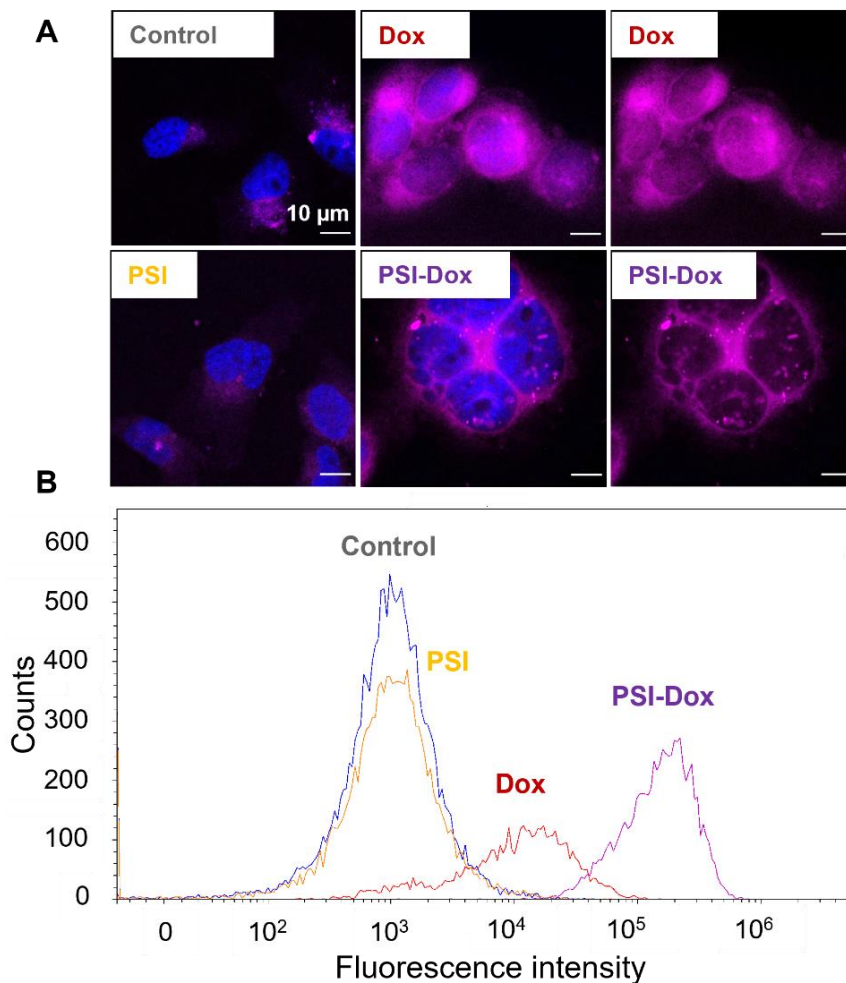
Figure 34.: *Visualization of the internalization of PSI-Dox conjugates by confocal microscopy (A). Nuclei (DAPI, blue); BCB in the cytoplasm (purple), scale bar: 10 µm. Validation of the internalization by flow cytometry (B) (**KT2**).*

To detect the autofluorescence of the cells, untreated cells were also observed under a confocal microscope along with neat PSI, Dox and PSI-Dox treated MDA-MB-231 cells (**Figure 34. A**). In the case of the control images (Control, and PSI-treated cells), only a weak signal (purple color) can be observed, which is generated by the autofluorescence of the MDA-MB-231 cells. Regarding Dox-treated cells, more fluorescence signal can be observed. The intracellular distribution of this signal is different in the case of PSI-Dox conjugate compared to free Dox. Regarding PSI-Dox conjugates, the fluorescent signal can be mainly seen in the cytoplasmic area. However, in Dox-treated cells, the purple signs are located in the nuclei as well. Regarding PSI-Dox conjugates, more fluorescence signal are located to a well-defined area (intense dots), in contrast to the homogenous cytoplasmic staining of the Dox-treated cells.

According to the flow cytometric results, the measured fluorescence intensity signals regarding Dox- and PSI-Dox-treated cells are much higher compared to the control and the PSI-treated cells. In addition, the peak of the conjugate represents higher fluorescence intensity than in the case of the free Dox-treated cells (**Figure 34. B**), suggesting that the uptake of the Dox can be enhanced by conjugation to PSI.

4.3.5. Cytokine release profile – anti-inflammatory effect of Pred-loaded fibers

To determine the anti-inflammatory effect of Pred the level of 13 different cytokines were measured in the supernatant of the MDA-MB-231 cells after culturing them in the presence of Pred (0-400 µM), as well as neat and Pred-containing (400 µM) fibrous polymer meshes (Pred/PVA, Pred/PSI, Pred/PCL) (**Figure 35.**).
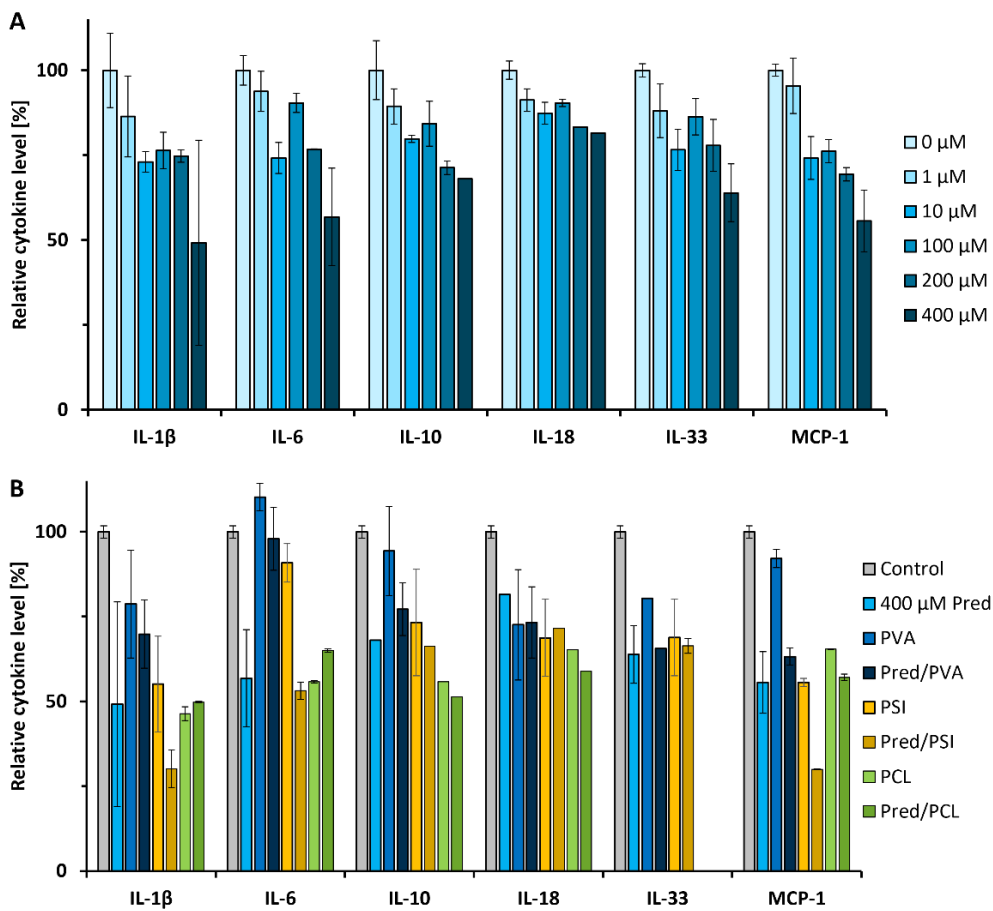
*Figure 35.: Relative cytokine level produced by MDA-MB-231 cells treated with a concentration series of Pred (A) and with different neat (PVA, PSI, PCL) and Pred-loaded fibrous meshes (400 µM related to Pred) (B). Cytokine level values were normalized to the untreated control (0 µM, Control) (**KT2**).*

According to the experimental data, only five interleukin (IL)-type cytokines (IL-1β, IL-6, IL-10, IL-18, IL-33) and the monocyte chemoattractant protein (MCP-1) were detectable in the case of the MDA-MB-231 cells. According to the results, Pred has a concentration-dependent effect on the levels of the detected interleukins and MCP-1. 400 µM Pred has a greater inhibition capacity (30-50%) in the case of the most investigated cytokines (only exception is IL-18 with approximately 20%) compared to the lower concentrations (0-200 µM).

In the case of IL-1β, IL-6 and MCP-1, the decrease in the cytokine level was 51%, 43% and 41% respectively, which are the most considerable results. While in the case of IL-18, IL-33, and IL-10, the decrease was 18%, 36%, and 32% respectively.

Considering the nanofibrous neat PVA, PSI, and PCL samples, the level of IL-18 and IL-33 was slightly decreased after introducing PVA, while in the case of the treatment with PSI fibers inhibited the production of all the investigated cytokines (except the IL-6). Neat PCL fibers generated a decrease under the detection limit of the IL-33 level and 35-54% decrease regarding the other five cytokines.

400 µM Pred-loaded PVA expressed a similar effect on the levels of cytokines such as free Pred in this adequate concentration. The only exception is IL-6, where no difference compared to the control was observed.

In the case of Pred/PSI fibers, the IL-1β, IL-6 and MCP-1 levels decreased. Regarding Pred/PCL samples, no effect of Pred can be noted compared to neat PCL fibers.

5. Discussion

5.1. Physicochemical and mechanical characterization of electrospun meshes

5.1.1. Chemical characterization of the meshes by ATR-FTIR and ^{1}H-NMR

Based on our FTIR results regarding PSI-DA conjugates (**Figure 13.**), the characteristic peaks belonging to the imid bond of the succinimide ring (1700, 1384, 1207, and 1160 cm^{-1}), are decreasing with the increasing DA content (164). The existence of these peaks, even in the case of PSI-DA DG1 conjugates, show that there are still unmodified succinimide rings in every conjugates. In the spectra of PSI-DA-AE 1:2, these characteristic peaks of imide bonds cannot be seen, which proves that every monomer was successfully modified.

Besides the changes of the imid peaks, the characteristic peaks referring to the amide bonds (1600, 1390, 1355, 1660, and 1540 cm^{-1}) are increasing, due to DA grafting, since generation of the amide bonds indicates the presence of opened succinimide rings. The intensity of these peaks is lower regarding PSI-DA DG4 than the other grafted polymer types, which proves that this conjugate has less DA than PSI-DA DG2 or PSI-DA DG1.

The characteristic peaks of -OH groups (around 3270 cm^{-1}) also can be observed in the case of PSI-DA-AE 1:2 conjugates referring to the successful modification of PSI with AE.

The FT-IR spectra of the different PSI-DA conjugates in powder form (**Figure 13. A**) are similar to the previous results based on the work of Juriga et al., which confirms the successful chemical modification and refers to the reproducible synthesis of PSI-DA conjugates (164). All the above-mentioned characteristic peaks appear also in the FTIR spectra of the nanofibrous form of the conjugates (**Figure 13. B**), which also confirm that the electrospinning process does not have any influence on the chemical structure of the conjugates (**KT1**).

Regarding Pred-containing PVA and PCL samples (**Figure 14.**), the characteristic peak of Pred at 1680 cm^{-1} occurs in the FTIR spectra of Pred/PVA and Pred/PCL fibrous meshes, which verifies the presence of Pred in the fibrous meshes. However due to the relatively small amount of the incorporated Pred, the difference between the spectra of the neat and drug-containing fibers is moderate. According to the spectrum of

70

Pred/PVA fibers, the intensity of the characteristic peaks relating to Pred is higher compared to that of Pred/PCL fibers. This difference can be explained by the drug-polymer incompatibility theory (69,70), which means that this incompatibility effect (i.e., the distinct chemical nature of the polymer and the drug molecule) forces the migration of the hydrophobic drug molecules to the surface of the hydrophilic polymer. Therefore, in Pred/PVA samples, the drug is supposed to be accumulated mainly on the surface of the fibers.

Regarding Pred/PCL samples the distribution of the Pred in PCL fibers can be more homogenous due to the higher drug-polymer compatibility, which is manifested in strong Van der Waals interactions between the apolar drug molecules and the apolar polymer chains (70). This phenomenon can explain why the characteristic peak of Pred (1680 cm^{-1}) is less intense by this polymer than in the case of PVA. In addition, not only the van der Waals interactions, but also hydrogen bonding, hydrophobic interactions and electrostatic interactions between the drug molecule and the polymer can also enhance the homogeneity of the drug distribution inside the fiber (70,230).

Nevertheless, in the FT-IR spectrum of Pred/PSI fibers, the characteristic peak of Pred at 1680 cm^{-1} overlaps with the characteristic peak of PSI, therefore the presence of the Pred in the PSI fibers could not be confirmed by this measurement.

Concerning Dox/PSI and PSI-Dox samples (**Figure 15.**), the characteristic FTIR peaks of Dox (1282 cm^{-1} and between 1500 and 1700 cm^{-1}) are observable. However, due to the modest amount of Dox, only a slight difference can be noticed on their spectra compared to those of the neat fibers (231). By this method, the Dox-containing PSI-based samples (PSI-Dox and Dox/PSI) cannot be distinguished from each other, therefore, ^{1}H-NMR measurements were carried out to explore aby difference in the chemical structure.

The NMR spectrum of PSI-Dox conjugate (**Figure 16.**) also prove the presence of Dox (1.02, 1.06, 1.16, 1.92, 2.97 ppm) in the PSI fibers, and the position of the observed characteristic peaks of the modified (4.65 ppm – methine proton) and unmodified (3.23 ppm, 2.74 ppm – methylene peaks, and 5.28 ppm – methine group) succinimide rings is in good correlation with the literature (98).

In our case, the theoretical degree of grafting regarding PSI-Dox conjugate is around 1:800, which is in accordance with the NMR results showing the molar ratio between

Dox and PSI (corresponding the degree of grafting) somewhere between 1:500 and 1:1000 (**KT2**).

5.1.2. Powder X-ray Diffractometry (XRD)

Hence electrospinning can induce the amorphization of drug molecules possessing poor water solubility (232), the crystal structure of fibrous Pred-containing PVA, PSI, and PCL samples were investigated besides the stock materials (physical mixtures of polymers and Pred, and polymers alone) (**KT2**).

Based on our results, Pred has a completely crystalline structure (most intensive characteristic peaks can be found between $2\theta = 13\text{-}20°$), and its structure does not change when it is physically mixed with the different polymers (**Figure 17.**).

Regarding the applied polymers, PVA and PCL are semi-crystalline polymers according to the literature (233,234) and our presented XRD results (characteristic peaks of PVA ($2\theta = 18\text{-}25°$) and PCL ($2\theta = 20\text{-}25°$)) as well (**KT2**). The crystal structure of PSI is similar to those of an amorphous polymer, but there is no exact information in the literature regarding XRD measurements of PSI (235,236).

After electrospinning of neat polymers, we found that the crystalline fraction of PVA was reduced (the peak at $2\theta = 23°$ vanished), while the crystal structure of PSI and PCL polymers remained unchanged (**KT2**).

Regarding Pred-containing nanofibrous samples, the characteristic peaks of Pred ($2\theta = 13\text{-}20°$) disappeared in Pred/PSI and Pred/PCL samples, while in the case of Pred/PVA samples, the disappearance is only partial. These results prove our initial hypothesis that the electrospinning of Pred with polymers, generate complete or partial amorphization of the Pred. In the case of Pred/PVA samples, the partial amorphization can be explained by the polarity difference of this polymer compared to PSI and PCL. This difference can also explain the FT-IR results: the hydrophobic Pred can be homogenously incorporated into the Pred/PSI and Pred/PCL fibers. In contrast, Pred molecules could be forced to the surface of the hydrophilic PVA fibers due to the drug-polymer incompatibility (69,70), which corresponds to the partial amorphization of Pred in Pred/PVA fibers, and the XRD results described by Zupancic et al. (233).

5.1.3. Morphological study of the electrospun fibers by SEM and two-photon microscopy, determination of fiber diameter

During the electrospinning process, it is crucial to choose the appropriate composition of the solvent to achieve smooth, homogenous fibers without beads and damage. In addition, several electrospinning parameters can also affect the diameter and the morphology of the fibers, such as the applied voltage, the polymer feeding rate in the syringe pump (**Table 1.** and **Table 2.**), and the chemical composition of the polymers or in this case: the chemical structure of the conjugates (**Figure 5.**) as well.

In the case of PSI-DA conjugates, THF was introduced to the solvent mixture to eliminate the malformations of the fibers by reducing the surface tension and the boiling point of the applied polymer solution, respectively (**Table 1.**). During the electrospinning of PSI-DA DG1 conjugate membranes, this DMF-THF solvent mixture generated bands and irregular shapes of fibers, so EtOH was also added to the mixture to further reduce the boiling point and the surface tension of the polymer solution (**Table 1.**) (**KT1**).

Our results show that the increasing amount of DA on the polymer chain generates thinner fibers (613 ± 172, 179 ± 27, 78 ± 15 nm for DG4, DG2 and DG1, respectively) (**Table 3.** and **Figure 18.**) (**KT1**). The conjugates may form more hydrogen bonds due to the presence of more DA, which can enhance the intramolecular interactions through the catechol-groups between the polymer chains (70,230), but the differences in the electrospinning parameters can also be the reason of the different diameters.

According the two-photon images (**Figure 18. B**), the PSI-DA DG1 fibrous mesh contained some beads and malformations, which could be caused by the deviations in the flow of the polymer solution in the syringe. The green autofluorescence of the fibers might be the consequence of the secondary structure of the polymer chains similarly to other biopolymers such as polyamides that can provide an autofluorescence signal (164,237).

Since PSI can be modified with different primer amine group containing molecules, such as DA (164) (**KT1**), PSI-Dox conjugates can also be produced by nucleophile addition. The fiber diameter of Dox-loaded and Dox-conjugated PSI fibers with same Dox content were investigated to compare the effect of the drug in loaded and conjugated form (**Table 2.**). Incorporating Dox into PSI fibers generated mildly thinner

fibers (Dox/PSI: 467 ± 107 nm; PSI-Dox (545 ± 90 nm) compared to the cases of neat PSI fibers (584 ± 113 nm), but the difference was not remarkable. The surface of the Dox-containing fibers (Dox/PSI and PSI-Dox) (**Figure 20.**) was smooth, such as in the case of neat PSI fibers (**Figure 19.**), therefore this relatively small amount of Dox did not affect the fiber diameter and the morphology considerably (**KT2**).

Moreover, hydrophobic Pred was loaded in different amounts (0.5%, 1%) into PVA, PSI, and PCL fibers to elucidate the effect of loading into polymers with different hydrophobicity. Regarding the fiber morphology (**Figure 19.**), smooth fibers can be seen, and the diameter is consistent along the PVA and PSI fibers, which means that the incorporation of the drug did not affect the morphology of the fiber surface. However, in the case of neat and drug-containing PCL, the fiber diameter is altering along the fiber, which leads to a wide range in distribution of the fiber diameter values (**KT2**), but this effect is not originated from the drug incorporation hence neat PCL fibers show the same surface morphology (238,239).

Regarding fiber diameter (**Table 4.**), incorporation of Pred with different amounts did not affect notably the PSI and PCL meshes but generated clear observable changes in the case of PVA samples. The measured fiber diameter is directly proportional to the amount of the incorporated Pred (157 ± 61, 212 ± 56, 497 ± 117 nm, regarding 0, 0.5, and 1% Pred-content, respectively), which also can be explained by the drug-, polymer incompatibility theory (70,230), as well as the influence of the incorporated drug on the viscosity and conductivity of the polymer solution used for electrospinning (**Table 8.**). In the literature, the changes in the fiber diameter are mainly explained by the viscosity change of the polymer solutions after incorporation of drugs. For e.g., decreased viscosity, therefore decreased fiber diameters were measured in the case of incorporating a curcumin- and β-cyclodextrin-based inclusion complex (67) or ibuprofen (65) with different concentrations into PVA polymer. On the other hand, increased viscosity and increased fiber diameters were measured in the case of PVA solution after loading a nonsteroid anti-inflammatory drug, meloxicam (62), which is in good correlation to our results related to Pred/PVA samples (**Table 8.**) (**KT2**).

*Table 8.: Viscosity and conductivity of the different solutions used in electrospinning and the average fiber diameter of electrospun fibers containing different amounts of Pred (**KT2**).*

Polymer	Property	Neat	0.5% Pred	1% Pred
PVA	Viscosity (mPa s)	229.5 ± 3.5	282 ± 6	249 ± 3
	Conductivity (μS/cm)	144 ± 2	175.2 ± 2.3	174.9 ± 3
	Fiber diameter (nm)	157 ± 61	212 ± 56	497 ± 117
PSI	Viscosity (mPa s)	2325 ± 87.5	3150 ± 100	3230 ± 30
	Conductivity (μS/cm)	11.30 ± 0.06	11.06 ± 0.06	10.57 ± 0.12
	Fiber diameter (nm)	584 ± 113	426 ± 84	616 ± 102
PCL	Viscosity (mPa s)	99.3 ± 5	186.5 ± 0.5	189 ± 1
	Conductivity (μS/cm)	2.84 ± 0.2	2.28 ± 0.2	2.38 ± 0.15
	Fiber diameter (nm)	583 ± 255	546 ± 261	610 ± 299

Concerning the fiber diameter change in the case of PSI samples, the explanation is also can be found in the viscosity and the conductivity changes beside the drug-polymer interactions (**Table 8.**) (**KT2**). According to the literature, the paracetamol-loaded PSI fibers are thicker than the neat PSI fibers (99). In addition, incorporation of different salts (LiCl, $MgCl_2$, $CaCl_2$) has slight influence on the fiber diameter of PSI, that mainly can be explained by the changed conductivity of the solution and the ion-polymer interactions (240).

Decreased fiber diameters were observed in the case of PCL fibers with incorporation of doxycycline until a certain concentration (241), α-lactalbumin (204), or in the case of different hydrophobic plant extracts (242,243). In contrast, increased diameters of PCL fibers were reached by loading increasing concentration related to diclofenac sodium salt or introducing 20(S)-protopanaxidol (244). The increased fiber diameter in the above-mentioned articles is mainly explained by the higher conductivity, the viscosity- and surface tension change of the polymer solutions due to the different incorporated molecules.

According to our results and the literature data, the fiber diameter (**Table 4.**), the morphology (**Figure 19.**) and the crystallinity (**Figure 17.**) are not only dependent on the electrospinning parameters (flow rate, distance, voltage etc.) (**Table 2.**) and the

physicochemical properties of the polymer solution (viscosity, conductivity, surface tension etc.) (**Table 8.**) (63) but loading of different types and amounts of drugs also influences these parameters (**KT2**).

5.1.4. The mechanical performance of the fibrous meshes

The appropriate mechanical properties of drug-containing fibrous polymer-based samples are essential for biomedical applications. According to the demonstrated results and the literature, the mechanical properties of these types of scaffolds can be affected by the physicochemical features of the polymer solution, and the chosen parameters during the electrospinning process, since these applied parameters have a high influence on the fiber diameter and distribution, the homogeneity, and the adhesion of the fibers (245). In addition, the amount of the incorporated drug also influences the physicochemical features of the fibers regarding the mechanical parameters (**KT1** and **KT2**).

The outcomes of our fiber diameter analysis show that with the increasing amount of DA on the polymer chain the fiber diameter decreases (**Table 5.**), which is in good correlation with the literature (246,247). The decreasing tendency in the fiber diameter ends up with decreasing tendency of the specific load capacity (0.039 ± 0.008 $Nm^2 \cdot g^{-1}$, 0.022 ± 0.007 $Nm^2 \cdot g^{-1}$, and 0.010 ± 0.005 $Nm^2 \cdot g^{-1}$ for DG4, DG2 and DG1 respectively), which means the specific load capacity has in strong correlation with the fiber diameter and the DA content of the polymers. The results have high standard errors of the mean, which can be explained by the macroscopically noticeable inhomogeneity in the thickness of the fibrous sample due to the different distances from the syringe during the electrospinning process (**KT1**).

Regarding the initial modulus values (**Table 5.**), there are no correlation with the specific load capacity and no dependence on DA content (it is between 0.3 and 0.5 $N \cdot mm^{-1}$ for all the PSI-DA conjugates). The possible explanation for this observation are that the elevated DA content promotes the formation of more hydrogen bonds, which could strengthen the fibers, or the DA content is able to alter the crystalline part of the polymer (**KT1 and KT2**) (70).

In the case of Pred-loading into polymers with different polarity (PVA, PSI, PCL), diverse effect could be observed regarding the mechanical performance of the samples (**Table 6.** and **Figure 22.**). In the case of PVA, the higher content of Pred expressed

more significant decreasing effect on the specific load capacity (0.151 ± 0.006, 0.164 ± 0.009, and 0.081 ± 0.005 $Nm^2 \cdot g^{-1}$ for PVA with 0, 0.5, and 1% Pred-content, respectively), the initial modulus (2.794 ± 0.339, 1.972 ± 0.212, and 0.650 ± 0.104 $Nm^2 \cdot (mm \cdot g^{-1})$ for PVA with 0, 0.5, and 1% Pred-content, respectively) (**Table 6.**), and the maximum elongation of the fibrous meshes (7.8 ± 0.7, 3.8 ± 0.2, and 2.6 ± 0.2 mm for PVA with 0, 0.5, and 1% Pred-content, respectively) (**Figure 22.**) compared to PSI and PCL. The possible explanation can be the increased fiber diameter (**Table 6.**), since, in general, the thinner fibers provide higher strength and modulus due to the strong interactions between the individual fibers (246–248). Additionally, the drug-polymer interactions could also affect the mechanical properties (69,70). Gutschmidt et al. noticed increased mechanical performance regarding hydrophilic soy protein-loaded PVA fibers (66), which is exactly the opposite effect compared to the hydrophobic Pred-loaded PVA fibers (**KT2**). Concerning PSI samples, the presence of the drug altered the mechanical properties although it did not significantly affect the fiber diameter: the specific load capacity is decreasing (0.233 ± 0.009, 0.126 ± 0.005, 0.136 ± 0.009 $Nm^2 \cdot g^{-1}$) but the initial modulus is increasing (0.701 ± 0.0019, 1.680 ± 0.099, 2.373 ± 0.270 $Nm^2 \cdot (mm \cdot g^{-1})$) with the increasing Pred content (0, 0.5, 1%) (**Table 6.**) (**KT2**).

Pred/PCL samples show similarity to Pred/PSI fibers regarding the unaltered fiber diameter accompanied by changes in the mechanical performance (**Table 6.**). According to the deformation curves (**Figure 22.**), we can conclude that there are also changes in the fiber microstructure in the case of both Pred/PCL and Pred/PSI samples, which is in good correlation with the literature (248,249). In the case of PCL, The amount of the loaded Pred (0, 0.5, 1%) directly correlates with the specific load capacity (0.018 ± 0.004, 0.139 ± 0.004, 0.165 ± 0.012 $Nm^2 \cdot g^{-1}$), the initial modulus (0.007 ± 0.001, 0.043 ± 0.003, 0.050 ± 0.006 $Nm^2 \cdot (mm \cdot g^{-1})$), and the maximal elongation values (7.6 ± 0.3, 35.4 ± 0.9, and 44.8 ± 0.7 mm) (**Figure 22.**). Consequently, higher Pred content leads to stronger PCL meshes. In the literature some similar examples can be found for the drug-concentration-dependent changes in the mechanical properties regarding vitamin D and/or curcumin (250) or cilostazol (251) loading into PCL fibers beside the effect of chloramphenicol (252).

The significantly smaller initial modulus values of PCL-based samples compared to the PVA and PSI meshes (**Table 6.**) can be explained by the short Hookean region (initial linear ascendant period) of the mechanical curves regarding PCL-based fibers (**Figure 22.**). Compared to the PVA and PSI meshes Pred/PCL fibers reaches significantly larger elongation values (**Figure 22.**), which also can be explained by the strong interactions between the hydrophobic Pred and PCL (**KT2**).

5.2. Disintegration, solubility, and drug release of fibrous meshes

5.2.1. Disintegration of fibrous, neat PVA, PSI, and PCL polymer meshes

PVA, PSI, and PCL-based fibers take different time intervals to reach the 100% relative transparency values in PBS (**Figure 23.**). As PVA is a hydrophilic polymer, these type of meshes reaches the 100% relative transparency value in the shortest time (6 h) due to the swelling of the fibers (65). Since hydrophobic PSI can hydrolyse to hydrophilic poly(aspartic acid) (PASP) above neutral pH values (79), the rate of disintegration of these meshes is between hydrophilic PVA and totally hydrophobic PCL meshes. Since PCL it a totally hydrophobic polymer, there is no transparency change in the aqueous environment at pH 7.4 (**KT2**).

5.2.2. Solubility of fibrous PSI-DA conjugates and drug release from the fibrous conjugates (PSI-DA, PSI-Dox) and drug-loaded (Pred/PVA, Pred/PSI, Dox/PSI, Pred/PCL) fibers

Although, the main aim was to create a proper delivery system for DA in order to protect the drug from the early deactivation before filling its final role, its conjugation to polymers can alter the solubility beside other important physicochemical parameters (98,164). Based on the outcomes of our solubility results, DA-containing fibrous meshes showed time-dependent dissolution kinetics (42.3, 7.6 and 6.6% were dissolved from the DG4, DG2, and DG1 conjugates after 65 hours, respectively) (**Figure 24. A**). The difference in the dissolution of the samples with different degrees of grafting could be the consequence of the hydrolysis of the rings in free succinimide monomers, generating aspartic acid monomers. These aspartic acid monomers compose the major part of the dissolved PSI-DA DG4 fibrous conjugate. The hydrolysis of the polymer chain can be the reason for the altered tendency in the dissolutions, showing up in a

form of a sudden increase in the DA concentration after 8 h of measurement (164) (**KT2**).

Based on the previous publication of our research group about the dissolution and DA release kinetics of the powder form of PSI-DA conjugates (164), the kinetics of the DA release is mainly determined by the dissolution of the conjugates. In the case of the fibrous PSI-DA conjugates, the dissolution and the release investigations showed a completely different mechanism (**KT1**). According to our results (**Table 7.**), the amount of the released DA (DG1: 13.4%, DG2: 14.5%) is higher than the amount of the DA on the dissolved conjugates (DG1: 6.6%, DG2: 7.6%) regarding PSI-DA DG1 and PSI-DA DG2 fibrous samples. The reason for this could be found in the nanoformulation of the PSI-DA conjugates by electrospinning, which resulted in a higher specific surface area providing a faster release of DA.

In the presence of α-chymotrypsin enzyme, DA release was enhanced (DG1: 45.1%, DG2: 38.0%, DG4: 49.2%) (**Table 7.**) due to the nanoformulation accompanied by higher specific surface area. Nanosized membranes may absorb higher concentrations related to the enzyme on their surface (253), therefore the enzymatic activity around the PSI fibers can enhance in our case the release of DA (**KT1**).

Regarding the PSI-DA fibrous conjugates, the dissolution, and the kinetics of the hydrolysis of the amide bond between the DA and the polymer can be separated into two independent steps. In the previous publication of our research group (164), the hydrolysis of the amide bond was found to follow first-order kinetics and mainly occurred after the polymer conjugates were dissolved in the medium. On the contrary, the results of our investigation proved that this mechanism of the DA release kinetics regarding the fibrous form of the conjugates differs from the previously published kinetics regarding due to the higher specific surface of the fibrous conjugates (**KT1**). The dissolution of the conjugates was the limiting step of the DA-release when the conjugates were in powder form. On the contrary, the DA-release occurs from the surface of the fibrous conjugates, therefore dissolution has no significant effect on the release kinetics (164).

As it was mentioned before, in the case of Pred-loaded PVA, PCL and PSI meshes as well as Dox/PSI, and PSI-Dox conjugates, the drug release was measured at two

different pH values (7.4 and 6.5) to mimic not only the physiological but also the cancer-related environments.

In the case of Pred/PVA meshes (**Figure 26.**), the burst release of the drug can be explained by the swelling of the hydrophilic PVA fibers. Due to the drug-polymer incompatibility (69,70), relatively high percentage of the Pred may be located on the surface of the fibers, therefore these molecules do not have to overcome the diffusion from the inner fiber parts to the surface. Compared to the release at pH 7.4 (100% after 6 hours), the release at pH 6.5 is slower (86.8% after 6 hours) – the reason could be the pH-dependent swelling behaviour of PVA polymer (65), and the pH 7.45 medium can intensify the repulsive forces between Pred and PVA (254).

Considering the drug release from Pred/PSI (**Figure 26.**), Dox/PSI and PSI-Dox conjugate (**Figure 25.**) meshes, significant difference can be observed between the two investigated pH values. The difference can be explained by the hydrolysis of the PSI polymer chain to PASP at pH 7.4, which could be also observed during the disintegration measurements. The hydrolysis enhances the release of the drugs, such as in the case of PASP hydrogels (255) and in the case of Dox conjugated PSI nanomicelles and nanoaggregates (89,90,93). At pH 6.5 the drug release is mainly dependent on the diffusion of the drugs from the inner parts of the fibers to the surface of the fibers, which results in a more prolonged release profile.

By comparing Dox/PSI and PSI-Dox nanofibers (**Figure 25.**), the release is noticeably slower in the case of PSI-Dox conjugates (PSI-Dox: 13.18%, and 30.67%, while Dox/PSI: 23.15%, and 87.53% after 200 hours at pH 6.5 and 7.4, respectively) due to the chemical bond between the drug and the polymer in this case. During the release of the drug, first the amide bond should be hydrolysed between the drug and the polymer, and this could be the limiting step (164).

Regarding Pred/PCL fibers (**Figure 26.**), there is no significant difference between the release a different environmental pH values, since PCL has no functional groups that can be influenced by the pH (239). Consequently, PCL have no degradation products in aqueous environment hence it cannot induce acidosis (241). The initial burst release can refer to desorption of Pred molecules from the surface of PCL fibers (244), while in the case of the linear part of the controlled release, diffusion and permeation processes can

dominate. Similar release kinetics were observed in the case of doxycycline (241), α-lactalbumine (204), acyclovir (249) and 20(S)-protopanayadiol-loaded (244) PCL fibers.

5.3. *In vitro* experiments

5.3.1. Presence of D1 and D2 DA receptors on PDLSCs and SH-SY5Y cells

Due to the fact that the SH-SY5Y cell line consisting of neuroblastoma cells, and it has concentration-dependent viability regarding DA, the relevance to test them in connection with PSI-DA conjugates is proved by the literature (256,257). According to our investigations, we could confirm that undifferentiated SH-SY5Y cells owe DA receptors. However, in the case of PDLSC, there was no available information in the literature regarding the presence of DA receptors before our study. Our immunofluorescence labeling analysis (**Figure 27.**) reveals that PDLSCs also express D1 and D2 dopamine receptors. These outcomes can be in connection with the neurogenic differentiation capacity of this stem cell type (258). Due to having DA receptors, PDLSCs are able to provide a suitable and healthy cell model for the investigation of the effect of DA (**KT1**).

According to the immunofluorescence labeling analysis of DA receptors, the SH-SY5Y neuroblastoma cell line along with PDLSCs may possess DA transporters that can mediate DA uptake (259).

5.3.2. Effect of DA, Dox, and Pred on cell viability and cell morphology

According to our cell viability results (**Figure 28**.), the SH-SY5Y cells can tolerate higher DA concentrations (200 µM) than PDLSCs (100 µM), which could be explained by the higher number of DA receptors or supposedly DA transporters (259) due to its neural origin. Consequently, the ability of SH-SY5Y cells to uptake DA could be higher than their capacity to store it in vesicles, therefore the concentration dependent DA effect could be different compared to PDLSCs (**KT1**).

Concerning the cytotoxic concentration of DA, Haque and co-workers found that 184 µM DA reduces the number of the viable SH-SY5Y cells by 50% by the end of a 24 hour-long treatment (172), while in other studies 50 µM (177), 500 µM (178), and 600 µM (260) concentrations related to DA also caused similarly decreased SH-SY5Y cell viability (177,178,260). According to our results, 200 µM free DA did not prove to be

cytotoxic, when applied for 24 hours, but this concentration induced cell death after 72 hours. In contrast, if DA was conjugated to PSI (PSI-DA-AE 1:2), it proved to be cytotoxic for SH-SY5Y cells neither at 200 μM concentration after 72 hours (**Figure 28.**). The different effects between the conjugated form of DA and the free DA on both cell types can be explained by the prolonged release of DA (164) from the conjugates, which provides less available free DA for the cells in the culturing medium. In addition, the conjugation of DA to the PSI prevents its degradation and the formation of oxidative quinones, which could express negative effects on the cell viability (172).

Regarding the morphology of the undifferentiated SH-SY5Y cells, the individual cells owe short neurites and generally grow in clumps (164,256), while PDLSCs have elongated shape long projections and with several connections between the cells. This normal morphology can be seen on the phase contrast images related to the control groups (**Figure 28.**) and the cell cultures treated with low-concentration DA or PSI-DA-AE 1:2 conjugate. The cells treated with high concentration related to DA undergo autophagy according to the literature (260) – in line with our results where floating dead cells can be observed, which could be the consequence of autophagy but definitely indicate moribund cells.

To investigate the effect of different concentrations of Dox and Pred on cell viability, MDA-MB-231 breast cancer cell line was used as a model (261). We observed concentration-dependent effect of Dox in decreasing cell viability (**Figure 29.**), which is in good correlation with the literature regarding the IC50 values as well (between 0.5 and 1 μM) (193,262–264).

In general, Dox – such as DA – can force the cells to apoptosis, through regulating the expression of genes related to caspase enzymes. Similarly to DA, Dox can also trigger oxidative damage, but the main mechanism behind its cytotoxic effect is the intercalation ability between DNA helixes generating free radicals, and ruptured DNA (265).

Pred was applied because of its potential anti-inflammatory ability but the non-cytotoxic effect regarding MDA-MB-231 cells in a concentration range between 0-400 μM was revealed, which is in good correlation with the literature (215).

5.3.3. Cytotoxicity of neat, DA-, Dox-containing fibrous meshes

We demonstrated that none of the neat PVA, PSI, and PCL meshes exerted cytotoxic effect on MDA-MB-231 cells (**Figure 30.**). Moreover, PSI did not prove to be cytotoxic regarding PDLSCs and SH-SY5Y cells (**Figure 31.**) although this type of neat polymer slightly lowered the cell viability after 72 hours of treatment. A feasible explanation could be the hydrolysis of PSI, which sightly shifts the pH of the culturing medium to the acidic range. According to our results and the literature (44,75,107), these fibrous polymers are promising basis for implantable drug-delivery systems.

By applying PSI-DA and PSI-Dox fibrous conjugates, the concentration of the free DA and Dox concentration available for the cells in the culturing medium remains lower than the revealed cytotoxic concentration based on the cell viability results, due to the prolonged drug release (**Figure 28.** and **29.**) (164) (**KT1**). Therefore, the fibrous samples can be applied in higher concentrations related to the drugs then the free forms. Although a decisive amount of the fibrous conjugate samples is dissolved by the end of the 72 hour-long treatment, there still could be remaining drug attached to the polymer chains, which soes not influence cell viability remarkably (**KT1**).

The different tendencies in cell viability of PDLSCs and the SH-SY5Y cell line after treatments with different PSI-DA conjugates (**Figure 31.**) could be explained by the different sources of these cells. Since SH-SY5Y neuroblastoma cells are practically premature neurons, they may express more DA receptors and more DA transporters, which pump DA from the culturing medium back into cytosol or isolate the DA into vesicles for storage and they release it later (173). Nevertheless, PDLSCs could be more sensitive to the presence of DA, due to their ectomesenchymal origin (258,266). The hypothesis is that the PDLSCs may not have enough DA transporter to regulate the uptake and the efflux of DA, therefore less free DA can be harmful for this cell type after 72 hours compared to SH-SY5Y cells. Due to our cell viability and cytotoxicity results (**Figure 28.** and **31.**), the proper distinct amount of DA can even exert a positive effect on cell proliferation (**KT1**).

In the case of PSI-DA DG4 fibrous conjugates, the DA release is the fastest compared to the other conjugates (**Figure 24.**), so regarding SH-SY5Y cells treated with this type of fibrous conjugates, the level of free DA is supposed to be too low after 72 h to promote cell growth. In contrast, in the case of PDLSCs this adequate free DA

concentration can enhance cell proliferation, as these cells are more sensitive to the free DA according to the concentration-dependent cell viability results (**KT1**). In the phase-microscopic and two-photon microscopic images a decisive number of connections can be observed between the adhered cells with normal morphology regarding both PDLSCs and SH-SY5Y cells, which can be the consequence of the proper DA concentration (**Figure 31.**).

Regarding PSI-Dox fibrous conjugates, the same tendency can be observed compared to the treatment with free Dox as we have seen at PSI-DA vs. DA (**Figure 31.**) (**KT1**): due to the prolonged Dox release, the available amount of free Dox is less in the case of the conjugate, in this way more Dox can be introduced to the cells without cytotoxic effect (**Figure 32.**). The difference between Dox/PSI and PSI-Dox samples can be also explained by the different release kinetics. By loading Dox into PSI fibers, the release is faster compared to PSI-DA conjugates where Dox is chemically bound (**Figure 25.**). Therefore Dox/PSI samples are proved to be more cytotoxic than the PSI-Dox conjugate (164) (**KT2**).

It is important to mention that Dox can be conjugated to PSI polymer not only by the primer amine groups, but there are also different linkers presented in the literature (90,93). Regarding the pH sensitive linker-based nanoparticle conjugates (89,90,93), as high cytotoxic effect can be observed as in the case of free Dox, which can be explained by the different cellular internalization methods and the different drug release kinetics of nanoparticles compared to the nanofibrous Dox-containing meshes.

5.3.4. Cell-internalization of PSI-DA and PSI-Dox conjugates

In general, small free drug molecules such as Dox, can be internalized by the cells via plasma membrane diffusion (90,267) or such as DA, by transporter-mediated uptake (268). On the other hand, polymer-drug conjugates can be internalized by cells via different types of endocytosis, namely: fluid-phase-, adsorptive-, and receptor-mediated endocytosis. During fluid-phase endocytosis, there is no interaction between the conjugates and the cell surface. On the contrary, in the case of adsorptive endocytosis, there is a nonspecific binding of hydrophobic moieties or positive charges of the drug with the plasma membrane (267).

Regarding the cellular internalization of PSI-DA conjugates, the fluorescent BCB stain (269) was also conjugated to the PSI chain (**Figure 12.**) in a relatively small amount, hence the conjugates can be followed by confocal microscopy and flow cytometry. Although in high doses, BCB could have a cytotoxic effect (270,271), the molecule contains primer amino group, therefore it can be easily conjugated to the PSI main chain with a cost-effective nucleophilic addition process (78). In the case of PSI-Dox conjugates, there was no need to further conjugate a fluorescent stain, due to the fact that Dox itself can provide fluorescent signal (196).

The confocal microscopy results (**Figure 33. A** and **Figure 34. A**) do not confirm clearly the endosomal drug-delivery of the conjugates (267). In the case of PSI-DA conjugates, a homogeneously distributed fluorescent sign can be seen in the cytoplasm instead of well-separated signs by the individual endosomes. Based on these observations, we could assume that the conjugates are able to escape from the endosomes due to the hydrolyzation of the polymer chain, which leads to a membrane destabilization process in the case of the endosomes (272). Regarding PSI-Dox conjugates, the weak fluorescence signal of the untreated control cells and neat PSI treated cells stands for the background signal from the autofluorescence of different proteins. The more intense signal from the cytoplasm regarding Dox and PSI-Dox treated cells compared to the control can be a consequence of the higher cellular internalization. It is important to mention that the significant difference in the intracellular distribution of the fluorescent signal regarding Dox and PSI-Dox can be the consequence of that the free Dox can be internalized by simple passive diffusion (90) and in free form it can also reach the cell nuclei (265). In the case of PSI-Dox, the brighter dots in the cytoplasm may refer to the endosomal presence of the conjugates (**Figure 34. A**).

The afore mentioned lower cytotoxic effect of PSI-Dox conjugates compared to free Dox can also be explained by this observation: PSI-Dox conjugates are not able to reach the cell nuclei (**KT2**).

Our flow cytometry analysis (**Figure 33.**) confirmed the cellular uptake of both PSI-DA and PSI-Dox conjugates. In the case of PSI-DA conjugates, the examined cells gave extra fluorescent signal thanks to the BCB conjugation. Regarding PSI-Dox conjugates, these results underline the cytotoxicity results: although the cellular uptake of PSI-Dox

was significantly higher compared to the uptake of free Dox, decisive amount of Dox remains conjugated to the polymer chain even after the uptake. Consequently, Dox is not able to exert the cytotoxic effect in this case because the PSI can protect and keep the drug in inactive form.

According to our results (**Figure 33.**) and the literature (14,142), the uptake in the case of PSI-DA conjugates could be strongly related to the presence and the number of different DA receptors and transporters on the examined cells, therefore the uptake of the conjugates could be more complex than fluid-phase endocytosis. Due to the presence of DA receptors on PDLSCs and SH-SY5Y cells, PSI-DA conjugates are supposedly taken up via receptor-mediated endocytosis, which is based on cell-specific targeting moieties, which role could be played by DA. These results are in good correlation with the literature in connection with DA and receptor-mediated endocytosis. For example, Y. Liu et al. concluded that the uptake of polyethylene glycol nanoparticles by D2 receptor-rich Kupffer cells was enhanced by using polydopamine coating (273). This theory about the mechanism of receptor-mediated endocytosis related to PSI-DA conjugates can also confirm the viability difference between the investigated cell types due to the different DA receptor or DA transporter content. According to these findings, the role of DA may not only be the drug but the targeting agent as well.

Regarding Dox, several kinds of nanomicelle and nanoaggregate-based carriers built on PSI and its derivatives have already been described (89,91,195,196). Amongst these drug-delivery systems, the number of such systems are small in which Dox was conjugated to the PSI chain (90,93). In addition, the internalization and the intracellular distribution of these systems was similar to our PSI-Dox conjugates. However, after a certain time, Dox could appear in the nucleus (90,195), which can be explained by the faster drug release in the case of these nanocarriers compared to our fibrous PSI-Dox conjugates. However, it is important to mention that this prolonged release can be crucial for the application of the meshes as an implantable drug cargo.

5.3.5. Production of cytokines by MDA-MB-231 cells treated with neat and Pred-loaded meshes

Since none of the neat PVA, PSI, PCL meshes and Pred reduced viability of MDA-MB-231 cells (**Figure 29. CD** and **30.**), the potential anti-inflammatory effect of Pred (0-400

µM) and Pred-loaded PVA, PSI, and PCL meshes (400 µM), beside the neat fibers was investigated by measuring the level of 13 cytokines produced by MDA-MB-231 cells (**Figure 35.**).

Almost all cell types secrete cytokines when the immune system is activated. These small proteins can be divided into pro-inflammatory and anti-inflammatory cytokines according to their mechanism: whether they activate the immune cells (pro) or inhibit the inflammation process (anti) (274). Amongst the investigated cytokines, the following interleukines (ILs): IL-1β, IL-18, and IL-33 and monocyte chemoattractant protein (MCP-1) are members of the pro-inflammatory group, while IL-6 and IL-10 belong to anti-inflammatory cytokines (274).

The secretion of all the above-mentioned cytokines was demonstrated also by other groups in the case of MDA-MB-231 cells (275,276), the only exception is IL-33, therefore its production can be considered as our new results regarding the control (untreated) MDA-MB-231 cells.

Although the effect of Pred on cytokine secretion regarding MDA-MB-231 cells has not been investigated yet, the level of IL-10 and IL-33 was found to be reduced by Pred in the nasal mucus of patients (277). However, other types of glucocorticoids were tested related to cancer cells regarding cytokine production. Our results (**Figure 35.**) are in a good correlation with these papers: in general glucocorticoids inhibit the gene expression of several pro-inflammatory interleukins namely: IL-1β, IL-6, IL-10, IL-18, and MCP-1 (215). According to our results, Pred exerts decreasing effect on the cytokine level produced by MDA-MB-231 breast cancer cells (the relative cytokine level after the incubation with 400 µM Pred was 49.2, 56.8, 68.0, 81.5, 63.9, 55.6% regarding IL-1β, IL-6, IL-10, IL-18, IL-33, MCP-1, respectively.). Therefore, the relevance of loading Pred – as an anti-inflammatory agent – into Dox-containing implantable meshes to support the cancer therapy is proved (**KT2**).

The controversial results regarding neat PSI (decreased cytokine levels were measured: 55, 91, 73, 69, 69, 56% regarding IL-1β, IL-6, IL-10, IL-18, IL-33, MCP-1, respectively) (**Figure 35.**) can be explained by its hydrolyzation to PASP form, which is followed with a slight decrease in the pH of the cell culturing medium, negatively affecting cell proliferation (278). Although regarding peripheral blood mononuclear cells, the anti-inflammation effect of PCL-based nanoparticles was demonstrated (279),

the slightly decreased level of cytokines related to PCL in our case (decreased cytokine levels were measured: 46, 56, 56, 65, 65% regarding IL-1β, IL-6, IL-10, IL-18, MCP-1, respectively) can be rather the consequence of potential adsorption. Since PCL fibers have totally hydrophobic characteristic, the small proteins such as cytokines can be absorbed to the fiber surface, hence less cytokines can be determined in the supernatant (253). As PSI is also a hydrophobic polymer, the same process may occur during the treatment with PSI-based fibrous systems. The different cytokine levels triggered by the different kinds of Pred-loaded polymer samples can be explained by the unique drug release profiles of the different meshes (**Figure 26.**), which entail the different amount of released Pred after a certain time period. In conclusion, by applying different polymers, different kinetics of prolonged Pred release can be obtained according to the requirements and the therapeutic purpose (**KT2**).

6. Conclusions

The main outcomes of my thesis are the following:

1. I successfully created dopamine (DA)-conjugated polysuccinimide (PSI-DA) fibers with different degrees of grafting (DG: 1, 2, 4) by electrospinning. The increasing amount of DA on the polymer chain leads to thinner fibers (average diameters are 613 ± 172 nm, 179 ± 27 nm, and 78 ± 15 nm for DG4, DG2 and DG1, respectively) with lower specific load capacity (0.039 ± 0.008 $Nm^2 \cdot g^{-1}$, 0.022 ± 0.007 $Nm^2 \cdot g^{-1}$, and 0.010 ± 0.005 $Nm^2 \cdot g^{-1}$ for DG4, DG2 and DG1 respectively). However, the initial modulus of the meshes is independent of the DA content and it is between 0.3 and 0.5 $N \cdot mm^{-1}$ for all the PSI-DA conjugates (**KT1**).

2. The solubility of the hydrophobic neat PSI increased significantly by the catechol side chain of DA: 42.3, 7.6 and 6.6% were dissolved from the DG4, DG2, and DG1 conjugates, respectively. The hydrolysis of free succinimide rings in the case of the PSI-DA DG4 generates a sudden increase in the concentration of dissolved conjugates after 8 h. PSI-DA conjugates provide prolonged drug release in PBS solution and the DG4 conjugate released more DA within 65 h (20.5%) than DG2 (14.5%) or DG1 conjugates (13.4%). The kinetic analysis confirmed that the release of DA occurs from the solid surface of the fibers and not from the dissolved conjugates. The DA release was significantly higher in the presence of the α-chymotrypsin enzyme, reaching 49.2%, 38.0%, and 45.1% after 65 h regarding DG4, DG2, and DG1 conjugates, respectively than in PBS without enzymes (**KT1**).

3. The PSI-DA-AE 1:2 conjugate can be applied in higher DA concentrations without toxic effect compared to free DA on periodontal ligament stem cells (PDLSCs) and SH-SY5Y neuroblastoma cell line. A treatment with 200 µM DA for 72 h eliminates all the PDLSCs and prevents the growth of SH-SY5Y cells. However, PSI-DA-AE 1:2 conjugates with 200 µM DA-content are not toxic for PDLSCs and enable proliferation of SH-SY5Y cells. Moreover, both PDLSCs and SH-SY5Y cells capable to proliferate for 24 h to 72 h in the presence of fibrous PSI-DA conjugates with 300 µM DA-content. I demonstrated by immunofluorescence labeling that the PDLSCs possess D1R and D2R dopamine

receptors. The flow cytometric and confocal microscopic studies proved that the PSI-DA conjugates can be internalized by both PDLSCs and SH-SY5Y cells (**KT1**).

4. Incorporation of prednisone (Pred) into PSI or ε-polycaprolactone (PCL) do not affect notably fiber diameter, it is 420-460 nm for PSI, while 540-610 nm for PCL regarding both neat and Pred-containing meshes. In the case of poly(vinyl alcohol) (PVA), the average fiber diameter is directly proportional to the Pred amount: 157 ± 61 (neat), 212 ± 56 (0.5% Pred), and 497 ± 117 nm (1% Pred). Higher Pred content leads to lower specific load capacity (0.151 ± 0.006, 0.164 ± 0.009, and 0.081 ± 0.005 $Nm^2 \cdot g^{-1}$ for 0, 0.5, and 1% Pred-content, respectively), initial modulus (2.794 ± 0.339, 1.972 ± 0.212, and 0.650 ± 0.104 $Nm^2 \cdot (mm \cdot g^{-1})$ for PVA with 0, 0.5, and 1% Pred-content respectively), and maximal elongation (7.8 ± 0.7, 3.8 ± 0.2, and 2.6 ± 0.2 mm for PVA with 0, 0.5, and 1% Pred-content respectively) of PVA fibers. In the case of PSI, the specific load capacity is decreasing (0.233 ± 0.009, 0.126 ± 0.005, 0.136 ± 0.009 $Nm^2 \cdot g^{-1}$) but the initial modulus is increasing (0.701 ± 0.0019, 1.680 ± 0.099, 2.373 ± 0.27 $Nm^2 \cdot (mm \cdot g^{-1})$) with the increasing Pred content (0, 0.5, 1%). Regarding PCL, the amount of the loaded Pred (0, 0.5, 1%) directly correlates with the specific load capacity (0.018 ± 0.004, 0.139 ± 0.004, 0.165 ± 0.012 $Nm^2 \cdot g^{-1}$), the initial modulus (0.007 ± 0.001, 0.043 ± 0.003, 0.050 ± 0.006 $Nm^2 \cdot (mm \cdot g^{-1})$), and the maximal elongation (7.6 ± 0.3, 35.4 ± 0.9, 44.8 ± 0.7 mm). The hydrophilic PVA provides burst release of Pred, while hydrophobic PSI and PCL show more prolonged release. At pH 7.4, the Pred release is faster from PVA and PSI (after 6 h 100% for PVA and 27.4% for PSI) than at pH 6.5 (after 6 h 86.8% for PVA and 15.3% for PSI) but in the case of PCL such difference is not remarkable. Pred reduces the level of 6 cytokines (IL-1β, IL-6, IL-10, IL-18, IL-33, MCP-1) produced by MDA-MB-231 breast cancer cells, justifying its relevance as an anti-inflammatory agent in a potential implantable nanofibrous mesh. (The relative cytokine level after incubation with 400 µM Pred is 49.2, 56.8, 68.0, 81.5, 63.9, 55.6% respectively.) (**KT2**).

5. I successfully conjugated PSI with doxorubicin (Dox) and fabricated nanofibers by electrospinning from this conjugate (PSI-Dox) and from Dox-loaded PSI

fibers (Dox/PSI). In the case of PSI-Dox, the chemical bond between the drug and the polymer provides noticeably slower release of Dox (reaching only 13.18%, and 30.67% after 200 h at pH 6.5 and 7.4, respectively) compared to Dox/PSI (reaching 23.15%, and 87.53% after 200 h at pH 6.5 and 7.4, respectively). In both cases, the release is faster and more complete at pH 7.4 compared to pH 6.5 due to the hydrolysis of PSI. The fibrous PSI-Dox conjugate mesh is less cytotoxic (the relative cell viability is 111% and 254% after 24 and 72 h, respectively) for the MDA-MB-231 breast cancer cell line compared to Dox/PSI (the relative cell viability is 68% and 23% after 24, and 72 h, respectively) because of the prolonged drug release and the different cellular uptake. Although PSI enhances the internalization of Dox by the MDA-MB-231 cells, significantly less drug can enter the cell nuclei, therefore the conjugated Dox is not able to exert strong cytotoxic effect (**KT2**).

7. Summary

Functionalized biocompatible electrospun nanofibrous systems can be promising candidates for pharmaceutical applications as drug-delivery systems due to the high specific surface and the amorphous structure, which leads to higher bioavailability of the drug. Moreover, the early deactivation, degradation, and fast clearance from circulation can also be avoided by the conjugation of drugs onto polymers.

The aim of this work was to create dopamine (DA)-, prednisone (Pred)-, and doxorubicin (Dox)-containing fibrous drug-loaded and drug-conjugated biocompatible polymer-based drug-delivery systems by electrospinning for different biomedical purposes, and to characterize them physiochemically, mechanically, and biologically.

The chemical composition and structure of the drug-delivery systems were investigated by FT-IR, NMR, and XRD measurements, morphology of the fibers was observed by SEM and the mechanical performance was also studied. The drug release was examined under normal physiological conditions while the *in vitro* investigations (cytotoxicity, internalization) were carried out on human periodontal ligament stem cells (PDLSCs), SH-SY5Y neuroblastoma cells, and MDA-MB-231 triple-negative breast cancer.

The presence of different drugs can influence the fiber diameter and the mechanical performance as well, but this effect can be controversial according to the physicochemical features of the drugs and the polymers. By loading or conjugating hydrophobic drugs into polymers with different polarities, the drug release can be tailored. In the case of drug loading into hydrophilic PVA, a burst release can be provoked, while applying hydrophobic PSI or PCL, the release is more prolonged. By conjugating DA or Dox to the PSI polymer chain, more prolonged drug release can be achieved compared to the drug loading and the drug can be tolerated in higher concentrations by the cells. The confocal microscopy analysis in line with the flow cytometry proves the enhanced cellular internalization of the conjugates and the immunofluorescence labeling analysis confirm the presence of DA receptors (D1R, D2R) on both PDLSC and SH-SY5Y cells.

According to the outcomes, by applying biocompatible polymers with different polarities, the release and the bioavailability of the introduced drug can be precisely tailored for a prolonged local therapy based on implanting nanofibrous drug delivery systems.

8. Összefoglalás

Az elektrosztatikus szálképzéssel előállított, biokompatibilis polimer alapú hatóanyag-hordozó rendszerek nagy fajlagos felületüknek és a hatóanyag emelkedett biohasznosulásához vezető amorf kristályszerkezetüknek köszönhetően ígéretes jelöltek lehetnek különböző gyógyszeres terápiák esetén. A hatóanyag polimerhez történő konjugálásával elkerülhető a hatóanyag inaktiválódása a funkciójának betöltése előtt, valamint degradációja és gyors kiürülése a szervezetből.

Célom dopamin-, prednizon-, és doxorubicin-tartalmú nanoszálas, hatóanyaggal töltött és konjugált biokompatibilis polimer-alapú hatóanyag-hordozó rendszerek előállítása elektrosztatikus szálképzéssel, ill. fizikokémiai, mechanikai és biológiai karakterizálásuk.

A kémiai szerkezetvizsgálat FT-IR, NMR, és XRD módszerek segítségével történt, míg a szálas struktúrák morfológiáját SEM mikroszkóppal, mechanikai tulajdonságait egyirányú elmozdulás kontrollált húzást biztosító készülékkel vizsgáltuk. A hatóanyag felszabadulásának vizsgálata normál fiziológiai körülmények között történt, az *in vitro* kísérletek során pedig humán foggyökérhártya eredetű őssejtek (PDLSC), SH-SY5Y neuroblasztóma- és MDA-MB-231 emlőtumor sejtvonalakat használtunk.

A hatóanyagok jelenléte eltérően befolyásolja az átlagos szálátmérőt és a mechanikai tulajdonságokat a hatóanyag és a polimer fizikokémiai tulajdonságaitól függően. Hidrofób jellegű hatóanyagok töltése vagy konjugálása különböző polaritással rendelkező polimerek esetén eltérő profilú hatóanyag-felszabadulást biztosít. A hidrofil PVA esetén egy kezdetben pillanatszerű, majd gyors hatóanyag felszabadulás érhető el, míg a hidrofób PSI és PCL esetében a felszabadulás ehhez képest jelentősen elnyújtott.

A konfokális mikroszkóppal készült felvételek és az áramlási citometria vizsgálatok bizonyítják a konjugátumok megnövekedett mértékű internalizációját a hatóanyag szabad formájához képest, továbbá az immuncitokémiai analízis igazolja a D1 és D2 dopamin receptorok jelenlétét a PDLSC és SH-SY5Y sejtek felszínén.

A fentebb bemutatott eredmények alapján a különböző polaritással rendelkező polimerekből előállított komplex nanoszálas hatóanyag hordozó rendszerek a jövőben alkalmasak lehetnek klinikai terápia során lokálisan kifejtve hatásukat, ugyanis alkalmazásukkal a hatóanyag felszabadulása és a biohasznosulása megfelelően szabályozható.

9. References

1. Chow, Dominic; Nunalee, Michelle; Lim, Dong Woo; J. Simnick, Andrew; Chilkoti A. Peptide-based Biopolymers in Biomedicine and Biotechnology. Mater Sci Eng. 2008;62:125–155. doi: 10.1016/j.mser.2008.04.004.

2. Sindhu KA, Prasanth R, Thakur VK. Medical Applications of Cellulose and its Derivatives: Present and Future. Nanocellulose Polym Nanocomposites Fundam Appl. 2014;9781118871:437–477. doi: 10.1002/9781118872246.ch16.

3. Rakes K M, Ajit B, Abu Bakar M. Pectin based formulations for biomedical applications: A review. Asian J Pharm Clin Res. 2012;5:1–7. doi: 10.1002/9781118301234.ch1

4. Jaipan P, Nguyen A, Narayan RJ. Gelatin-based hydrogels for biomedical applications. MRS Commun. 2017;7:416–426. doi: 10.1557/mrc.2017.92.

5. Parenteau-Bareil R, Gauvin R, Berthod F. Collagen-based biomaterials for tissue engineering applications. Materials (Basel). 2010;3:1863–1887. doi: 10.3390/ma3031863.

6. Kim S, Moon MJ, Surendran SP, Jeong YY. Biomedical applications of hyaluronic acid-based nanomaterials in hyperthermic cancer therapy. Pharmaceutics. 2019;11:1–19. doi: 10.3390/pharmaceutics11070306.

7. Janmey PA, Winer JP, Weisel JW. Fibrin gels and their clinical and bioengineering applications. J R Soc Interface. 2009;6:1–10. doi: 10.1098/rsif.2008.0327.

8. Tawakkal ISMA, Cran MJ, Miltz J, Bigger SW. A review of poly(lactic acid)-based materials for antimicrobial packaging. J Food Sci. 2014;79. doi: 10.1111/1750-3841.12534.

9. Petri DFS. Xanthan gum: A versatile biopolymer for biomedical and technological applications. J Appl Polym Sci. 2015;132. doi: 10.1002/app.42035.

10. Vert M. Biopolymers and Artificial Biopolymers in Biomedical Applications, an Overview. Biorelated Polym. 2001;63–79. doi: 10.1007/978-1-4757-3374-7_6.

11. Cholkar K, Acharya G, Trinh HM, Singh G. Therapeutic Applications of Polymeric Materials. Emerg. Nanotechnologies Diagnostics, Drug Deliv. Med. Devices. Elsevier; 2017. doi: 10.1016/B978-0-323-42978-8.00001-2.

12. Viswanathan P, Muralidaran Y, Ragavan G. Challenges in oral drug delivery: A

nano-based strategy to overcome. Nanostructures Oral Med. Elsevier Inc.; 2017. doi: 10.1016/B978-0-323-47720-8/00008-0.

13.   Duncan R. Polymer conjugates as anticancer nanomedicines. Nat Rev Cancer. 2006;6:688–701. doi: 10.1038/nrc1958.

14.   Khandare J, Minko T. Polymer-drug conjugates: Progress in polymeric prodrugs. Prog Polym Sci. 2006;31:359–397. doi: 10.1016/j.progpolymsci.2005.09.004.

15.   L Zhang, FX Gu, JM Chan, AZ Wang RL and OF. Therapeutic, Nanoparticles in Medicine: Applications and Developments. Educ Policy Anal Arch. 2007;8:761–769. doi: 10.1038/sj.clp.

16.   Xu H, Yao Q, Cai C, Gou J, Zhang Y, Zhong H, Tang X. Amphiphilic poly(amino acid) based micelles applied to drug delivery: The in vitro and in vivo challenges and the corresponding potential strategies. J Control Release. 2015;199:84–97. doi: 10.1016/j.jconrel.2014.12.012.

17.   Lelle M, Kaloyanova S, Freidel C, Theodoropoulou M, Musheev M, Niehrs C, Stalla G, Peneva K. Octreotide-Mediated Tumor-Targeted Drug Delivery via a Cleavable Doxorubicin-Peptide Conjugate. Mol Pharm. 2015;12:4290–4300. doi: 10.1021/acs.molpharmaceut.5b00487.

18.   Sun H, Meng F, Dias AA, Hendriks M, Feijen J, Zhong Z. α-Amino acid containing degradable polymers as functional biomaterials: Rational design, synthetic pathway, and biomedical applications. Biomacromolecules. 2011;12:1937–1955. doi: 10.1021/bm200043u.

19.   Paz-Ares L, Ross H, O'Brien M, Riviere A, Gatzemeier U, Von Pawel J, Kaukel E, Freitag L, Digel W, Bischoff H, Garcya-Campelo R, Iannotti N, Reiterer P, Bover I, Prendiville J, Eisenfeld AJ, Oldham FB, Bandstra B, Siger JW, Bonomi P. Phase III trial comparing paclitaxel poliglumex vs docetaxel in the second-line treatment of non-small-cell lung cancer. Br J Cancer. 2008;98:1608–1613. doi: 10.1038/sj.bjc.6604372.

20.   Hudecz F. Polimer terapeutikumok. Magy Tudomány. 1998;1–10.

21.   Schiffman JD, Schauer CL. A review: Electrospinning of biopolymer nanofibers and their applications. Polym Rev. 2008;48:317–352. doi: 10.1080/15583720802022182.

22.   Doostmohammadi M, Forootanfar H, Ramakrishna S. Regenerative medicine and

drug delivery: Progress via electrospun biomaterials. Mater Sci Eng C. 2020;109:110521. doi: 10.1016/j.msec.2019.110521.

23. Formhals A. Process and apparatus for preparing artificial threads. 1934.

24. Formhals A. Method of Producing Artificial Fibers. 1939.

25. Formhals A. Method and Apparatus for Spinning. 1944.

26. Fang X, Reneker DH. DNA fibers by electrospinning. J Macromol Sci Part B Phys. 1997;32:169–173. doi: 10.1080/00222348.2014.928156.

27. Agarwal S, Wendorff JH, Greiner A. Use of electrospinning technique for biomedical applications. Polymer (Guildf). 2008;49:5603–5621. doi: 10.1016/j.polymer.2008.09.014.

28. Ahmed J, Gultekinoglu M, Edirisinghe M. Bacterial cellulose micro-nano fibres for wound healing applications. Biotechnol Adv. 2020;107549. doi: 10.1016/j.biotechadv.2020.107549.

29. Tao F, Cheng Y, Shi X, Zheng H, Du Y, Xiang W, Deng H. Applications of chitin and chitosan nanofibers in bone regenerative engineering. Carbohydr Polym. 2020;230:115658. doi: 10.1016/j.carbpol.2019.115658.

30. Augustine R, Rehman SRU, Ahmed R, Zahid AA, Sharifi M, Falahati M, Hasan A. Electrospun chitosan membranes containing bioactive and therapeutic agents for enhanced wound healing. Int J Biol Macromol. 2020;156:153–170. doi: 10.1016/j.ijbiomac.2020.03.207.

31. Mokhena TC, Mochane MJ, Mtibe A, John MJ, Sadiku ER, Sefadi JS. Electrospun alginate nanofibers toward various applications: A review. Materials (Basel). 2020;13:1–24. doi: 10.3390/ma13040934.

32. Brenner EK, Schiffman JD, Thompson EA, Toth LJ, Schauer CL. Electrospinning of hyaluronic acid nanofibers from aqueous ammonium solutions. Carbohydr Polym. 2012;87:926–929. doi: 10.1016/j.carbpol.2011.07.033.

33. Jiang H, Fang D, Hsiao BS, Chu B, Chen W. Optimization and characterization of dextran membranes prepared by electrospinning. Biomacromolecules. 2004;5:326–333. doi: 10.1021/bm034345w.

34. Lu WP, Guo Y. Electrospinning of Collagen and Its Derivatives for Biomedical Applications. Nov Asp Nanofibers. IntechOpen Limited, London, 2018, Chapter

3. doi: 10.5772/intechopen.73581.

35. Maleknia L, Rezazadeh Majdi Z. Electrospinning of gelatin nanofiber for biomedical application. Orient J Chem. 2014;30:2043–2048. doi: 10.13005/ojc/300470.

36. Sasithorn N, Martinová L, Horáková J, Mongkholrattanasit R. Fabrication of Silk Fibroin Nanofibres by Needleless Electrospinning. Electrospinning - Mater Tech Biomed Appl., IntechOpen Limited, London, 2016; Chapter 5. doi: 10.5772/65835.

37. Hadjiargyrou M. Incorporation of DNA into Electrospun Nanofibrous Scaffolds: Fundamental Characterization Studies and Gene Delivery. Nanofibers - Prod Prop Funct Appl. IntechOpen Limited, London, 2011; Chapter 18. doi: 10.5772/23504.

38. Sasikala ARK, Unnithan AR, Yun YH, Park CH, Kim CS. An implantable smart magnetic nanofiber device for endoscopic hyperthermia treatment and tumor-triggered controlled drug release. Acta Biomater. 2016;31:122–133. doi: 10.1016/j.actbio.2015.12.015.

39. Parwe SP, Chaudhari PN, Mohite KK, Selukar BS, Nande SS, Garnaik B. Synthesis of ciprofloxacin-conjugated poly (L-lactic acid) polymer for nanofiber fabrication and antibacterial evaluation. Int J Nanomedicine. 2014;9:1463–1477. doi: 10.2147/IJN.S54971.

40. Pitarresi G, Fiorica C, Palumbo FS, Calascibetta F, Giammona G. Polyaspartamide-polylactide electrospun scaffolds for potential topical release of Ibuprofen. J Biomed Mater Res - Part A. 2012;100 A:1565–1572. doi: 10.1002/jbm.a.34095.

41. Jalvandi J, White M, Gao Y, Truong YB, Padhye R, Kyratzis IL. Polyvinyl alcohol composite nanofibres containing conjugated levofloxacin-chitosan for controlled drug release. Mater Sci Eng C. 2017;73:440–446. doi: 10.1016/j.msec.2016.12.112.

42. Ye L, Wu X, Duan HY, Geng X, Chen B, Gu YQ, Zhang AY, Zhang J, Feng ZG. The in vitro and in vivo biocompatibility evaluation of heparin-poly(ε-caprolactone) conjugate for vascular tissue engineering scaffolds. J Biomed Mater Res - Part A. 2012;100 A:3251–3258. doi: 10.1002/jbm.a.34270.

43. Oh GW, Ko SC, Je JY, Kim YM, Oh JH, Jung WK. Fabrication, characterization and determination of biological activities of poly(ε-caprolactone)/chitosan-caffeic acid composite fibrous mat for wound dressing application. Int J Biol Macromol. 2016;93:1549–1558. doi: 10.1016/j.ijbiomac.2016.06.065.

44. Aslam M, Kalyar MA, Raza ZA. Polyvinyl alcohol: A review of research status and use of polyvinyl alcohol based nanocomposites. Polym. Eng. Sci. John Wiley and Sons Inc.; 2018. p. 2119–2132. doi: 10.1002/pen.24855.

45. Paradossi G, Cavalieri F, Chiessi E, Spagnoli C, Cowman MK. Poly(vinyl alcohol) as versatile biomaterial for potential biomedical applications. J Mater Sci Mater Med. 2003;14:687–691. doi: 10.1023/A:1024907615244.

46. Yamaoka T, Tabata Y, Ikada Y. Comparison of Body Distribution of Poly(vinyl alcohol) with Other Water-soluble Polymers after Intravenous Administration. J Pharm Pharmacol. 1995;47:479–486. doi: 10.1111/j.2042-7158.1995.tb05835.x.

47. Hyon S-H, Ikada Y. Porous and transparent poly(vinyl alcohol) gel and method of manufacturing the same. Tamatsukurimotomachi, Japan; 1987.

48. Noguchi T, Yamamuro T, Oka M, Kumar P, Kotoura Y, Hyon S-H, Ikada Y. Poly(vinyl Alcohol) Hydrogel As an Artificial Articular Cartilage: Evaluation of Biocompatibility. J Appl Biomater. 1991;2:101–107. doi: 10.1002/jab.770020205.

49. Peppas NA, Benner RE. Proposed method of intracordal injection and gelation of poly (vinyl akohol) solution in vocal cords: polymer considerations. Biomaterials. 1980;1:158–162. doi: 10.1016/0142-9612(80)90039-3.

50. Hyon S-H, Cha W-I, Ikada Y, Kita M, Ogura Y, Honda Y. Poly (Vinyl Alcohol) Hydrogels as Soft Contact Lens Material. J Biomater Sci Polym Ed. 1994;5:397–406. doi: 10.1163/156856294X00103.

51. Daza JHU, Righetto GM, Chaud MV, da Conceição Amaro Martins V, Lopes Baratella da Cunha Camargo I, Maria de Guzzi Plepis A. PVA/anionic collagen membranes as drug carriers of ciprofloxacin hydrochloride with sustained antibacterial activity and potential use in the treatment of ulcerative keratitis. J Biomater Appl. 2020;35:301–312. doi: 10.1177/0885328220931733.

52. Gutiérrez MC, García-Carvajal ZY, Jobbágy M, Rubio F, Yuste L, Rojo F, Ferrer ML, Del Monte F. Poly(vinyl alcohol) scaffolds with tailored morphologies for

drug delivery and controlled release. Adv Funct Mater. 2007;17:3505–3513. doi: 10.1002/adfm.200700093.

53. Weis C, Odermatt EK, Kressler J, Funke Z, Wehner T, Freytag D. Poly(vinyl alcohol) membranes for adhesion prevention. J Biomed Mater Res - Part B Appl Biomater. 2004;70:191–202. doi: 10.1002/jbm.b.30007.

54. Mallapragada SK, Peppas NA, Colombo P. Crystal dissolution-controlled release systems. II. Metronidazole release from semicrystalline poly(vinyl alcohol) systems. J Biomed Mater Res. 1997;36:125–130. doi: 10.1002/(SICI)1097-4636(199707)36:1<125::AID-JBM15>3.0.CO;2-H.

55. Vashisth P, Nikhil K, Roy P, Pruthi PA, Singh RP, Pruthi V. A novel gellan-PVA nanofibrous scaffold for skin tissue regeneration: Fabrication and characterization. Carbohydr Polym. 2016;136:851–859. doi: 10.1016/j.carbpol.2015.09.113.

56. Parikh V, Kadiwala J, Hidalgo Bastida A, Holt C, Sanami M, Miraftab M, Shakur R, Azzawi M. Small diameter helical vascular scaffolds support endothelial cell survival. Nanomedicine Nanotechnology, Biol Med. 2018;14:2598–2608. doi: 10.1016/j.nano.2018.08.005.

57. Mozafari M, Moztarzadeh, Jalali, Alhosseini N, Asgari, Dodel, Samadikuchaksaraei, Kargozar. Synthesis and characterization of electrospun polyvinyl alcohol nanofibrous scaffolds modified by blending with chitosan for neural tissue engineering. Int J Nanomedicine. 2012;25. doi: 10.2147/ijn.s25376.

58. Wang L, Deng F, Wang W, Li A, Lu C, Chen H, Wu G, Nan K, Li L. Construction of Injectable Self-Healing Macroporous Hydrogels via a Template-Free Method for Tissue Engineering and Drug Delivery. ACS Appl Mater Interfaces. 2018;10:36721–36732. doi: 10.1021/acsami.8b13077.

59. Chahala S, Hussain FSJ, Yusoff MM. Characterization of modified cellulose (MC)/poly (vinyl alcohol) electrospun nanofibers for bone tissue engineering. Procedia Eng. Elsevier Ltd; 2013. p. 683–688. doi: 10.1016/j.proeng.2013.02.088.

60. Oktay B, Kayaman-Apohan N, Erdem-Kuruca S, Süleymanoğlu M. Fabrication of collagen immobilized electrospun poly (vinyl alcohol) scaffolds. Polym Adv Technol. 2015;26:978–987. doi: 10.1002/pat.3512.

61. Molnár K, Voniatis C, Fehér D, Ferencz A, Fónyad L, Reiniger L, Zrínyi M, Wéber G, Jedlovszky-Hajdú A. Biocompatibility study of poly(Vinyl alcohol)-based electrospun scaffold for hernia repair. Express Polym Lett. 2018;12:676–687. doi: 10.3144/expresspolymlett.2018.58.

62. Ngawhirunpat T, Opanasopit P, Rojanarata T, Akkaramongkolporn P, Ruktanonchai U, Supaphol P. Development of meloxicam-loaded electrospun polyvinyl alcohol mats as a transdermal therapeutic agent. Pharm Dev Technol. 2009;14:73–82. doi: 10.1080/10837450802409420.

63. Steffens L, Morás AM, Arantes PR, Masterson K, Cao Z, Nugent M, Moura DJ. Electrospun PVA-Dacarbazine nanofibers as a novel nano brain-implant for treatment of glioblastoma: in silico and in vitro characterization. Eur J Pharm Sci. 2020;143. doi: 10.1016/j.ejps.2019.105183.

64. Nguyen TH, Kim YH, Song HY, Lee BT. Nano Ag loaded PVA nano-fibrous mats for skin applications. J Biomed Mater Res - Part B Appl Biomater. 2011;96 B:225–233. doi: 10.1002/jbm.b.31756.

65. Sequeira RS, Miguel SP, Cabral CSD, Moreira AF, Ferreira P, Correia IJ. Development of a poly(vinyl alcohol)/lysine electrospun membrane-based drug delivery system for improved skin regeneration. Int J Pharm. 2019;570. doi: 10.1016/j.ijpharm.2019.118640.

66. Gutschmidt D, Hazra RS, Zhou X, Xu X, Sabzi M, Jiang L. Electrospun, sepiolite-loaded poly(vinyl alcohol)/soy protein isolate nanofibers: Preparation, characterization, and their drug release behavior. Int J Pharm. 2021;594. doi: 10.1016/j.ijpharm.2020.120172.

67. Sharma D, Satapathy BK. Optimally controlled morphology and physico-mechanical properties of inclusion complex loaded electrospun polyvinyl alcohol based nanofibrous mats for therapeutic applications. J Biomater Sci Polym Ed. 2021;32:1182–1202. doi: 10.1080/09205063.2021.1909414.

68. Bhattarai RS, Das A, Alzhrani RM, Kang D, Bhaduri SB, Boddu SHS. Comparison of electrospun and solvent cast polylactic acid (PLA)/poly(vinyl alcohol) (PVA) inserts as potential ocular drug delivery vehicles. Mater Sci Eng C. 2017;77:895–903. doi: 10.1016/j.msec.2017.03.305.

69. Zeng J, Yang L, Liang Q, Zhang X, Guan H, Xu X, Chen X, Jing X. Influence of

the drug compatibility with polymer solution on the release kinetics of electrospun fiber formulation. J Control Release. 2005;105:43–51. doi: 10.1016/j.jconrel.2005.02.024.

70. Goonoo N, Bhaw-Luximon A, Jhurry D. Drug loading and release from electrospun biodegradable nanofibers. J. Biomed. Nanotechnol. American Scientific Publishers; 2014. p. 2173–2199. doi: 10.1166/jbn.2014.1885.

71. Kim J-H, Lee HJ, Yoon S-W. Preparation and Swelling Behavior of Biodegradable Superabsorbent Gels Based on Polyaspartic Acid. J Ind Eng Chem. 2002;8:138–142.

72. Matsubara K, Nakato T, Tomida M. H and 13 C NMR Characterization of Poly(succinimide) Prepared by Thermal Polycondensation of L-Aspartic Acid. Macromolecules. 1997;30:2305–2312. doi: 10.1021/ma961579h.

73. Alford DD, Wheeler AP, Pettigrew CA. Biodegradation of Thermally Synthesized Polyaspartate. J. Environ. Polym. Degrad. 1994;2:225-236.

74. Neri P, Antoni G, Benvenuti F, Cocola F, Gazzei G. Synthesis of a,ß -Poly[(2-hydroxyethyl)-DL-aspartamide], a New Plasma Expander. J Med Chem. 1973;16:893–897. doi: 10.1021/jm00266a006.

75. Jalalvandi E, Shavandi A. Polysuccinimide and its derivatives: Degradable and water soluble polymers (review). Eur. Polym. J. Elsevier Ltd; 2018. p. 43–54. doi: 10.1016/j.eurpolymj.2018.08.056.

76. Koskan LP, Meah RYA. Production of polysuccinimide and polyaspartic acid from maleic anhydride and ammonia. 1994.

77. Nakato T, Kusuno A, Kakuchi T. Synthesis of poly(succinimide) by bulk polycondensation of L-aspartic acid with an acid catalyst. J Polym Sci Part A Polym Chem. 2000;38:117–122. doi: 10.1002/(SICI)1099-0518(20000101)38:1<117::AID-POLA15>3.0.CO;2-F.

78. Sikes SC. Preparation of high molecular weight polysuccinimides. 2006.

79. Adelnia H, Tran HDN, Little PJ, Blakey I, Ta HT. Poly(aspartic acid) in Biomedical Applications: From Polymerization, Modification, Properties, Degradation, and Biocompatibility to Applications. ACS Biomater. Sci. Eng. American Chemical Society; 2021. p. 2083–2105. doi: 10.1021/acsbiomaterials.1c00150.

80. Li L, Wu J, Zhao M, Wang Y, Zhang H, Zhang X, Gui L, Liu J, Mair N, Peng S. Poly-α,β-DL-aspartyl-L-cysteine: A novel nanomaterial having a porous structure, special complexation capability for Pb(II), and selectivity of removing Pb(II). Chem Res Toxicol. 2012;25:1948–1954. doi: 10.1021/tx300265c.

81. Xu M, Zhao Y, Feng M. Polyaspartamide derivative nanoparticles with tunable surface charge achieve highly efficient cellular uptake and low cytotoxicity. Langmuir. 2012;28:11310–11318. doi: 10.1021/la3025028.

82. Jalalvandi E, Cabral J, Hanton LR, Moratti SC. Cyclodextrin-polyhydrazine degradable gels for hydrophobic drug delivery. Mater Sci Eng C. 2016;69:144–153. doi: 10.1016/j.msec.2016.06.058.

83. Das P, Jana NR. Dopamine functionalized polymeric nanoparticle for targeted drug delivery. RSC Adv. 2015;5:33586–33594. doi: 10.1039/c5ra03302k.

84. Sharma A, Srivastava A. Pronounced influence of pH, metal-ion and solvent isotope on the thermoresponse of synthetic amphiphilic polypeptides. Polym Chem. 2013;4:5119–5128. doi: 10.1039/c3py00741c.

85. Zhao D, Li B, Han J, Yang Y, Zhang X, Wu G. PH responsive polypeptide based polymeric micelles for anticancer drug delivery. J Biomed Mater Res - Part A. 2015;103:3045–3053. doi: 10.1002/jbm.a.35434.

86. Cavallaro G, Goffredi M, la Manna G, Pitarresi G, Liveri VT, Giammona G. Dielectric Behavior of Aqueous Solutions of α,β-Poly(aspartyl hydrazide) and α,β-Poly(N-hydroxyethyl aspartamide): An Investigation of the Structural and Dynamic Properties. J Bioact Compat Polym. 1994;9:101–110. doi: 10.1177/088391159400900106.

87. Mendichi R, Giammona G, Cavallaro G, Schieroni AG. Molecular characterization of a,b-poly(asparthylhydrazide) a new synthetic polymer for biomedical applications. Polymer (Guildf). 1999;40:7109–7116. doi: 10.1016/S0032-3861(99)00079-8.

88. Lu C, Wang X, Wu G, Wang J, Wang Y, Gao H, Ma J. An injectable and biodegradable hydrogel based on poly(α,β- aspartic acid) derivatives for localized drug delivery. J Biomed Mater Res - Part A. 2014;102:628–638. doi: 10.1002/jbm.a.34725.

89. Yoon SR, Yang HM, Park CW, Lim S, Chung BH, Kim JD. Charge-conversional

poly(amino acid)s derivatives as a drug delivery carrier in response to the tumor environment. J Biomed Mater Res - Part A. 2012;100 A:2027–2033. doi: 10.1002/jbm.a.34048.

90. Wang X, Wu G, Lu C, Zhao W, Wang Y, Fan Y, Gao H, Ma J. A novel delivery system of doxorubicin with high load and pH-responsive release from the nanoparticles of poly (α,β-aspartic acid) derivative. Eur J Pharm Sci. 2012;47:256–264. doi: 10.1016/j.ejps.2012.04.007.

91. Cao L, Xiao Y, Lu W, Liu S, Gan L, Yu J, Huang J. Nanomicelle drug with acid-triggered doxorubicin release and enhanced cellular uptake ability based on mPEG-graft-poly(N-(2-aminoethyl)-L-aspartamide)-hexahydrophthalic acid copolymers. J Biomater Appl. 2018;32:826–838. doi: 10.1177/0885328217741522.

92. An H, Zhu L, Shen J, Li W, Wang Y, Qin J. Self-healing PEG-poly(aspartic acid) hydrogel with rapid shape recovery and drug release. Colloids Surfaces B Biointerfaces. 2020;185. doi: 10.1016/j.colsurfb.2019.110601.

93. Lim CW, Kim D. Bone targeting nano-aggregates prepared from self-assembled polyaspartamide graft copolymers for pH sensitive DOX delivery. Biomater Sci. 2021;9:1660–1667. doi: 10.1039/d0bm01473g.

94. Di Meo C, Cilurzo F, Licciardi M, Scialabba C, Sabia R, Paolino D, Capitani D, Fresta M, Giammona G, Villani C, Matricardi P. Polyaspartamide-Doxorubicin Conjugate as Potential Prodrug for Anticancer Therapy. Pharm Res. 2015;32:1557–1569. doi: 10.1007/s11095-014-1557-2.

95. Debnath K, Shekhar S, Kumar V, Jana NR, Jana NR. Efficient Inhibition of Protein Aggregation, Disintegration of Aggregates, and Lowering of Cytotoxicity by Green Tea Polyphenol-Based Self-Assembled Polymer Nanoparticles. ACS Appl Mater Interfaces. 2016;8:20309–20318. doi: 10.1021/acsami.6b06853.

96. Debnath K, Jana NR, Jana NR. Quercetin Encapsulated Polymer Nanoparticle for Inhibiting Intracellular Polyglutamine Aggregation. ACS Appl Bio Mater. 2019;2:5298–5305. doi: 10.1021/acsabm.9b00518.

97. Németh C, Gyarmati B, Gacs J, Salakhieva D V., Molnár K, Abdullin T, László K, Szilágyi A. Fast dissolving nanofibrous matrices prepared by electrospinning of polyaspartamides. Eur Polym J. 2020;130. doi:

10.1016/j.eurpolymj.2020.109624.

98. Németh C, Gyarmati B, Abdullin T, László K, Szilágyi A. Poly(aspartic acid) with adjustable pH-dependent solubility. Acta Biomater. 2017;49:486–494. doi: 10.1016/j.actbio.2016.11.065.

99. Barczikai D, Kacsari V, Domokos J, Szabó D, Jedlovszky-Hajdu A. Interaction of silver nanoparticle and commonly used anti-inflammatory drug within a poly(amino acid) derivative fibrous mesh. J Mol Liq. 2021;322. doi: 10.1016/j.molliq.2020.114575.

100. Luk BT, Zhang L. Current advances in polymer-based nanotheranostics for cancer treatment and diagnosis. ACS Appl. Mater. Interfaces. American Chemical Society; 2014. p. 21859–21873.

101. Nicolas J, Mura S, Brambilla D, Mackiewicz N, Couvreur P. Design, functionalization strategies and biomedical applications of targeted biodegradable/biocompatible polymer-based nanocarriers for drug delivery. Chem Soc Rev. 2013;42:1147–1235. doi: 10.1039/c2cs35265f.

102. Licciardi M, Di Stefano M, Craparo EF, Amato G, Fontana G, Cavallaro G, Giammona G. PHEA-graft-polybutylmethacrylate copolymer microparticles for delivery of hydrophobic drugs. Int J Pharm. 2012;433:16–24. doi: 10.1016/j.ijpharm.2012.04.052.

103. Craparo EF, Teresi G, Bondi' ML, Licciardi M, Cavallaro G. Phospholipid-polyaspartamide micelles for pulmonary delivery of corticosteroids. Int J Pharm. 2011;406:135–144. doi: 10.1016/j.ijpharm.2010.12.024.

104. Triolo D, Craparo EF, Porsio B, Fiorica C, Giammona G, Cavallaro G. Polymeric drug delivery micelle-like nanocarriers for pulmonary administration of beclomethasone dipropionate. Colloids Surfaces B Biointerfaces. 2017;151:206–214. doi: 10.1016/j.colsurfb.2016.11.025.

105. Yao X, Xie C, Chen W, Yang C, Wu W, Jiang X. Platinum-incorporating poly(N-vinylpyrrolidone)-poly(aspartic acid) pseudoblock copolymer nanoparticles for drug delivery. Biomacromolecules. 2015;16:2059–2071. doi: 10.1021/acs.biomac.5b00479.

106. Huang YT, Wang WC, Hsu CP, Lu WY, Chuang WJ, Chiang MY, Lai YC, Chen HY. The ring-opening polymerization of ε-caprolactone and l-lactide using

aluminum complexes bearing benzothiazole ligands as catalysts. Polym Chem. 2016;7:4367–4377. doi: 10.1039/c6py00569a.

107. Malikmammadov E, Tanir TE, Kiziltay A, Hasirci V, Hasirci N. PCL and PCL-based materials in biomedical applications. J Biomater Sci Polym Ed. 2018;29:863–893. doi: 10.1080/09205063.2017.1394711.

108. Hoskins JN, Grayson SM. Synthesis and degradation behavior of cyclic poly(ε-caprolactone). Macromolecules. 2009;42:6406–6413. doi: 10.1021/ma9011076.

109. Díaz E, Sandonis I, Valle MB. In vitro degradation of poly(caprolactone)/nHA composites. J Nanomater. 2014;2014. doi: 10.1155/2014/802435.

110. Abedalwafa M, Wang F, Wang L, Li C. Biodegradable poly-epsilon-caprolactone (PCL) for tissue engineering applications: a review. Rev. Adv. Mater. Sci. 2013;34:123-140.

111. Gleadall A, Pan J, Kruft MA, Kellomäki M. Degradation mechanisms of bioresorbable polyesters. Part 1. Effects of random scission, end scission and autocatalysis. Acta Biomater. 2014;10:2223–2232. doi: 10.1016/j.actbio.2013.12.039.

112. Gleadall A, Pan J, Kruft MA, Kellomäki M. Degradation mechanisms of bioresorbable polyesters. Part 2. Effects of initial molecular weight and residual monomer. Acta Biomater. 2014;10:2233–2240. doi: 10.1016/j.actbio.2014.01.017.

113. Hissink CE, Steendam R, Meyboom R, Adrianus T, Flipsen S. Biodegradable multi-block co-polymers. 2007.

114. Maquet V, Pagnoulle C, Evrard B, Jerome R, Foidart J-M, Frankenne F. Active Substance Delivery System Comprising A Hydrogel Atrix And Microcarriers. 2008.

115. Kasinathan N, Amirthalingam M, Reddy ND, Jagani H V., Volety SM, Rao JV. In-situ implant containing PCL-curcumin nanoparticles developed using design of experiments. Drug Deliv. 2016;23:1017–1025. doi: 10.3109/10717544.2014.927021.

116. Hsu KH, Fang SP, Lin CL, Liao YS, Yoon YK, Chauhan A. Hybrid Electrospun Polycaprolactone Mats Consisting of Nanofibers and Microbeads for Extended Release of Dexamethasone. Pharm Res. 2016;33:1509–1516. doi:

10.1007/s11095-016-1894-4.

117. Qi P, Bu Y, Xu J, Qin B, Luan S, Song S. pH-responsive release of paclitaxel from hydrazone-containing biodegradable micelles. Colloid Polym Sci. 2017;295:1–12. doi: 10.1007/s00396-016-3968-6.

118. Chi Y, Zhu S, Wang C, Zhou L, Zhang L, Li Z, Dai Y. Glioma homing peptide-modified PEG-PCL nanoparticles for enhanced anti-glioma therapy. J Drug Target. 2016;24:224–232. doi: 10.3109/1061186X.2015.1070854.

119. Raval JP, Naik DR, Amin KA, Patel PS. Controlled-release and antibacterial studies of doxycycline-loaded poly(ε-caprolactone) microspheres. J Saudi Chem Soc. 2014;18:566–573. doi: 10.1016/j.jscs.2011.11.004.

120. Alex AT, Joseph A, Shavi G, Rao JV, Udupa N. Development and evaluation of carboplatin-loaded PCL nanoparticles for intranasal delivery. Drug Deliv. 2016;23:2144–2153. doi: 10.3109/10717544.2014.948643.

121. Chandy T, Wilson RF, Rao GHR, Das GS. Changes in cisplatin delivery due to surface-coated poly (lactic acid)-poly(ε-caprolactone) microspheres. J Biomater Appl. 2002;16:275–291. doi: 10.1106/088532802024246.

122. Dong CM, Guo YZ, Qiu KY, Gu ZW, Feng X De. In vitro degradation and controlled release behavior of D,L-PLGA50 and PCL-b-D,L-PLGA50 copolymer microspheres. J Control Release. 2005;107:53–64. doi: 10.1016/j.jconrel.2005.05.024.

123. Davoodi P, Srinivasan MP, Wang CH. Synthesis of intracellular reduction-sensitive amphiphilic polyethyleneimine and poly(ε-caprolactone) graft copolymer for on-demand release of doxorubicin and p53 plasmid DNA. Acta Biomater. 2016;39:79–93. doi: 10.1016/j.actbio.2016.05.003.

124. Leng M, Hu S, Lu A, Cai M, Luo X. The anti-bacterial poly(caprolactone)-poly(quaternary ammonium salt) as drug delivery carriers. Appl Microbiol Biotechnol. 2016;100:3049–3059. doi: 10.1007/s00253-015-7126-8.

125. Jassal M, Sengupta S, Bhowmick S. Functionalization of electrospun poly(caprolactone) fibers for pH-controlled delivery of doxorubicin hydrochloride. J Biomater Sci Polym Ed. 2015;26:1425–1438. doi: 10.1080/09205063.2015.1100495.

126. Monteiro APF, Rocha CMSL, Oliveira MF, Gontijo SML, Agudelo RR,

Sinisterra RD, Cortés ME. Nanofibers containing tetracycline/β-cyclodextrin: Physico-chemical characterization and antimicrobial evaluation. Carbohydr Polym. 2017;156:417–426. doi: 10.1016/j.carbpol.2016.09.059.

127. Hutmacher DW. Scaffolds in tissue engineering bone and cartilage. Biomaterials. 2000;21:2529-2543. doi: 10.1016/S0142-9612(00)00121-6.

128. Rai B, Teoh SH, Hutmacher DW, Cao T, Ho KH. Novel PCL-based honeycomb scaffolds as drug delivery systems for rhBMP-2. Biomaterials. 2005;26:3739–3748. doi: 10.1016/j.biomaterials.2004.09.052.

129. Lee JB, Kim JE, Bae MS, Park SA, Balikov DA, Sung HJ, Jeon HB, Park HK, Um SH, Lee KS, Kwon IK. Development of poly(ε-Caprolactone) scaffold loaded with simvastatin and beta-cyclodextrin modified hydroxyapatite inclusion complex for bone tissue engineering. Polymers (Basel). 2016;8. doi: 10.3390/polym8020049.

130. Patel JJ, Modes JE, Flanagan CL, Krebsbach PH, Edwards SP, Hollister SJ. Dual Delivery of EPO and BMP2 from a Novel Modular Poly-ε-Caprolactone Construct to Increase the Bone Formation in Prefabricated Bone Flaps. Tissue Eng - Part C Methods. 2015;21:889–897. doi: 10.1089/ten.tec.2014.0643.

131. Yilgor P, Hasirci N, Hasirci V. Sequential BMP-2/BMP-7 delivery from polyester nanocapsules. J Biomed Mater Res - Part A. 2010;93:528–536. doi: 10.1002/jbm.a.32520.

132. Yilgor P, Yilmaz G, Onal MB, Solmaz I, Gundogdu S, Keskil S, Sousa RA, Reis RL, Hasirci N, Hasirci V. An in vivo study on the effect of scaffold geometry and growth factor release on the healing of bone defects. J Tissue Eng Regen Med. 2013;7:687–696. doi: 10.1002/term.1456.

133. Dziadek M, Menaszek E, Zagrajczuk B, Pawlik J, Cholewa-Kowalska K. New generation poly(ε-caprolactone)/gel-derived bioactive glass composites for bone tissue engineering: Part I. Material properties. Mater Sci Eng C. 2015;56:9–21. doi: 10.1016/j.msec.2015.06.020.

134. Saito E, Suarez-Gonzalez D, Murphy WL, Hollister SJ. Biomineral Coating Increases Bone Formation by Ex Vivo BMP-7 Gene Therapy in Rapid Prototyped Poly(l-lactic acid) (PLLA) and Poly(ε-caprolactone) (PCL) Porous Scaffolds. Adv Healthc Mater. 2015;4:621–632. doi: 10.1002/adhm.201400424.

135. Qu X, Xia P, He J, Li D. Microscale electrohydrodynamic printing of biomimetic PCL/nHA composite scaffolds for bone tissue engineering. Mater Lett. 2016;185:554–557. doi: 10.1016/j.matlet.2016.09.035.

136. Habraken WJEM, Wolke JGC, Jansen JA. Ceramic composites as matrices and scaffolds for drug delivery in tissue engineering. Adv. Drug Deliv. Rev. 2007;59:234–248. doi: 10.1016/j.addr.2007.03.011.

137. Croisier F, Atanasova G, Poumay Y, Jérôme C. Polysaccharide-Coated PCL Nanofibers for Wound Dressing Applications. Adv Healthc Mater. 2014;3:2032–2039. doi: 10.1002/adhm.201400380.

138. Chen H, Huang J, Yu J, Liu S, Gu P. Electrospun chitosan-graft-poly (ε-caprolactone)/poly (ε-caprolactone) cationic nanofibrous mats as potential scaffolds for skin tissue engineering. Int J Biol Macromol. 2011;48:13–19. doi: 10.1016/j.ijbiomac.2010.09.019.

139. Gong CY, Wu QJ, Wang YJ, Zhang DD, Luo F, Zhao X, Wei YQ, Qian ZY. A biodegradable hydrogel system containing curcumin encapsulated in micelles for cutaneous wound healing. Biomaterials. 2013;34:6377–6387. doi: 10.1016/j.biomaterials.2013.05.005.

140. Baker SC, Rohman G, Southgate J, Cameron NR. The relationship between the mechanical properties and cell behaviour on PLGA and PCL scaffolds for bladder tissue engineering. Biomaterials. 2009;30:1321–1328. doi: 10.1016/j.biomaterials.2008.11.033.

141. Cooper A, Bhattarai N, Zhang M. Fabrication and cellular compatibility of aligned chitosan-PCL fibers for nerve tissue regeneration. Carbohydr Polym. 2011;85:149–156. doi: 10.1016/j.carbpol.2011.02.008.

142. Klein MO, Battagello DS, Cardoso AR, Hauser DN, Bittencourt JC, Correa RG. Dopamine: Functions, Signaling, and Association with Neurological Diseases. Cell. Mol. Neurobiol. Springer New York LLC; New York, 2019. p. 31–59. doi: 10.1007/s10571-018-0632-3.

143. Christenson JG, Dairman W, Udenfriend S. Preparation and Properties of a Homogeneous Aromatic L-Amino Acid Decarboxylase from Hog Kidney'. Arch. Biochem. Biophys. 1970;141:356-367 doi: 10.1016/0003-9861(70)90144-x.

144. Nagatsu T, Levitt M, Udenfriend S. Tyrosine Hydroxylase. J Biol Chem.

1964;239:2910–2917. doi: 10.1016/S0021-9258(18)93832-9.

145. Fernstrom JD, Fernstrom MH. Tyrosine, Phenylalanine, and Catecholamine Synthesis and Function in the Brain. J Nutr. 2007;137:1539S-1547S. doi: 10.1093/jn/137.6.1539S.

146. Segura-Aguilar J, Paris I, Muñoz P, Ferrari E, Zecca L, Zucca FA. Protective and toxic roles of dopamine in Parkinson's disease. J. Neurochem. Blackwell Publishing Ltd; New York 2014. p. 898–915. doi: 10.1111/jnc.12686.

147. Eisenhofer G, Kopin IJ, Goldstein DS. Catecholamine metabolism: A contemporary view with implications for physiology and medicine. Pharmacol. Rev. 2004;56:331–349. doi: 10.1124/pr.56.3.1.

148. Chen J, Song J, Yuan P, Tian Q, Ji Y, Ren-Patterson R, Liu G, Sei Y, Weinberger DR. Orientation and cellular distribution of membrane-bound catechol-O-methyltransferase in cortical neurons: Implications for drug development. J Biol Chem. 2011;286:34752–34760. doi: 10.1074/jbc.M111.262790.

149. Liu C, Kershberg L, Wang J, Schneeberger S, Kaeser PS. Dopamine Secretion Is Mediated by Sparse Active Zone-like Release Sites. Cell. 2018;172:706-718.e15. doi: 10.1016/j.cell.2018.01.008.

150. Agnati LF, Zoli M, Stromberg I, Fuxe K. Intercellular communication in the brain: wiring versus volume transmission. Neuroscience. 1995;69:711-726. doi: 10.1016/0306-4522(95)00308-6.

151. Floresco SB, West AR, Ash B, Moorel H, Grace AA. Afferent modulation of dopamine neuron firing differentially regulates tonic and phasic dopamine transmission. Nat Neurosci. 2003;6:968–973. doi: 10.1038/nn1103.

152. Harrington KA, Augood SJ, Kingsbury AE, Foster OJF, Emson PC. Dopamine transporter (DAT) and synaptic vesicle amine transporter (VMAT2) gene expression in the substantia nigra of control and Parkinson's disease. Mol. Brain Res. 1996;36:157-162. doi: 10.1016/0169-328x(95)00278-z.

153. Miller GW, Gainetdinov RR, Levey AI, Caron MG. Dopamine transporters and neuronal injury. TiPS. 1999;20:424–429. doi: 10.1016/S0165-6147(99)01379-6.

154. Luttrell ML, Lefkowitz RJ. The role of β-arrestins in the termination and transduction of G-protein-coupled receptor signals. J Cell Sci. 2002;115:455–

465. doi: 10.1242/jcs.115.3.455.

155. Missale C, Nash SR, Robinson SW, Jaber M, Caron MG. Dopamine Receptors: From Structure to Function. Physiol. Rev. 1998;78:189-225. doi: 10.1152/physrev.1998.78.1.189.

156. Baik JH. Dopamine signaling in reward-related behaviors. Front. Neural Circuits. Frontiers Media S.A.; 2013;11:152- doi: 10.3389/fncir.2013.00152.

157. Goto Y, Otani S, Grace AA. The Yin and Yang of dopamine release: a new perspective. Neuropharmacology. 2007;53:583–587. doi: 10.1016/j.neuropharm.2007.07.007.

158. Grace AA, Floresco SB, Goto Y, Lodge DJ. Regulation of firing of dopaminergic neurons and control of goal-directed behaviors. Trends Neurosci. 2007;5:220–227. doi: /10.1016/j.tins.2007.03.003.

159. Baik JH. Dopamine signaling in food addiction: Role of dopamine D2 receptors. BMB Rep. 2013;46:519–526. doi: 10.5483/BMBRep.2013.46.11.207.

160. Beaulieu J-M, Espinoza S, Gainetdinov RR. Dopamine receptors - IUPHAR Review 13. Br J Pharmacol. 2015;172:1–23. doi: 10.1111/bph.12445/abstract.

161. Greengard P. The Neurobiology of Slow Synaptic Transmission. Neuroscience. 2001;294:1024–1030. doi: 10.1126/science.294.5544.1024.

162. Wang B, Jeon YS, Bhang SH, Kim JH. Bioinspired dopamine-conjugated polyaspartamide as a novel and versatile adhesive material. Express Polym Lett. 2017;11:601–610. doi: 10.3144/expresspolymlett.2017.58.

163. Kalčić I, Zorc B, Butula I. Macromolecular prodrugs. VII. Polymer-dopamine conjugates. Int J Pharm. 1996;136:31–36. doi: 10.1016/0378-5173(96)04484-5.

164. Juriga D, Laszlo I, Ludanyi K, Klebovich I, Chae CH, Zrinyi M. Kinetics of dopamine release from poly(aspartamide)-based prodrugs. Acta Biomater. 2018;76:225–238. doi: 10.1016/j.actbio.2018.06.030.

165. Naki T, Matshe W, Ubanako P, Adeyemi SA, Balogun MO, Sinha Ray S, Choonara YE, Aderibigbe BA. Dopamine-Loaded Polymer-Drug Conjugates for Potential Synergistic Anti-Cancer Treatment. Polym Technol Mater. 2022;61:1003–1020. doi: 10.1080/25740881.2022.2029895.

166. Dong H, Wang K, Zhou D, Ito Y, Hu L, Zhang Z, Zhu X. Enrichment and immobilization of semiconducting single-walled carbon nanotubes by dopamine

functionalized conjugated polymer. React Funct Polym. 2020;153:104616. doi: 10.1016/j.reactfunctpolym.2020.104616.

167. Lu Z, Wang W, Zhang J, Bártolo P, Gong H, Li J. Electrospun highly porous poly(L-lactic acid)-dopamine-SiO2 fibrous membrane for bone regeneration. Mater Sci Eng C. 2020;117. doi: 10.1016/j.msec.2020.111359.

168. Ansari AQ, Ansari SJ, Khan MQ, Khan MF, Qureshi UA, Khatri Z, Ahmed F, Kim IS. Electrospun Zein nanofibers as drug carriers for controlled delivery of Levodopa in Parkinson syndrome. Mater Res Express. 2019;6. doi: 10.1088/2053-1591/ab16bf.

169. Richards ML, Sadee W. Human neuroblastoma cell lines as models of catechol uptake. Brain Res. 1986;384:132–137. doi: 10.1016/0006-8993(86)91228-X.

170. Yamakawa K, Izumi Y, Takeuchi H, Yamamoto N, Kume T, Akaike A, Takahashi R, Shimohama S, Sawada H. Dopamine facilitates α-synuclein oligomerization in human neuroblastoma SH-SY5Y cells. Biochem Biophys Res Commun. 2010;391:129–134. doi: 10.1016/j.bbrc.2009.11.015.

171. Mena MA, Garcia de Yebenes J, Dwork A, Fahn S, Latov N, Herbert J, Flaster E, Slonim D. Biochemical properties of monoamine-rich human neuroblastoma cells. Brain Res. 1989;486:286–296. doi: 10.1016/0006-8993(89)90514-3.

172. Haque ME, Asanuma M, Higashi Y, Miyazaki I, Tanaka KI, Ogawa N. Apoptosis-inducing neurotoxicity of dopamine and its metabolites via reactive quinone generation in neuroblastoma cells. Biochim Biophys Acta - Gen Subj. 2003;1619:39–52. doi: 10.1016/S0304-4165(02)00440-3.

173. Lopes FM, da Motta LL, De Bastiani MA, Pfaffenseller B, Aguiar BW, de Souza LF, Zanatta G, Vargas DM, Schönhofen P, Londero GF, de Medeiros LMm Freire VN, Dafre AL, Castro MAAm Parsons RB, Klamt F. RA Differentiation Enhances Dopaminergic Features, Changes Redox Parameters, and Increases Dopamine Transporter Dependency in 6-Hydroxydopamine-Induced Neurotoxicity in SH-SY5Y Cells. Neurotox Res. 2017;31:545–559. doi: 10.1007/s12640-016-9699-0.

174. Presgraves P. S, Ahmed T, Borwege S, Joyce N. J. Terminally Differentiated SH-SY5Y Cells Provide a ModelSystem for Studying Neuroprotective Effects of Dopamine Agonists. Neurotox Res. 2004;5:579–598. doi: 10.1007/BF03033178.

175. Storch A, Kaftan A, Burkhardt K, Schwarz J. 6-Hydroxydopamine toxicity towards human SH-SY5Y dopaminergic neuroblastoma cells: independent of mitochondrial energy metabolism. J Neural Transm. 2000;107:281-293. doi: 10.1007/s007020050023.

176. Izumi Y, Sawada H, Sakka N, Yamamoto N, Kume T, Katsuki H, Shimohama S, Akaike A. P-Quinone Mediates 6-Hydroxydopamine-Induced Dopaminergic Neuronal Death and Ferrous Iron Accelerates the Conversion of P-Quinone Into Melanin Extracellularly. J Neurosci Res. 2005;79:849–860. doi: 10.1002/jnr.20382.

177. Ham A, Kim B, Koo U, Nam KW, Lee SJ, Kim KH, Shin J, Mar W. Spirafolide from bay leaf (Laurus nobilis) prevents dopamine-induced apoptosis by decreasing reactive oxygen species production in human neuroblastoma SH-SY5Y cells. Arch Pharm Res. 2010;33:1953–1958. doi: 10.1007/s12272-010-1210-5.

178. Kawajiri S, Machida Y, Saiki S, Sato S, Hattori N. Zonisamide reduces cell death in SH-SY5Y cells via an anti-apoptotic effect and by upregulating MnSOD. Neurosci Lett. 2010;481:88–91. doi: 10.1016/j.neulet.2010.06.058.

179. Kim SE, Yun YP, Han YK, Lee DW, Ohe JY, Lee BS, Song HR, Park K, Choi BJ. Osteogenesis induction of periodontal ligament cells onto bone morphogenic protein-2 immobilized PCL fibers. Carbohydr Polym. 2014;99:700–709. doi: 10.1016/j.carbpol.2013.08.053.

180. Lee JS, Lee JC, Heo JS. Polydopamine-assisted BMP-2 immobilization on titanium surface enhances the osteogenic potential of periodontal ligament stem cells via integrin-mediated cell-matrix adhesion. J Cell Commun Signal. 2018;12:661–672. doi: 10.1007/s12079-018-0468-0.

181. Slingerland M, Guchelaar HJ, Gelderblom H. Liposomal drug formulations in cancer therapy: 15 years along the road. Drug Discov. Today. 2012;17:160–166. doi: 10.1016/j.drudis.2011.09.015.

182. Rivankar S. An overview of doxorubicin formulations in cancer therapy. J. Cancer Res. Ther. Medknow Publications; 2014;10:853–858. doi: 10.4103/0973-1482.139267.

183. Momparler RL, Karon M, Siegel Stuart E, Avila Felicidad. Effect of Adriamycin

on DNA, RNA, and Protein Synthesis in Cell-free Systems and lntact Cells. Cencer Res. 1976;36:2891–1976.

184. Waterhouse DN, Tardi PG, Mayer LD, Bally MB. A Comparison of Liposomal Formulations of Doxorubicin with Drug Administered in Free Form Changing Toxicity Profiles. Drug Saf. 2001;24:903–920. doi: 10.2165/00002018-200124120-00004.

185. Pai VB, Nahata MC. Cardiotoxicity of Chemotherapeutic Agents: Incidence, Treatment and Prevention. Drug Saf. 2000;22:263–302. doi: 10.2165/00002018-200022040-00002.

186. Birtle AJ. Anthracyclines and Cardiotoxicity. Clin Oncol. 2000;12:146–152. doi: 10.1053/clon.2000.9141.

187. Tardi PG, Boman NL, Cullis PR. Liposomal Doxorubicin. J. Drug Target. 1996;4:129-140. doi: 10.3109/10611869609015970.

188. Immordino LM, Dosio F, Cattel L. Stealth liposomes: review of the basic science, rationale, and clinical applications, existing and potential. Int J Nanomedicine. 2006;1:297–315.

189. Schnyder A, Huwyler J. Drug Transport to Brain with Targeted Liposomes. J Am Soc Exp Neurother. 2005;2:99–107. doi: 10.1602/neurorx.2.1.99.

190. Shao K, Hou Q, Duan W, Go ML, Wong KP, Li QT. Intracellular drug delivery by sulfatide-mediated liposomes to gliomas. J Control Release. 2006;115:150–157. doi: 10.1016/j.jconrel.2006.07.024.

191. Bromberg L, Alakhov V. Effects of polyether-modified poly(acrylic acid) microgels on doxorubicin transport in human intestinal epithelial Caco-2 cell layers. J. Control. Release. 2003;88:11-22. doi: 10.1016/s0168-3659(02)00419-4.

192. Itokazu M, Kumazawa S, Wada E, Wenyi Y. CANCER LETTERS ELSEVIER Sustained release of adriamycin from implanted hydroxyapatite blocks for the treatment of experimental osteogenic sarcoma in mice. Cancer Lett. 1996;107:11-18. doi: 10.1016/0304-3835(96)04337-6.

193. Nagy KS, Toth K, Pallinger E, Takacs A, Kohidai L, Jedlovszky-Hajdu A, Mathe D, Kovacs N, Veres DS, Szigeti K, Molnar K, Krisch E, Puskas JE. Folate-targeted monodisperse peg-based conjugates made by chemo-enzymatic methods

for cancer diagnosis and treatment. Int J Mol Sci. 2021;22. doi: 10.3390/ijms221910347.

194. Sanyakamdhorn S, Agudelo D, Tajmir-Riahi HA. Review on the targeted conjugation of anticancer drugs doxorubicin and tamoxifen with synthetic polymers for drug delivery. J Biomol Struct Dyn. 2017;35:2497–2508. doi: 10.1080/07391102.2016.1222971.

195. Yu J, Li X, Luo Y, Lu W, Huang J, Liu S. Poly(ethylene glycol) shell-sheddable magnetic nanomicelle as the carrier of doxorubicin with enhanced cellular uptake. Colloids Surfaces B Biointerfaces. 2013;107:213–219. doi: 10.1016/j.colsurfb.2013.02.009.

196. Zhang Y, Xiao Y, Huang Y, He Y, Xu Y, Lu W, Yu J. Poly(ethylene glycol) shell-sheddable TAT-modified core cross-linked nano-micelles: TAT-enhanced cellular uptake and lysosomal pH-triggered doxorubicin release. Colloids Surfaces B Biointerfaces. 2020;188. doi: 10.1016/j.colsurfb.2020.110772.

197. Yang SR, Lee HJ, Kim JD. Histidine-conjugated poly(amino acid) derivatives for the novel endosomolytic delivery carrier of doxorubicin. J Control Release. 2006;114:60–68. doi: 10.1016/j.jconrel.2006.05.016.

198. Hao W, Zheng Z, Zhu L, Pang L, Ma J, Zhu S, Du L, Jin Y. 3D printing-based drug-loaded implanted prosthesis to prevent breast cancer recurrence post-conserving surgery. Asian J Pharm Sci. 2021;16:86–96. doi: 10.1016/j.ajps.2020.06.002.

199. Gao Y, Wang J, Han H, Xiao H, Jin WK, Wang S, Shao S, Wang Z, Yang W, Wang L, Weng L. A nanoparticle-containing polycaprolactone implant for combating post-resection breast cancer recurrence. Nanoscale. 2021;13:14417–14425. doi: 10.1039/d1nr04125h.

200. Fong YT, Chen CH, Chen JP. Intratumoral delivery of doxorubicin on folate-conjugated graphene oxide by in-situ forming thermo-sensitive hydrogel for breast cancer therapy. Nanomaterials. 2017;7:388. doi: 10.3390/nano7110388.

201. Li X, He Y, Hou J, Yang G, Zhou S. A Time-Programmed Release of Dual Drugs from an Implantable Trilayer Structured Fiber Device for Synergistic Treatment of Breast Cancer. Small. 2020;16. doi: 10.1002/smll.201902262.

202. Darbasizadeh B, Mortazavi SA, Kobarfard F, Jaafari MR, Hashemi A,

Farhadnejad H, Feyzi-barnaji B. Electrospun Doxorubicin-loaded PEO/PCL core/sheath nanofibers for chemopreventive action against breast cancer cells. J Drug Deliv Sci Technol. 2021;64. doi: 10.1016/j.jddst.2021.102576.

203. Balakrishnan B, Jayakrishnan A. Self-cross-linking biopolymers as injectable in situ forming biodegradable scaffolds. Biomaterials. 2005;26:3941–3951. doi: 10.1016/j.biomaterials.2004.10.005.

204. Guo X, Liu Y, Bera H, Zhang H, Chen Y, Cun D, Foderà V, Yang M. α-Lactalbumin-Based Nanofiber Dressings Improve Burn Wound Healing and Reduce Scarring. ACS Appl Mater Interfaces. 2020;12:45702–45713. doi: 10.1021/acsami.0c05175.

205. Abasalta M, Asefnejad A, Khorasani MT, Saadatabadi AR. Fabrication of carboxymethyl chitosan/poly(ε-caprolactone)/doxorubicin/nickel ferrite core-shell fibers for controlled release of doxorubicin against breast cancer. Carbohydr Polym. 2021;257. doi: 10.1016/j.carbpol.2021.117631.

206. Ignatova M, Yossifova L, Gardeva E, Manolova N, Toshkova R, Rashkov I, Alexandrov M. Antiproliferative activity of nanofibers containing quaternized chitosan and/or doxorubicin against MCF-7 human breast carcinoma cell line by apoptosis. J Bioact Compat Polym. 2011;26:539–551. doi: 10.1177/0883911511424655.

207. Rasouli S, Montazeri M, Mashayekhi S, Sadeghi-Soureh S, Dadashpour M, Mousazadeh H, Nobakht A, Zarghami N, Pilehvar-Soltanahmadi Y. Synergistic anticancer effects of electrospun nanofiber-mediated codelivery of Curcumin and Chrysin: Possible application in prevention of breast cancer local recurrence. J Drug Deliv Sci Technol. 2020;55. doi: 10.1016/j.jddst.2019.101402.

208. Yuan Z, Wu W, Zhang Z, Sun Z, Cheng R, Pan G, Wang X, Cui W. In situ adjuvant therapy using a responsive doxorubicin-loaded fibrous scaffold after tumor resection. Colloids Surfaces B Biointerfaces. 2017;158:363–369. doi: 10.1016/j.colsurfb.2017.06.052.

209. Wei X, Liu C, Wang Z, Luo Y. 3D printed core-shell hydrogel fiber scaffolds with NIR-triggered drug release for localized therapy of breast cancer. Int J Pharm. 2020;580. doi: 10.1016/j.ijpharm.2020.119219.

210. Habibi Jouybari M, Hosseini S, Mahboobnia K, Boloursaz LA, Moradi M, Irani

M. Simultaneous controlled release of 5-FU, DOX and PTX from chitosan/PLA/5-FU/g-C3N4-DOX/g-C3N4-PTX triaxial nanofibers for breast cancer treatment in vitro. Colloids Surfaces B Biointerfaces. 2019;179:495–504. doi: 10.1016/j.colsurfb.2019.04.026.

211. Li H, Zhu J, Chen S, Jia L, Ma Y. Fabrication of aqueous-based dual drug loaded silk fibroin electrospun nanofibers embedded with curcumin-loaded RSF nanospheres for drugs controlled release. RSC Adv. 2017;7:56550–56558. doi: 10.1039/c7ra12394a.

212. Major A, Smith SM. DA-R-EPOCH vs R-CHOP in DLBCL: How Do We Choose?

213. Krasselt M, Baerwald C. Efficacy and safety of modified-release prednisone in patients with rheumatoid arthritis. Drug Des Devel Ther. 2016;10:1047–1058. doi: 10.2147/DDDT.S87792.

214. Jin Y, Fan M. Treatment of gynecomastia with prednisone: case report and literature review. J Int Med Res. 2019;47:2288–2295. doi: 10.1177/0300060519840896.

215. Lin KT, Wang LH. New dimension of glucocorticoids in cancer treatment. Steroids. Elsevier Inc.; 2016;111:84–88. doi: 10.1016/j.steroids.2016.02.019.

216. Kumar R, Thompson EB. Gene regulation by the glucocorticoid receptor: Structure:function relationship. J Steroid Biochem Mol Biol. 2005;94:383–394. doi: 10.1016/j.jsbmb.2004.12.046.

217. Schoneveld OJLM, Gaemers IC, Lamers WH. Mechanisms of glucocorticoid signalling. Biochim Biophys Acta - Gene Struct Expr. 2004;1680:114–128. doi: 10.1016/j.bbaexp.2004.09.004.

218. Perretti M, Ahluwalia A. The microcirculation and inflammation: Site of action for glucocorticoids. Microcirculation. Nature Publishing Group; 2000;7:147–161.

219. Liberman AC, Druker J, Perone MJ, Arzt E. Glucocorticoids in the regulation of transcription factors that control cytokine synthesis. Cytokine Growth Factor Rev. 2007;18:45–56. doi: 10.1016/j.cytogfr.2007.01.005.

220. Zhang JM, An J. Cytokines, inflammation, and pain. Int. Anesthesiol. Clin. 2007;45:27–37. doi: 10.1097/AIA.0b013e318034194e.

221. Ferrari F, Bertoni M, Bonferoni CM, Rossi S, Caramella C, Bolhuis GK.

Dissolution enhancement of an insoluble drug by physical mixture with a superdisintegrant: optimization with a simplex lattice design. Pharm. Dev. Technol. 1996;1:159-164. doi: 10.3109/10837459609029890.

222. Spies CM, Cutolo M, Straub RH, G-R B, Buttgereit F. Prednisone chronotherapy. Clin Exp Rheumatol. 2011;29:S42–S45.

223. Poller B, Strachan C, Broadbent R, Walker GF. A minitablet formulation made from electrospun nanofibers. Eur J Pharm Biopharm. 2017;114:213–220. doi: 10.1016/j.ejpb.2017.01.022.

224. Wang Y, Tao M, Wei H, Arslan Ahmad M, Ma Y, Mao X, Hao L, Ao Q. Poly (ε-Caprolactone-co-l,l-Lactide) Vascular External Sheath Carrying Prednisone for Improving Patency Rate of the Vein Graft. Tissue Eng Part A. 2021;28:394–404. doi: 10.1089/ten.tea.2021.0118.

225. Celebioglu A, Wang N, Kilic ME, Durgun E, Uyar T. Orally Fast Disintegrating Cyclodextrin/Prednisolone Inclusion-Complex Nanofibrous Webs for Potential Steroid Medications. Mol Pharm. 2021;18:4486–4500. doi: 10.1021/acs.molpharmaceut.1c00677.

226. Tawfik EA, Scarpa M, Abdelhakim HE, Bukhary HA, Craig DQM, Barker SA, Orlu M. A potential alternative orodispersible formulation to prednisolone sodium phosphate orally disintegrating tablets. Pharmaceutics. 2021;13:1–17. doi: 10.3390/pharmaceutics13010120.

227. Jafari-Aghdam N, Adibkia K, Payab S, Barzegar-Jalali M, Parvizpur A, Mohammadi G, Sabzevari A. Methylprednisolone acetate-Eudragit® RS100 electrospuns: Preparation and physicochemical characterization. Artif Cells, Nanomedicine Biotechnol. 2016;44:497–503. doi: 10.3109/21691401.2014.965309.

228. Zhang S, Wang XJ, Li WS, Xu XL, Hu JB, Kang XQ, Qi J, Ying XY, You J, Du YZ. Polycaprolactone/polysialic acid hybrid, multifunctional nanofiber scaffolds for treatment of spinal cord injury. Acta Biomater. 2018;77:15–27. doi: 10.1016/j.actbio.2018.06.038.

229. Yao Y, Ding J, Wang Z, Zhang H, Xie J, Wang Y, Hong L, Mao Z, Gao J, Gao C. ROS-responsive polyurethane fibrous patches loaded with methylprednisolone (MP) for restoring structures and functions of infarcted myocardium in vivo.

Biomaterials. 2020;232. doi: 10.1016/j.biomaterials.2019.119726.

230. Yoshida M, Langer R, Lendlein A, Lahann J. From advanced biomedical coatings to multi-functionalized biomaterials. Polym Rev. 2006;46:347–375. doi: 10.1080/15583720600945394.

231. Bansal R, Singh R, Kaur K. Quantitative analysis of doxorubicin hydrochloride and arterolane maleate by mid IR spectroscopy using transmission and reflectance modes. BMC Chem. 2021;15. doi: 10.1186/s13065-021-00752-3.

232. Son YJ, Kim WJ, Yoo HS. Therapeutic applications of electrospun nanofibers for drug delivery systems. Arch. Pharm. Res. 2014;37:69–78. doi: 10.1007/s12272-013-0284-2.

233. Zupančič Š, Preem L, Kristl J, Putrinš M, Tenson T, Kocbek P, Kogermann K. Impact of PCL nanofiber mat structural properties on hydrophilic drug release and antibacterial activity on periodontal pathogens. Eur J Pharm Sci. 2018;122:347–358. doi: 10.1016/j.ejps.2018.07.024.

234. Enayati MS, Behzad T, Sajkiewicz P, Rafienia M, Bagheri R, Ghasemi-Mobarakeh L, Kolbuk D, Pahlevanneshan Z, Bonakdar SH. Development of electrospun poly (vinyl alcohol)-based bionanocomposite scaffolds for bone tissue engineering. J Biomed Mater Res - Part A. 2018;106:1111–1120. doi: 10.1002/jbm.a.36309.

235. Nita LE, Chiriac AP, Popescu CM, Neamtu I, Alecu L. Possibilities for poly(aspartic acid) preparation as biodegradable compound. J Optoelectron. Adv. Mater. 2006;8:663-666.

236. Molnar K, Juriga D, Nagy PM, Sinko K, Jedlovszky-Hajdu A, Zrinyi M. Electrospun poly(aspartic acid) gel scaffolds for artificial extracellular matrix. Polym Int. 2014;63:1608–1615. doi: 10.1002/pi.4720.

237. Juriga D, Kalman EE, Toth K, Barczikai D, Szöll D, Földes A, Nagy KS. Analysis of Three-Dimensional Cell Migration in Dopamine-Modified Poly(aspartic acid)-Based Hydrogels. Gels. 2022;8. doi: https://doi.org/10.3390/gels8020065.

238. Milosevic M, Stojanovic DB, Simic V, Grkovic M, Bjelovic M, Uskokovic PS, Kojic M. Preparation and modeling of three-layered PCL/PLGA/PCL fibrous scaffolds for prolonged drug release. Sci Rep. 2020;10. doi: 10.1038/s41598-020-

68117-9.

239. Tran T, Hernandez M, Patel D, Wu J. Temperature and pH responsive microfibers for controllable and variable ibuprofen delivery. Adv Mater Sci Eng. 2015;2015:6. doi: 10.1155/2015/180187.

240. Juhasz AG, Molnar K, Idrissi A, Jedlovszky-Hajdu A. Salt induced fluffy structured electrospun fibrous matrix. J Mol Liq. 2020;312:113478. doi: 10.1016/j.molliq.2020.113478.

241. Jia LN, Zhang X, Xu HY, Hua F, Hu XG, Xie Q, Wang W, Jia J. Development of a Doxycycline Hydrochloride-Loaded Electrospun Nanofibrous Membrane for GTR/GBR Applications. J Nanomater. 2016;2016. doi: 10.1155/2016/6507459.

242. Salles THC, Volpe-Zanutto F, De Oliveira Sousa IM, MacHado D, Zanatta AC, Vilegas W, Lancellotti M, Foglio MA, D'Avila MA. Electrospun PCL-based nanofibers Arrabidaea chica Verlot - Pterodon pubescens Benth loaded: Synergic effect in fibroblast formation. Biomed Mater. 2020;15. doi: 10.1088/1748-605X/ab9bb1.

243. Ramalingam R, Dhand C, Leung CM, Ong ST, Annamalai SK, Kamruddin M, Verma NK, Ramakrishna S, Lakshminarayanan R, Arunachalam KD. Antimicrobial properties and biocompatibility of electrospun poly-ε-caprolactone fibrous mats containing Gymnema sylvestre leaf extract. Mater Sci Eng C. 2019;98:503–514. doi: 10.1016/j.msec.2018.12.135.

244. Liu DQ, Cheng ZQ, Feng QJ, Li HJ, Ye SF, Teng B. Polycaprolactone nanofibres loaded with 20(S)-protopanaxadiol for in vitro and in vivo anti-tumour activity study. R Soc Open Sci. 2018;5. doi: 10.1098/rsos.180137.

245. Tetteh G, Khan AS, Delaine-Smith RM, Reilly GC, Rehman IU. Electrospun polyurethane/hydroxyapatite bioactive Scaffolds for bone tissue engineering: The role of solvent and hydroxyapatite particles. J Mech Behav Biomed Mater. 2014;39:95–110. doi: 10.1016/j.jmbbm.2014.06.019.

246. Wong SC, Baji A, Leng S. Effect of fiber diameter on tensile properties of electrospun poly(ε-caprolactone). Polymer (Guildf). 2008;49:4713–4722. doi: 10.1016/j.polymer.2008.08.022.

247. Kim HH, Kim MJ, Ryu SJ, Ki CS, Park YH. Effect of fiber diameter on surface morphology, mechanical property, and cell behavior of electrospun poly(ε-

caprolactone) mat. Fibers Polym. 2016;17:1033–1042. doi: 10.1007/s12221-016-6350-x.

248. Lim CT, Tan EPS, Ng SY. Effects of crystalline morphology on the tensile properties of electrospun polymer nanofibers. Appl Phys Lett. 2008;92. doi: 10.1063/1.2857478.

249. Costa T, Ribeiro A, Machado R, Ribeiro C, Lanceros-Mendez S, Cavaco-Paulo A, Almeida A, das Neves J, Lúcio M, Viseu T. Polymeric Electrospun Fibrous Dressings for Topical Co-delivery of Acyclovir and Omega-3 Fatty Acids. Front Bioeng Biotechnol. 2019;7. doi: 10.3389/fbioe.2019.00390.

250. Al-Bishari AM, Al-Shaaobi BA, Al-Bishari AA, Al-Baadani MA, Yu L, Shen J, Cai L, Shen Y, Deng Z, Gao P. Vitamin D and curcumin-loaded PCL nanofibrous for engineering osteogenesis and immunomodulatory scaffold. Front Bioeng Biotechnol. 2022;10. doi: 10.3389/fbioe.2022.975431.

251. Rychter M, Milanowski B, Grześkowiak BF, Jarek M, Kempiński M, Coy EL, Borysiak S, Baranowska-Korczyc A, Lulek J. Cilostazol-loaded electrospun three-dimensional systems for potential cardiovascular application: Effect of fibers hydrophilization on drug release, and cytocompatibility. J Colloid Interface Sci. 2019;536:310–327. doi: 10.1016/j.jcis.2018.10.026.

252. Lanno GM, Ramos C, Preem L, Putrins M, Laidmaë I, Tenson T, Kogermann K. Antibacterial porous electrospun fibers as skin scaffolds for wound healing applications. ACS Omega. 2020;5:30011–30022. doi: 10.1021/acsomega.0c04402.

253. Asadian M, Rashidi A, Majidi M, Mehrjoo M, Emami BA, Tavassoli H, Asl MP, Bonakdar S. Nanofiber protein adsorption affected by electrospinning physical processing parameters. J Iran Chem Soc. 2015;12:1089–1097. doi: 10.1007/s13738-014-0569-5.

254. Rahmani E, Pourmadadi M, Zandi N, Rahdar A, Baino F. pH-Responsive PVA-Based Nanofibers Containing GO Modified with Ag Nanoparticles: Physico-Chemical Characterization, Wound Dressing, and Drug Delivery. Micromachines. 2022;13. doi: 10.3390/mi13111847.

255. Zrinyi M, Gyenes T, Juriga D, Kim JH. Volume change of double cross-linked poly(aspartic acid) hydrogels induced by cleavage of one of the crosslinks. Acta

Biomater. 2013;9:5122–5131. doi: 10.1016/j.actbio.2012.08.046.

256. Song J, Kim BC, Nguyen DTT, Samidurai M, Choi SM. Levodopa (L-DOPA) attenuates endoplasmic reticulum stress response and cell death signaling through DRD2 in SH-SY5Y neuronal cells under α-synuclein-induced toxicity. Neuroscience. 2017;358:336–348. doi: 10.1016/j.neuroscience.2017.06.060.

257. Wu X, Xu F ling, Wang B jie, Yao J. Analysis of the Promoter Region of Human Dopamine Receptor D1. J Mol Neurosci. 2018;65:438–443. doi: 10.1007/s12031-018-1116-0.

258. Kawanabe N, Murata S, Murakami K, Ishihara Y, Hayano S, Kurosaka H, Kamioka H, Takano-Yamamoto T, Yamashiro T. Isolation of multipotent stem cells in human periodontal ligament using stage-specific embryonic antigen-4. Differentiation. 2010;79:74–83. doi: 10.1016/j.diff.2009.10.005.

259. Lehmensiek V, Tan EM, Liebau S, Lenk T, Zettlmeisl H, Schwarz J, Storch A. Dopamine transporter-mediated cytotoxicity of 6-hydroxydopamine in vitro depends on expression of mutant α-synucleins related to Parkinson's disease. Neurochem Int. 2006;48:329–340. doi: 10.1016/j.neuint.2005.11.008.

260. Gómez-Santos C, Ferrer I, Santidrián AF, Barrachina M, Gil J, Ambrosio S. Dopamine induces autophagic cell death and α-synuclein increase in human neuroblastoma SH-SY5Y cells. J Neurosci Res. 2003;73:341–350. doi: 10.1002/jnr.10663.

261. Thomas CR, Ferris DP, Lee JH, Choi E, Cho MH, Kim ES, Stoddart JF, Shin JS, Cheon J, Zink JI. Noninvasive remote-controlled release of drug molecules in vitro using magnetic actuation of mechanized nanoparticles. J Am Chem Soc. 2010;132:10623–10625. doi: 10.1021/ja1022267.

262. Nigjeh SE, Yeap SK, Nordin N, Kamalideghan B, Ky H, Rosli R. Citral induced apoptosis in MDA-MB-231 spheroid cells. BMC Complement Altern Med. 2018;18. doi: 10.1186/s12906-018-2115-y.

263. Sabzi A, Rahmani A, Edalati M, Kahroba H, Dadpour MR, Salehi R, Zarebkohan A. Targeted co-delivery of curcumin and doxorubicin by citric acid functionalized Poly (ε-caprolactone) based micelle in MDA-MB-231 cell. Colloids Surfaces B Biointerfaces. 2020;194. doi: 10.1016/j.colsurfb.2020.111225.

264. Rezano A, Ridhayanti F, Rangkuti AR, Gunawan T, Winarno GNA, Wijaya I. Cytotoxicity of Simvastatin in Human Breast Cancer MCF-7 and MDA-MB-231 Cell Lines. Asian Pacific J Cancer Prev. 2021;22:33–42. doi: 10.31557/APJCP.2021.22.S1.33.

265. Pilco-Ferreto N, Calaf GM. Influence of doxorubicin on apoptosis and oxidative stress in breast cancer cell lines. Int J Oncol. 2016;49:753–762. doi: 10.3892/ijo.2016.3558.

266. Ansari S, Diniz IM, Chen C, Sarrion P, Tamayol A, Wu BM, Moshaverinia A. Human Periodontal Ligament- and Gingiva-derived Mesenchymal Stem Cells Promote Nerve Regeneration When Encapsulated in Alginate/Hyaluronic Acid 3D Scaffold. Adv Healthc Mater. 2017;6:1–10. doi: 10.1002/adhm.201700670.

267. Pang X, Jiang Y, Xiao Q, Leung AW, Hua H, Xu C. PH-responsive polymer-drug conjugates: Design and progress. J Control Release. 2016;222:116–129. doi: 10.1016/j.jconrel.2015.12.024.

268. Pogun S, Baumann MH, Kuhar MJ. Nitric oxide inhibits [3H]dopamine uptake. Brain Res. 1994;641:83–91. doi: 10.1016/0006-8993(94)91818-X.

269. Khandekar S V., Kulkarni MG, Devarajan P V. Polyaspartic acid functionalized gold nanoparticles for tumor targeted doxorubicin delivery. J Biomed Nanotechnol. 2014;10:143–153. doi: 10.1166/jbn.2014.1772.

270. Alcoba DD, Schneider J, Arruda L, Martiny PB, Capp E, von Eye Corleta H, Brum IS. Brilliant cresyl blue staining does not present cytotoxic effects on human luteinized follicular cells, according to gene/protein expression, as well as to cytotoxicity tests. Reprod Biol. 2017;17:60–68. doi: 10.1016/j.repbio.2016.12.003.

271. Vennerstrom JL, Makler MT, Angerhofer CK, Williams JA. Antimalarial dyes revisited: Xanthenes, azines, oxazines and thiazines. Antimicrob Agents Chemother. 1995;39:2671–2677. doi: 10.1128/AAC.39.12.2671.

272. Varkouhi AK, Scholte M, Storm G, Haisma HJ. Endosomal escape pathways for delivery of biologicals. J Control Release. 2011;151:220–228. doi: 10.1016/j.jconrel.2010.11.004.

273. Liu Y, Choi CKK, Hong H, Xiao Y, Kwok ML, Liu H, Tian XY, Choi CHJ. Dopamine Receptor-Mediated Binding and Cellular Uptake of Polydopamine-

Coated Nanoparticles. ACS Nano. 2021;15:13871–13890. doi: 10.1021/acsnano.1c06081.

274. Anaya JM, Shoenfeld Y, Rojas-Villarraga A, Levy RA, Cervera R. Cancer and Autoimmunity. El Rosario University Press, Bogota, 2000, Chapter 27: 455-475. doi: 10.1016/b978-0-444-50331-2.x5000-0.

275. Chen K, Satlof L, Stoffels G, Kothapalli U, Ziluck N, Lema M, Poretsky L, Avtanski D. Cytokine secretion in breast cancer cells – MILLIPLEX assay data. Data Br. 2020;28:104798. doi: 10.1016/j.dib.2019.104798.

276. Hernández-Bedolla MA, Carretero-Ortega J, Valadez-Sánchez M, Vázquez-Prado J, Reyes-Cruz G. Chemotactic and proangiogenic role of calcium sensing receptor is linked to secretion of multiple cytokines and growth factors in breast cancer MDA-MB-231 cells. Biochim Biophys Acta - Mol Cell Res. 2015;1853:166–182. doi: 10.1016/j.bbamcr.2014.10.011.

277. Tan LH, Lin C, Ungerer H, Kumar A, Qatanani A, Adappa ND, Palmer JN, Bosso J V., Reed D, Cohen NA, Kohanski MA. Steroid affected cytokines in aspirin-exacerbated respiratory disease. Int Forum Allergy Rhinol. 2022;12:1232–1241. doi: 10.1002/alr.22977.

278. Hackett AP, Trinick RE, Rose K, Flanagan BF, McNamara PS. Weakly acidic pH reduces inflammatory cytokine expression in airway epithelial cells. Respir Res. 2016;17:1–9. doi: 10.1186/s12931-016-0399-3.

279. Jesus S, Bernardi N, Da Silva J, Colaço M, Panaõ Costa J, Fonte P, Borges O. Unravelling the Immunotoxicity of Polycaprolactone Nanoparticles-Effects of Polymer Molecular Weight, Hydrolysis, and Blends. Chem Res Toxicol. 2020;33:2819–2833. doi: 10.1021/acs.chemrestox.0c00208.

10. Bibliography of the candidate's publications

Publications relevant to the dissertation

KT1: Krisztina Tóth, Krisztina S. Nagy, Zeliha Güler, Ákos György Juhász, Éva Pállinger, Gábor Varga, A. Sezai Sarac, Miklós Zrínyi, Angéla Jedlovszky-Hajdú, and Dávid Juriga. Characterization of Electrospun Polysuccinimide-Dopamine Conjugates and Effect on Cell Viability and Uptake. Macromolecular Bioscience. 2023; 2200397.

KT2: Krisztina Tóth, Nóra Fekete, Vivien Klaudia Simon, Bence Tóth, Árpád Ferenc Kovács, Éva Pállinger, István Antal, László Kőhidai, Angéla Jedlovszky-Hajdú, Dávid Juriga, Krisztina S. Nagy. Different implantable electrospun meshes for simultaneous application of prednisone and doxorubicin. Journal of Molecular Liquids. 2023;121854.

Publications not relevant to the dissertation

Dávid Juriga, Eszter Kálmán, Krisztina Tóth, Dóra Barczikai, Dávid Szöllősi, Anna Földes, Gábor Varga, Miklós Zrínyi, Angéla Jedlovszky-Hajdú, Krisztina S. Nagy. Analysis of Three-Dimensional Cell Migration in Dopamine-Modified Poly(aspartic acid)-Based Hydrogels. GELS. 2022; 8 (2) Paper 65.

László Mészáros, Balázs Tatár, Krisztina Tóth, Anna Földes, Krisztina S. Nagy, Angéla Jedlovszky-Hajdú, Tünde Tóth, Kolos Molnár. Novel, Injection Molded All-Polyethylene Composites for Potential Biomedical Implant Applications. Journal of Materials Research and Technology. 2022; 17:743-755.

Krisztina S. Nagy, Krisztina Tóth, Éva Pállinger, Angéla Takács, László Kőhidai, Angéla Jedlovszky-Hajdú, Domokos Máthé, Noémi Kovács, Dániel S. Veres, Krisztián Szigeti, Kristóf Molnár, Enikő Krisch, Judit E. Puskás. Folate-Targeted Monodisperse PEG-Based Conjugates Made by Chemo-Enzymatic Methods for Cancer Diagnosis and Treatment. International Journal of Molecular Sciences. 2021; 22 (19) Paper 10347.

11. Acknowledgements

First of all, I would like to express my gratitude to my supervisor, Dr. Krisztina S. Nagy, for her support and encouragement before and during my Ph.D. work and for educating me on in vitro cell culturing.

I highly appreciate the guidance and support of my consultant, Dr. Angéla Jedlovszky-Hajdú, who with Prof. Miklós Zrínyi provided me the opportunity to become a member of the Nanochemistry Research Group.

I must also acknowledge Prof. Miklós Kellermayer, who allowed me to work in the Department of Biophysics and Radiation Biology at Semmelweis University and I would like to offer my gratitude to Prof. Gábor Varga, Prof. László Kőhidai and Dr. Éva Pállinger for enabling the availability of the instruments and equipment for the in vitro research. I would like to thank Dr. Anna Földes for the useful suggestions that she shared with me regarding the in vitro experiments. I would like to offer my gratitude to Prof. István Antal, who supported my work by enabling the availability of the instruments for XRD measurements, and to Zsófia Garadi and Dr. Szabolcs Béni for the NMR measurements.

I must thank the following people who also provided assistance and care during the experimental work: Nóra Fekete, Eszter Kálmán, Bence Tóth, Vivien Simon.

I really appreciate the support of the recent and former members of the Nanochemistry Research Group: Ákos Juhász, Rita Pázmány, Ramóna Cseke-Gottscháll, Dr. Constantinos Voniatis, Bálint Budavári, Dr. Evelin Forró, Dóra Barczikai, Dr. Kristóf Molnár, and Elza Simon.

I highly appreciate the work of the pre-defense reviewers Dr. Dóra Haluszka and Dr. György Török, who endorsed a developed version of this thesis.

Special thanks should be given to Dr. Dávid Juriga for his constructive suggestions, his help in the experimental work, and his permanent support and motivation from the early beginning.

Last but not least, I appreciate the support that I have been receiving from my family and my friends.